WASM: Minerals, Energy and Chemical Engineering

Application of Electrostatic Solvent Extraction for Process Metallurgy

Zela Tanlega Ichlas

0000-0003-2550-5948

This thesis is presented for the Degree of
Doctor of Philosophy
of
Curtin University

April 2022

DECLARATION

To the best of my knowledge and belief this thesis contains no material previously published by any other person except where due acknowledgement has been made.

This thesis contains no material which has been accepted for the award of any other degree or diploma in any university.

Signature: Zela Tanlega Ichlas

Date: 15 April 2022

COPYRIGHT STATEMENT

I have obtained permission from the copyright owners to use any third-party copyright material reproduced in the thesis (e.g., questionnaires, artwork, unpublished letters), or to use any of my own published work (e.g., journal articles) in which the copyright is held by another party (e.g., publisher, co-author).

Signature: Zela Tanlega Ichlas

Date: 15 April 2022

ACKNOWLEDGEMENT

First of all, I would like to extend my gratitude to my supervisor, Dr Bogale Tadesse, for his guidance, encouragement and support. I would also like to thank my associate supervisors, Dr Richard Alorro and Dr Simon Assmann, for their knowledge and constructive suggestions.

This research is sponsored by the Minerals Research Institute of Western Australia (MRIWA). I would like to thank MRIWA for their financial support. Special thanks to Dr Penny Atkins, Dr Charmaine de Witt and Dr Geoffrey Batt from MRIWA for helping me with my many enquiries.

I am grateful to the faculty members, laboratory technical staff and support staff at the WA School of Mines, Curtin University, for their assistance. Special thanks to Mujesira Vukancic, Anusha Shanta Kumara, Melina Miralles, Sheree McCutcheon and Colin Tayler for their help and friendship throughout the course of my study. Thank are also due to Angelina Rossiter, Graeme Watson and David Collier for their assistance to fabricate the necessary components to modify the X-Y Table for my experiments.

I am also grateful to the staff at the WA School of Mines Kalgoorlie Library, Teresa Bennett and Mieke Boers, for their warm friendship and encouragement. Thank you for treating me so kindly.

I am thankful to my fellow HDR colleagues for their camaraderie. Thank you, Dr Ndisha Mbedzi, Daryl Gaw, Dr Lahiru Basnayaka, Dr Yasin Dagasan, Dr Ping Chang, Dr Yinping Chen, Elham Aghaei, April Calderon, Bona Lim and Izzan Nur Aslam, for your friendship, advice and support.

Last but not least, I would like to offer my deepest gratitude to my wife, Indahtyas Winasis, for helping me survive this journey and to all my family and friends for supporting me.

ABSTRACT

Solvent extraction (SX) is an essential separation technique in process metallurgy and its use has been increasing and expanding owing to the increasing need to process low-grade and complex ores. Current SX technology, however, has inherent limitations owing to the use of mechanical agitation, leading to poor mass transfer, loss of reagents and high power consumption. The use of electrostatic fields to induce mixing in SX, and hence referred to as electrostatic solvent extraction (ESX), can potentially circumvent these limitations without changing the chemistry of the process. This is because the technique allows the production of small droplets with narrow droplet size distribution that nevertheless exhibit a high degree of turbulence inside and outside these droplets. Moreover, the applied electrostatic field acts only at the liquid–liquid interface rather than in the bulk of the liquids, leading to low energy consumption.

In relatively recent years, significant advances have been made in efforts to develop the technique for applications in process metallurgy. These include the achievement of a volumetric throughput that is comparable with that of a conventional sieve-plate pulse column and the development of a technique to characterise droplet dispersion behaviours under the influence of electrostatic fields involving use of an advanced imaging technology. The imaging technology, however, allowed only a limited range of droplet size to be studied at a time, and the previous study on the subject focused on the behaviours of droplets ranging from 100 μm to 1400 μm. These behaviours include breakup, motion and oscillation. Given that one major advantage of ESX is that it can be operated with smaller droplets, the present study aimed to investigate the behaviours of the smaller droplets under more vigorous electrostatic field conditions, i.e., at higher field strengths, than those studied previously to address this gap.

This thesis consists of three main parts: (i) investigation of the effect of electrostatic fields on droplet dispersion behaviours, which include droplet breakup, motion and oscillation; (ii) investigation of the effect of electrostatic fields on droplet size and size distribution; and (iii) investigation of the effect of the changes in the dispersion characteristics in relation to properties of the electrostatic fields on mass transfer. These investigations were performed through systematic experimental works using an identical SX system and comparable experimental method to those used in the previous study so a direct comparison can be made. These experiments were performed using

an ESX column involving insulated parallel-plate electrodes with alternating current (AC) fields. Experiments involving an SX system with a slow extraction kinetics were also performed to help evaluate the performance of the ESX technique.

The investigation of the effect of AC fields on droplet breakup, motion and oscillation revealed that:

- The application of more vigorous AC fields from insulated electrodes could induce a breakup mechanism that was not previously observed in AC fields, namely an emulsion-like formation.
- The combination of breakup involving jetting and necking was found to be the predominant breakup mechanism in all the tested ranges. This mechanism was only observed at the highest tested fields strength and frequencies below 50 Hz in the previous study.
- Increases in strength and decreases in frequency of the AC fields increased the amplitude of droplet motion and oscillation. In the present study, to the best of the present author's knowledge, it was observed for the first time that droplets as small as 23 μm in diameter, which was the smallest observable size within the used imaging technology, exhibited significant motion and oscillation.
- It was found that the horizontal velocity of droplets with a diameter < 100 μm was generally smaller than the larger droplets, but the gap between them decreased with increasing field strength to the point that it was practically negligible at 4.25 kV/cm. This has not been previously observed.
- Increases in droplet motion increased the frequency of droplet coalescence, and the resulting droplets were often so unstable that they underwent redispersion after formation.
- Application of a vigorous electrostatic field could lead to the formation of a semi-permanent emulsion. The proclivity for the emulsion to form increased with increasing field strength and decreasing frequency.

The investigation of the effect of AC fields on droplet size and droplet size distribution revealed that:

- The increase in strength and decrease in frequency of the field decreased the droplet size. The trends of plots of the droplet Sauter mean diameter as a

function of either the field strength or frequency were almost linear, analogous to those previously observed at the lower field strengths.

- The effect of strength and frequency of the field was found to vary depending on whether droplet size distributions were in a regime where they were unimodal or multimodal. This has not been observed before.
- The formation of a semi-permanent emulsion formation was found to be related to the size of the droplets generated by the electrostatic fields that prevented them from settling. It was found that the smallest Sauter mean diameter at which the ESX technique can operate before an emulsion starts to form was 115 μm, which corresponds to 54 μm in average diameter.

The investigation of the effect of AC fields on mass transfer revealed that:

- The trend of the increasing cobalt extraction with increasing field strength and decreasing field frequency continued to increase almost linearly when the droplet size decreased to mainly below 100 μm in more vigorous fields compared with those previously studied, even under conditions that were near the regime where the semi-permanent emulsion formed.
- The ESX technique appeared to be able to overcome the slow extraction kinetics of the extraction of copper(II) from sulfate with LIX® 84-I, an oxime extractant, under the tested ranges. Moreover, the mass-transfer enhancement could still be increased further as the droplets appeared to be still large enough to allow the application of even more vigorous fields before the semi-permanent emulsion forms for this liquid–liquid system.

Overall, the results of the present study showed that increases in the strength and decreases in the frequency of the field, which have been previously identified to be favourable to enhancing mass transfer, continued to be favourable for mass transfer when dispersing smaller droplets under more vigorous electrostatic fields, but they also increase the proclivity for the formation of a semi-permanent emulsion, leading to poor phase disengagement. Hence, to achieve high mass-transfer rates and fast phase disengagement in ESX, a compromise must be made where the electrostatic field conditions are sufficiently vigorous to produce small droplets that exhibit high agitation but not too vigorous to form an emulsion.

TABLE OF CONTENTS

LIST OF FIGURES

LIST OF TABLES

CHAPTER 1
INTRODUCTION

1.1 BACKGROUND OF THE STUDY

Solvent extraction (SX) is an essential separation technique in process metallurgy. It is the only commercial separation technique that allows complete separation of chemically similar metals such as nickel and cobalt, and the rare earth metals. It is also applicable to a wide range of metal concentrations and pH values. These make the technique particularly useful in the exploitation of low grade and complex ores because they invariably generate highly contaminated dilute leach solutions.

The separation of metal of interest from impurities in SX (or vice versa) is achieved by contacting the contaminated leach solution with an immiscible organic phase containing an extractant with a high affinity towards the metal of interest. This results in two phases, namely loaded organic, which is the organic phase that contains the extracted metal, and raffinate, the residual aqueous phase containing little to no metal of interest. Hence, a conventional SX operation comprises at least one mixing step that is followed by a phase-separation step to obtain separate streams of each phase, as illustrated in Figure 1.1.

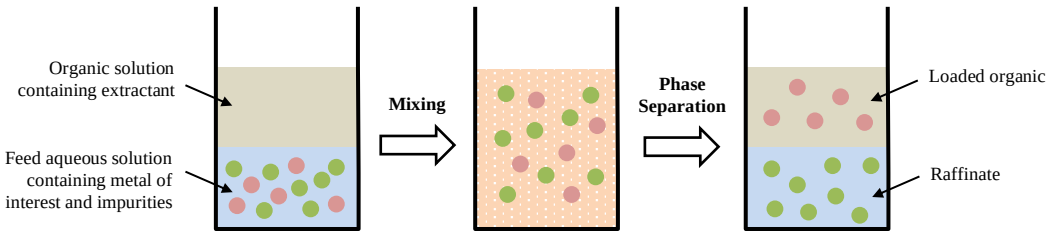

Figure 1.1. Simplified illustration of the mixing and phase separation steps in a conventional SX operation.

The mass transfer process during mixing is facilitated through the dispersion of one phase as droplets in another phase to increase the interfacial contact between the two phases. Therefore, it is logical that the size of the dispersed droplets significantly influences the mass-transfer efficiency because the smaller the droplets, the larger is the interfacial contact area. This, however, does not necessarily lead to a greater rate of mass transfer because as the size of the droplets decrease, they increasingly behave

like a rigid sphere. That is, the droplet interface becomes more immobile as the size decreases, leading to less internal circulation and droplet oscillation, which then impedes the transfer of solutes between the two phases. In addition, as the size of the droplets decreases, the time required for phase separation increases, leading to a large plant footprint to accommodate the slow phase separation step, which then leads to high solvent inventory. Hence, at a particular point, decreases in the droplet size would reduce the efficiency of the mass-transfer process and significantly hinder the phase disengagement process.

The size distribution of the produced droplets also has a pronounced influence on both the mass-transfer and phase-separation efficiencies. The former is because the smaller droplets in the dispersion become ineffective in the mass-transfer process more quickly than the larger droplets as they become depleted of the metal within a shorter contact time resulting in a loss of effective interfacial area (Chakraborty et al., 2003). The latter is because the larger droplets collide and coalesce at much faster rates than the smaller droplets, leading to entrainment loss of the remnant population of smaller droplets (Klink et al., 2011). It is, therefore, undesirable to produce dispersions with a wide droplet size distribution during the mixing step.

Despite this, the most common means of mixing in current commercial SX operations for process metallurgy applications is via mechanical agitation, which has poor control of the droplet size distribution. The poor droplet size control is mainly because the dispersion in a mechanically agitated contactor is promoted by high-shear flows that are generated by rotating impellers. High-shear mixing exhibits a highly variable breakup because the intensity of the breakup forces that act on the droplets depends on their position relative to the high-shear zone near the impeller (Park and Blair, 1975). Consequently, there is a tendency for the produced droplets to coalesce as they move away from this zone resulting in a broad distribution of droplet sizes even at equilibrium. Moreover, this dispersion process is inefficient in terms of power consumption because the energy is applied to the bulk of the phases but the actual mixing process is only adequate around the impeller (Wu and Patterson, 1989; Ng and Yianneskis, 2000).

The use of high-shear mixing also entails other operational limitations, including the susceptibility of the mechanically agitated contactor to produce ultrafine droplets that

exhibit rigid-sphere behaviour and to promote the formation of crud, a stable emulsion of suspended solids and solvent phases. These are detrimental to the economics of the operation as they lead to significant loss of the solvent and, moreover, accumulation of the latter also leads to plant downtime for maintenance (Ritcey, 1980; Vancas, 2003; Ritcey, 2006).

The development of pulsed-column technology as an alternative contactor circumvents some of the limitations of mechanically agitated contactors. Note that reciprocating plate column is another type of agitated column beside pulsed column, but it is not normally used for hydrometallurgical applications. Dispersion of droplets in a pulsed column is produced by passing the phases through column internals, such as perforated plates in the middle part of the vertical column, as depicted in Figure 1.2. Contact between the phases is enhanced by introducing the heavier phase from the top and the lighter phase from the bottom of the column to obtain counter-current flow of these two phases and also by applying pulsatile actions to induce turbulence within the column. This dispersion process provides low shear rates during mixing, thus virtually eliminating the probability of producing ultrafine droplets and accumulating crud. This process, however, is relatively gentle in nature and, hence, a pulsed column can only produce droplets of relatively large sizes, making pulsed columns typically unsuitable for SX systems that have slow kinetics as they would require excessively tall columns.

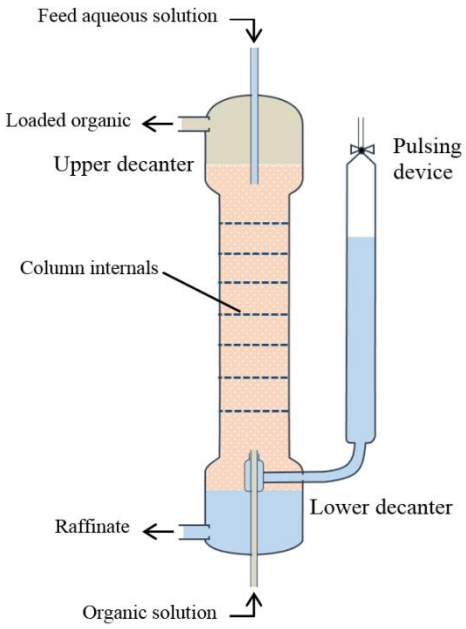

Figure 1.2. Schematic diagram of a pulsed column (Vancas, 2003).

Given the limitations of mechanically agitated contactors and pulsed columns inherent to the nature of their dispersion processes, it is reasonable to suggest that the use of an entirely new dispersion process is needed to achieve significant improvement in SX. The use of electrostatic fields is an attractive alternative as it promises to overcome the limitations of these conventional dispersion processes.

The basis of electrostatic dispersion is that the application of external electric fields can polarise conductive droplets that are immersed in a nonconductive continuum to effect droplet breakup and agitation. If a transient field is used, the polarised droplets will elongate and retract along the axis parallel to the electric field lines, making them oscillate in this direction following the frequency of the applied field (Torza et al., 1971; Wham and Byers, 1987; Vizika and Saville, 1992; Assmann, 2014; Guo et al., 2015; Yan et al., 2015). This results in an increase of the interfacial surface area and induces turbulence within and around the droplets. Droplet breakup can be achieved by increasing the strength of the electrostatic field to overcome the interfacial tension that holds the droplet together. This mechanism of droplet breakup is advantageous because a particular field strength should only break droplets larger than a particular size, thus promising good control of the droplet size distribution.

Use of an electrostatic field also promises the possibility of operating with much smaller droplets than those practically viable with conventional technologies. This is firstly because the imposed electrical stress at the droplet interface induces turbulence of fluids within and around the droplet (Taylor, 1966), which enhances the mass transfer rate and theoretically reduces the droplets tendency to rigid sphere behaviours. Consequently, the use of electrostatic fields allows the generation of small droplets that nevertheless exhibit high mass-transfer coefficients (Bailes, 1981; He et al., 1997). Secondly, application of electrostatic fields can also be made to enhance the rate of coalescence between the dispersed droplets during or after mixing as the induced polarisation promotes rapid rupture of the film at the droplet–droplet interface (Allan and Mason, 1962b; Brown and Hanson, 1965; Eow et al., 2001). This concept of phase separation, which is widely known as electrocoalescence, has been successfully used to enhance the coalescence of water in crude oil for decades (Atten, 1993; Eow and Ghadiri, 2002; Noik et al., 2006).

Moreover, the electrical means of droplet dispersion is much more efficient in terms of energy consumption than mechanical agitation. It is estimated that the electric energy consumption to produce a particular droplet size using electrostatic force can be less than 1% of that required using mechanical agitation (Scott and Sisson, 1988). This is possible because the applied electrostatic forces interact selectively with only one of the phases. Therefore, the applied energy is directly utilised to disperse the droplets, leading to minimal energy loss during mixing, which is usually associated with friction forces between moving parts and liquid in the case of mechanical agitation.

1.2 STATEMENTS OF THE PROBLEM

Despite the desirable features of using electrostatic fields to effect mixing for SX applications, and hence electrostatic solvent extraction (ESX), there is still no commercial application of this technology to date. This is because the fundamental understanding of the technique is still inadequate.

Assmann (2014) recently yielded significant advances towards the characterisation of droplet dispersion behaviours under the influence of electrostatic fields of various types. He developed a technique to determine the effect of different electrostatic field conditions on the mass transfer of a simulated hydrometallurgical SX system by utilising an advanced imaging technology consisting of a high-speed camera capable of capturing 500 frames per second (fps) with laser backlighting. This allows high-quality videos to be recorded, from which characterisation of the dispersion behaviours can be observed and quantified. These behaviours include the breakup, motion and oscillation of the individual droplet.

He characterised the behaviours of droplets ranging in diameter from 100 to 1400 µm at field strengths of 2.5–3.5 kV/cm at frequencies ranging from 20 to 60 Hz. One of his main recommendations for future work was to determine the behaviours of smaller droplets than those he studied. Specifically, it will be helpful to determine whether these droplets behave similarly to the larger droplets he studied. Under comparable experimental conditions, these smaller droplets would be formed at more vigorous electrostatic field conditions, i.e., at field strengths > 3.5 kV/cm. Addressing this is important to advance the development of ESX because, in theory, its major advantage

is that it can be operated with much smaller droplets than those in conventional contactors.

Furthermore, it is of particular interest in this study to investigate whether there is a limit where the droplets will start to behave drastically differently with increasing mixing intensity, as in the case of conventional SX contactors. As mentioned earlier, generation of smaller droplets is generally desirable in conventional contactors but only until a point where the generated droplets start to behave like a rigid sphere and exhibit poor phase separation. One particular observation reported by Steffens (2011), who studied various electrode configurations to produce dispersion in electrostatic fields using also a hydrometallurgical SX system, indicated that such a condition may exist with electrostatically induced dispersions. He observed that a swarm of ultrafine droplets that subsequently formed into an apparent stable emulsion was produced when transient electrostatic fields were imposed on droplets using parallel plate electrodes. He, however, did not explain nor specify the conditions that led to this phenomenon.

Moreover, Assmann (2014) found that the application of electrostatic fields can induce a droplet breakup mechanism involving a sudden burst of the droplet, creating formation of a momentary emulsion of ultrafine droplets that eventually disappear by coalescing to form larger droplets. The breakup mechanism, which he referred to as emulsion-like-formation, was observed in direct current (DC) and pulsed direct current (PDC) fields wherein uninsulated electrodes were used, but it was not observed in alternating current (AC) fields wherein insulated electrodes were used. The use of uninsulated electrodes is not desirable as they cannot operate with the high aqueous-phase flow rate required for a commercial application before arcing occurs (Scott et al., 1994; Steffens, 2011). In addition, corrosion may become a serious problem with uninsulated electrodes, given the presence of an electric current and aqueous solutions containing metal ions, which are often acidic, during operation (Warren and Byeseda, 1990). Therefore, it was also of particular interest in this study to determine whether such a momentary emulsion occurs under electrostatic fields using insulated electrodes and explore if and how this can be controlled to allow high mass-transfer rates and fast phase disengagement in ESX.

1.3 AIMS AND SCOPE OF THE STUDY

The present study aimed to investigate the behaviours of smaller droplets under more vigorous electrostatic field conditions than those studied previously. Specifically, it aimed to:

1. Characterise the behaviours of smaller droplets (< 100 μm) than those previously characterised (100–1400 μm) under the influence of electrostatic fields and determine their effect on mass transfer.
2. Determine the conditions that allow the formation of momentary emulsion under the influence of electrostatic fields and explore if and how these can be controlled to allow high mass-transfer rates and fast phase disengagement in ESX.
3. Evaluate the performance of the proposed ESX technique by performing SX of metals from aqueous solutions and determine conditions for high mass transfer rates and fast phase disengagement.

1.4 SIGNIFICANCE OF THE STUDY

SX plays a significant role in the purification processes of many important metals, particularly uranium, thorium, copper, nickel, cobalt and rare earth metals. The refining of these metals alone involves over 200 commercial SX operations across the world today (Mackenzie, 2015). The role of SX is still expected to grow as a result of the increasing exploitation of low-grade and complex ores due to the depletion of high-grade ores. This is because the processing of such ores often requires more vigorous leaching techniques that invariably generate highly contaminated pregnant leach solutions, and SX is currently the only commercially applicable separation technique that is able to purify these solutions. Development of a more efficient SX technique would therefore benefit the global mining industry and Australia will be the main beneficiary as it hosts one of the largest laterite nickel resources as well as substantial reserves of uranium and rare earth metals.

The present study contributes to extending the understanding of behaviours of droplets under the influence of electrostatic fields to a much wider range of droplet sizes. This knowledge would be valuable in optimisation of an ESX design and would contribute toward the development of commercial application of the technique.

1.5 THESIS ORGANISATION

There are seven chapters in this thesis, as outlined below:

Chapter 1 **-** Presents a brief overview of the SX operation in process metallurgy applications, statements of the problem and the objectives and significance of the present study.

Chapter 2 **-** Provides a review of studies relating to the use of electrostatic fields to induce dispersion in SX that are relevant to process metallurgy applications.

Chapter 3 **-** Presents descriptions of the experimental equipment, general procedures to perform the experiments and the experimental materials used in the present study.

Chapter 4 **-** Describes the results of the investigation on the effect of electrostatic fields on the breakup, motion and oscillation behaviours of droplets smaller than those previously studied.

Chapter 5 **-** Discusses the effect of the changes in the droplet behaviours in relation to the properties of the field on droplet size and droplet size distribution.

Chapter 6 **-** Describes the results of the investigation on the effect of the strength and frequency of electrostatic fields on mass transfer.

Chapter 7 **-** Provides summaries of the key findings from the present study and recommendations for future research efforts.

CHAPTER 2
REVIEW OF STUDIES ON ELECTROSTATIC DISPERSION IN SOLVENT EXTRACTION

2.1 INTRODUCTION

This chapter presents a detailed review of existing literature related to the application of electrostatic fields to induce droplet dispersion in another immiscible liquid, hence electrostatic dispersion. The chapter first introduces a brief overview of the mass transfer process in SX to appreciate the fundamental roles of the various physical variables involved in the process. The following sections provide an overview of the various phenomena induced on droplets by the application of electrostatic fields. These include droplet deformation, breakup, motion, oscillation and internal circulation. Subsequently, the effect of electrostatic fields and the configuration of the electrodes to impose these fields on droplet size distribution are discussed. The chapter then concludes with the identified gaps in the knowledge.

2.2 OVERVIEW OF MASS-TRANSFER PROCESS IN SOLVENT EXTRACTION

Mass transfer in SX involves diffusional transport of chemical species to, across and away from the interface of two immiscible liquids. The diffusion process is driven by the chemical potential as the macroscopic properties of the system tend towards uniformity. In most cases, chemical potential increases with increasing solute concentration and so, for convenience, the diffusion process is expressed in terms of concentration in this section, as it aims only to appreciate the fundamental role of the various physical variables that control the rate of mass transfer in SX. The Fick's first law gives the basic mathematical representation of a diffusion process as

$$j = \frac{1}{A}\frac{dn}{dt} = -k\frac{dC}{dx} \tag{2-1}$$

where the mass flux j per unit area, defined as n moles of the chemical species that are transferred through an area A in a time t, is proportional to the mass transfer coefficient and the gradient of concentration. It follows that mass transfer is positive in the

direction of decreasing concentration and the rate depends on the concentration difference, the mass-transfer coefficient and the interfacial area between the two liquids.

The concentration profile of a diffusing species between two immiscible liquids can be expressed by the simplified model illustrated in Figure 2.1. The model, which is known as the two-film theory, assumes the existence of two stagnant layers of finite thickness located on opposite sides of the interface and the mass transfer takes place exclusively via diffusion in these double stationary films, while the concentration of solute is uniform in the bulk of both liquids as a result of perfect mixing (Lewis and Whitman, 1924; Whitman, 1962). The diffusion that occurs on both sides of the interface can be formulated as

$$j_1 = -k_1(C_{1i} - C_1)/\delta_1 \quad (2\text{-}2)$$

$$j_2 = -k_2(C_2 - C_{2i})/\delta_2 \quad (2\text{-}3)$$

where C_1 and C_2 are the bulk concentrations in liquids 1 and 2, respectively, C_{1i} and C_{2i} are the concentrations at the sharp interface at each respective liquid, and δ is the thickness of the diffusion film.

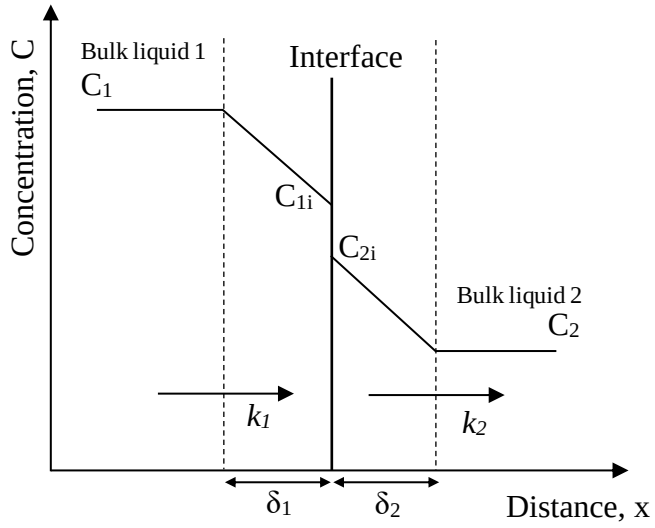

Figure 2.1. Theoretical concentration profile across an interface between two immiscible liquids.

In practice, SX is performed by mixing the bulk of the liquids to disperse one of the liquid phases as droplets, henceforth referred to as disperse phase, in another, referred to as continuous phase. In addition to the size of the produced droplets, which

determines the interfacial contact area, the mass transfer rate is also influenced by whether these droplets are internally circulating and oscillating. If these droplets behave like rigid spheres with an immobile interface, therefore internally stagnant, the mass-transfer coefficient k depends solely on the molecular diffusion process. The values of molecular diffusivity D_M for most extractable species in SX fall in the range 10^{-5}–10^{-6} cm^2/s in both water and organic solutions (Danesi, 2004). If the interface of the droplet is mobile, shear forces of the continuous phase acting on a moving droplet will lead to toroidal convective motions that circulate the liquid elements between the surface and centre of the droplet (Hadamard, 1911; Rybczyński, 1911; Scott, 1987b). This internal circulation enhances the mass-transfer rate by keeping the gradient concentration at a high level and reducing the thickness of the diffusion film. The occurrence of oscillation can further enhance the mass-transfer rate as it leads to turbulent mixing in the droplet interior. In the presence of turbulent eddies, eddy diffusivity D_E is operative and the molar rate of diffusion in a mass-transfer process can then be expressed as in Equation (2-4) (Kalinske and Pien, 1944; Davies, 1972b).

$$\frac{dn}{dt} = A(D_M + D_E)\frac{dC}{dx} \tag{2-4}$$

It follows that the mass-transfer rate between dispersing droplets and their surrounding liquid increases with increases in the interfacial area and the degree of turbulence within the droplet. In conventional SX contactors, where mixing is mechanically performed, however, the degree of internal turbulence decreases with decreases in droplet size. This is because the propensity for a droplet to oscillate decreases with its size (Schroeder and Kintner, 1965; Winnikow and Chao, 1966; Edge and Grant, 1971; Vacek and Nekovář, 1977). Moreover, as the droplet size decreases further to a regime where it no longer oscillates, its propensity to internally circulate decreases with its size to a point where the droplet characteristics reflect those of a rigid sphere (Wegener et al., 2014). Hence, the ideal conditions to maximise the mass-transfer process in SX, namely large interfacial area and intense internal turbulence, are mutually exclusive using the conventional mixing technology.

An alternative approach to mechanical agitation is the use of electrostatic force. The application of electrostatic fields to induce dispersion can generate a population of droplets smaller than those commonly produced through mechanical agitation and

induce intense turbulence within and around these small droplets, promising faster mass transfer rates. This is possible because the mechanism for droplet dispersion in electrostatic fields is totally different to those of mechanical agitation.

2.3 EFFECT OF ELECTROSTATIC FIELD ON DROPLET DISPERSION

2.3.1 Droplet Deformation and Breakup in Electrostatic Fields

The imposition of an electrostatic field to a neutrally charged conducting droplet that is immersed in a poorly conducting continuum can deform the shape of the droplet due to normal electrical stress that acts outwards on the droplet interface (Rayleigh, 1882; Allan and Mason, 1962a; Torza et al., 1971). This electrical stress is owing to induced polarisation of ions within the droplet (Scott, 1989). The most significant forms of electrostatic field-induced polarisation for a droplet immersed in a dielectric liquid are orientational and interfacial polarisation (Pohl, 1973). The former occurs due to alignment of polar molecules that have permanent dipole moments, such as water, with the applied electrostatic field. The latter occurs due to field discontinuity at the liquid–liquid interface, which causes electric charge within the droplet and migrating charge in the continuous phase to accumulate at the interface (Taylor, 1966; Melcher and Taylor, 1969). These two polarisation forms can coincide and create charge regions at opposite ends of the droplet, wherein either cation or anion species predominate over the other. These charge regions are then attracted to electrodes of the opposite charge, resulting in droplet deformation in the axis parallel to the applied field.

Droplet deformation under the influence of electrostatic fields can be described as a balance between electric stress ($\varepsilon_e\varepsilon_0 E_0^2$) and capillary stress ($\gamma/\alpha$) (Allan and Mason, 1962a; Karyappa et al., 2014). Here, a (m) is the droplet radius, ε_e (F/m) is the dielectric constant of the solvent, ε_0 (F/m) the permittivity of free space, E_0 (V/m) is the nominal electric field strength, and γ (N/m) is the interfacial tension. The relationship is known as the electric capillary number, *Ca*, which is a dimensionless parameter that can be used to measure the relative importance of the field strength and the droplet size in an electrostatic field as

$$Ca = \frac{a\varepsilon_e\varepsilon_0 E_0^2}{\gamma} \tag{2-5}$$

Taylor (1966) developed a theoretical correlation between droplet deformation and *Ca* as

$$D = (9F/16)Ca \tag{2-6}$$

where $D = (L-B)/(L+B)$ is the Taylor deformation parameter, L and B are the lengths of the major and minor axes, respectively, and F is known as Taylor discriminating factor. This factor is a linear function of three property ratios of the two liquids; namely, conductivity ratio $R = \sigma_2/\sigma_1$, dielectric constant ratio $Q = \varepsilon_1/\varepsilon_2$ and viscosity ratio $M = \mu_1/\mu_2$. This theory, however, is linearised and valid only for small deformations. Ajayi (1978) extended the leaky dielectric theory to include higher order terms. Still, even the extended theory failed to resolve the disagreement (Ha and Yang, 2000; Lac and Homsy, 2007; Karyappa et al., 2014). Moreover, the theory is valid only when the droplet is subjected to a uniform static field. Application of transient fields adds further complications to the theory as the magnitude of the imposed electric stress changes with time. Torza et al. (1971) and Vizika and Saville (1992) attempted to modify the theory to satisfy such a situation but discrepancies between theoretical prediction and experimental results remain. These show the complexities of physical processes involved in droplet deformation under the influence of electrostatic fields.

Despite these discrepancies, extensive theoretical investigations in the topic have provided the basis to determine the major variables that affect droplet deformation and their relationships in affecting the deformation. These variables include the physical properties of the two immiscible liquids; namely, interfacial tension, conductivity, dielectric constant and viscosity, and the properties of the electrostatic field; namely, type, strength and, in case of transient fields, frequency of the field.

It follows that when a droplet is imposed to a sufficiently strong electrostatic field, the electric stress can become large enough to overcome the capillary stress that holds the droplet together, resulting in the droplet breaking into a number of smaller daughter droplets. The droplet breakup can be achieved regardless of the types of field, whether it is DC, PDC or AC fields.

In addition to the strength of the field, the size of the daughter droplets also depends on the breakup mechanism of the mother droplets (Scott, 1987a; Scott et al., 1990; Assmann, 2014). The most common breakup mechanisms for droplets subjected to

electrostatic fields are jetting and necking (Allan and Mason, 1962a; Taylor, 1964; Torza et al., 1971; Ha and Yang, 2000; Eow and Ghadiri, 2003; Karyappa et al., 2014; Guo et al., 2015), which are illustrated in Figure 2.2. The former is characterised by the formation of conical ends and ejection of fine droplets from either end while the middle part of the droplet remains relatively large. The latter is characterised by thinning of the central part of the droplet as it elongates until it disintegrates to form two or more smaller droplets. Only in relatively recent years have other droplet breakup mechanisms that are distinctly different to jetting and necking under the influence of electrostatic fields been reported. These mechanisms include the so-called emulsion-like formation, irregular and combination mechanism (Assmann, 2014).

Figure 2.2. Schematic illustration of droplet deformation and disintegration via jetting and necking.

Assmann (2014) reported that aqueous droplets suspended in nonviscous organic solutions that are commonly used in hydrometallurgical SX applications could undergo a sudden burst producing an emulsion-like formation of ultrafine droplets, which would coalesce soon after they are formed to create larger droplets. He observed that this breakup mechanism occurred only under a limited set of operating conditions when either DC or PDC fields were used. Specifically, emulsion-like formation was observed only when small droplets were situated between two large elongated droplets, each contacting an uninsulated electrode and creating a localised region with substantially higher field strength. This particular circumstance, however, can lead to arcing, which can result in an intermittent electrostatic field.

Assmann (2014) also reported two other distinct mechanisms, which he referred to as irregular and combination mechanisms. The former is characterised by the formation of a detaching lobe with sporadic protrusions on its surface towards various directions that extend until it disintegrates. The latter is characterised by the occurrence of two or more droplet breakup mechanisms, e.g., breakup of a droplet through a combination of jetting and necking, indicating that these mechanisms are not mutually exclusive.

The irregular and combination mechanisms were observed regardless of the type of field, whether in DC, PDC or AC field.

Theoretically, emulsion-like formation and necking should be more favourable for mass transfer. The former produces a large interfacial area for mass transfer by the generation of ultrafine droplets, which coalesce soon after formation, minimising the probability of entrainment. The latter produces more uniform daughter droplets and minimises the generation of ultrafine droplets, which could become entrained in the continuous phase during the subsequent phase separation step. In the absence of any other external forces, however, droplets tend to undergo jetting breakup under the influence of electrostatic fields owing to the natural tendency for charge to accumulate at sharp points (Taylor, 1964; Sherwood, 1988; Betelú et al., 2006; Dubash and Mestel, 2007).

Researchers have shown through single droplet studies that decreases in viscosity ratio between the disperse and continuous phase can shift the breakup mechanism towards necking (Allan and Mason, 1962a; Torza et al., 1971; Sherwood, 1988; Karyappa et al., 2014; Mohamed et al., 2016). They attributed this shift to increasing deformation resistance by the outer phase owing to viscous stress, which led to increases in droplet propensity to form flatter ends rather than conical ends during elongation, leading to the formation of lobes and necks. The shift, however, only started when the viscosity of the continuous phase was two orders of magnitude higher than that of the disperse phase. Clearly, such large variations in solvent viscosity are not practical in hydrometallurgical SX. Similarly, making significant changes in liquid conductivity, dielectric constant, and interfacial to shift the droplet breakup mechanism from jetting is not a practical option (Sherwood, 1988; Ha and Yang, 1998; Raut et al., 2009; Steffens, 2011). Therefore, the effects of physical properties of the solutions on droplet dispersion were not pursued in the present study.

2.3.2 Effect of Electrostatic Fields on Droplet Breakup Mechanism

Regardless of field type, increases in the applied field strength result in greater droplet deformation (Torza et al., 1971; Vizika and Saville, 1992; Maruyama et al., 2003). This is because the electric stress imposed on a droplet intensifies as the field strength increases. The nature of droplet deformation, however, varies among the different

types of fields giving rise to possibilities to shift the predominant breakup mechanism from jetting for a given system.

Unlike in DC fields, where the droplet is subjected to constant field strengths, the field strengths imposed on droplets subjected to either PDC or AC fields vary with time, depending on the field frequency, as schematically illustrated in Figure 2.3. The droplet elongates in the field direction when the voltage approaches a peak, either positive or negative, and retracts back towards a spherical shape when the intensity approaches zero and hence, the droplet oscillates about a deformed shape.

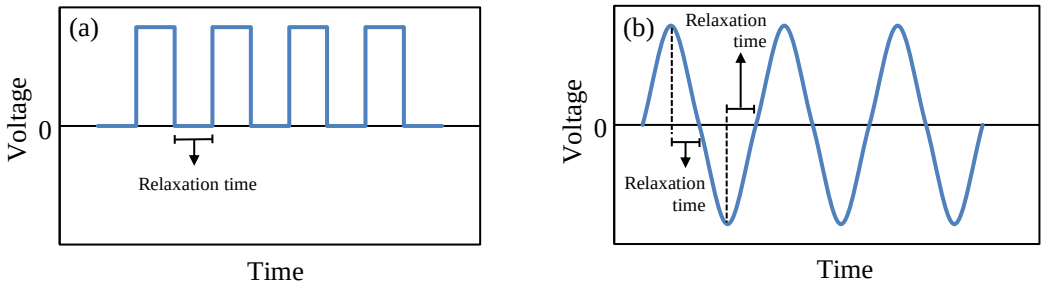

Figure 2.3. Typical waveform generated by (a) PDC fields and (b) AC fields.

Maruyama et al. (2003) observed that variations in dynamics of droplet deformation in DC and AC electrostatic fields affected the breakup mechanism. The observation was made by recording the deformation and breakup of a single water droplet suspended in a mixture of carbon tetrachloride and silicone oil, which had the same density as water, at various field strengths. Visual analysis of these recordings revealed that the predominant droplet breakup in DC fields was jetting, whereas it was predominantly necking in AC fields. They attributed this shift in breakup mechanism to necking in AC fields to the periodic changes in polarity that changed the tangential stress on the droplet from a maximum to zero. This then converted the droplet ends from conical shape to roundish shape, which preludes the necking mechanism. It appeared that this was also possible partly due to the contribution of viscous stress to hinder the formation of sharp points.

Assmann (2014) later corroborated this observation. He also specified the conditions that favour necking in AC fields for a system comprising of 300 mg/L cobalt sulphate solution as the disperse phase and 10% v/v CYANEX® 272, which is a commercial dialkyl phosphinic acid extractant, in ShellSol® 2046, a commercial aliphatic diluent, as the continuous phase. He reported that the droplet breakup mechanism in AC fields

at strengths ranging from 2.5 to 3.5 kV/cm shifted from jetting to necking when the frequency was set below 50 Hz, and the prevalence of necking increased with decreasing frequency.

In PDC fields, Scott (1987a) and Scott et al. (1990) reported that the droplet breakup mechanism is affected by the so-called natural droplet oscillation frequency, which is a frequency wherein droplets undergo a substantially higher amplitude of deformation than at either adjacent frequency. The natural oscillation frequency increases with decreases in droplet size, which is similar to the behaviour of droplet oscillation owing to gravity alone. Therefore, they attributed the enhanced elongation to the coupling of natural elongation that was unrelated to the electrostatic force and induced elongation by electrostatic force. They observed that at or below this natural oscillation frequency, the droplet became very unstable and underwent vigorous breakup to form very small daughter droplets compared with the original droplet. It was unclear whether this falls into the jetting or necking breakup category or even a completely different breakup mechanism, because the dynamics were not described in detail. At higher frequencies, however, the breakup mechanism shifted to what was apparently necking.

Assmann (2014) also investigated droplet breakup mechanisms in PDC fields and observed a similar phenomenon wherein the size of the daughter droplets decreased markedly at a particular frequency compared with either adjacent frequency. When investigating the behaviour of droplets of comparable size to that produced in the PDC fields but in the absence of a field, however, he observed that the droplets did not exhibit any form of oscillation. He then deemed that the significant decreases in the average droplet size were owing to a shift in droplet dispersion mechanism to necking and that at the other frequencies jetting was more favourable, which contradicts the observation made by Scott and his co-workers. Despite this discrepancy, these studies clearly show that it was possible to alter the predominant droplet breakup mechanism from jetting to necking by adjusting the frequency of the transient field.

2.3.3 Droplet Motion in Electrostatic Fields

A free neutrally charged droplet that is suspended in a perfect dielectric solution will become a dipole as a result of polarisation when subjected to electrostatic fields but, if the field is uniform, it will not experience a net displacement from its original position.

In the absence of other external forces, the droplet will only experience a displacement if it carries a net charge or there is a nonuniformity in the field.

Yamaguchi et al. (1988) observed that droplets situated between vertical rod electrodes exhibited lateral motion wherein they moved towards one electrode and reversed their direction towards the opposite electrode upon contact when subjected to DC fields. Assmann (2014) later observed similar lateral motion under the influence of PDC fields. This droplet behaviour indicates that the droplet initially migrated toward the electrodes owing to electrostatic attraction between the polarised droplet and the electrodes. The droplet then acquired the same charge as the electrode upon contact and was repelled towards and attracted by the opposite electrode. This, however, means that electrodes cannot be insulated for such a zigzag motion to occur in DC or PDC fields as direct contact between droplets and electrodes is required.

Subjecting droplets to AC fields may also induce zigzagging but the nature by which these droplets translate differs from those induced by DC or PDC fields. Previous investigators who studied the dispersion behaviours of a population of droplets in AC fields showed that droplets reversed their direction periodically at a rate that was in apparent synchrony with the periodic changes in the electrode polarity, and they do so without any direct contact with the electrodes (Reeves et al., 1999; Steffens, 2011; Assmann, 2014). This behaviour suggests that droplet zigzagging under the influence of AC fields can be achieved using insulated electrodes.

Yamaguchi et al. (1988) reported that the induced zigzagging of water droplets immersed in cyclohexane under the influence of DC fields increased the occurrence of droplet coalescence and redispersion. Note that droplets carrying a net charge create a dipole, so droplets of opposite sign attract each other. This electrostatic attraction increases the rate of coalescence between neighbouring droplets by increasing the film thinning rate when these droplets collide (Atten, 1992; Eow et al., 2001). It follows that, as droplets coalesce, the resulting droplets may become unstable and redisperse because the droplet size may exceed their stability limit. In theory, the occurrence of droplet coalescence and redispersion during emulsification in an SX column benefits the mass-transfer process because the concentration gradients are very high across a newly formed interface (Davies, 1972b).

Droplet coalescence and redispersion are also beneficial to narrow the droplet size distribution. Williams and Bailey (1986) showed that the proportion of the smallest and largest size fractions of water droplets with sizes ranging from 1.9 to 118.4 μm that were immersed in silicone oil under the influence of DC fields decreased as the imposition duration of the fields increased. This was shown by comparing the droplet size distribution of the dispersion at different times after the dispersion was subjected to the electrostatic field. The reduction of both small (< 7 μm) and large (> 13 μm) droplets shifted the distribution peaks toward sizes within the middle size fractions (9–13 μm). This then changed the shape of the diagrams from bimodal distribution to more of a unimodal distribution as the duration of the imposition increased. They attributed this to coalescence of the small droplets and breakup and redispersion of the large droplets. These findings clearly suggest that increases in the frequency of coalescence and redispersion of the resulting droplets in electrostatic fields are beneficial to enhancing mass transfer in SX.

Assmann (2014) reported that droplet coalescence and redispersion also occurred in AC fields. This is logical as dipole attraction between neutrally charged droplets can also be enhanced as long as they can be polarised. He, however, did not specify the extent of and the conditions that favour this phenomenon in AC fields. Hence, further investigation in this subject is warranted to improve the efficiency of an ESX column.

Yamaguchi et al. (1988) reported that the zigzag motion increased the residence time of the droplets in the column. This is desirable as it exhibits the potential to increase the holdup fraction of the disperse phase to allow complete mass transfer at shorter vertical translation, reducing the required height of the column to process a certain feed flow rate of the dispersed phase.

The strength of the applied field influences droplet zigzagging behaviour. Steffens (2011) reported that as the strength of the applied AC field increased from 2 to 5 kV/cm, the average horizontal velocity and the population of droplets that exhibited zigzag motion increased. These results in agreement with findings reported by Assmann (2014) at field strengths ranging from 2.5 to 3.5 kV/cm. The latter author attributed this to the increase in the amounts of incidental charges that were acquired by the droplets as the strength of the field increased. These observations clearly

indicate that the droplet net charge plays a significant role in inducing the zigzag motion under the influence of AC fields.

Variation in the amount of net charge on the droplet may lead to droplets behaving differently in electrostatic fields. Assmann (2014), for example, reported that for a given population of droplets that was subjected to an AC field, some droplets were oscillating while falling solely in the gravity direction, some were zigzagging while remaining spherical, and the remaining droplets were oscillating and zigzagging but in varying degrees when subjected to AC fields. The occurrence of free-falling droplets is undesirable as it reduces the droplet residence time in the column to allow complete extraction of the solute within the droplets. Notably, such behaviour was not observed in DC or PDC fields, reinforcing the argument that a different mechanism of charge acquisition was at play with the use of insulated electrodes.

2.3.4 Effect of Electrostatic Fields on Droplet Oscillation

The application of transient electrostatic fields on droplets may cause them to oscillate about their spherical shape due to the periodic cycling of the electrostatic force imposed on the droplets. This is evident from consistent observations on the frequency of forced oscillation that is in apparent synchrony with the frequency of the field, i.e., with the use of high-speed imaging equipment, researchers have shown that droplets of various sizes and physical properties exhibited oscillation at a fixed frequency that is either about the same as the field frequency in PDC fields or twice that of the field in AC fields because the voltage reaches two peaks in one cycle (Torza et al., 1971; Kaji et al., 1985; Assmann, 2014; Guo et al., 2015; Yan et al., 2015; Li et al., 2017).

The benefits of droplet oscillation to the mass-transfer process are twofold. First, it increases the amount of surface area per unit droplet volume, thus providing more reacting sites for mass transfer. Second, it induces internal mixing, which provides periodic renewal of the reactant in the boundary layer with fresh reactant from the interior of the droplet. Trinh et al. (1982) provided experimental evidence on the internal fluid mixing resulting from oscillation by using dye particles as a tracer.

Wham and Byers (1987) reported the effect of droplet oscillation on the rate of mass transfer from a single stationary water droplet that was fluidised in a continuous flow of 2-ethylhexanol in the presence and absence of a field. This experimental technique

was devised to minimise the translational motion of the droplet so the increase in the mass-transfer rate can virtually be ascribed solely to the oscillation. They showed that mass transfer coefficients of water from the droplet increased up to 35% when it was forced to oscillate in PDC fields at a frequency of up to 50 Hz compared with when no field was applied. Meanwhile, the measured changes in the average surface area owing to the forced droplet oscillation were only less than 1% in all cases, which were too small to account for the increased mass-transfer coefficient.

Increases in the strength of transient fields, both PDC and AC fields, result in increases in the amplitude of droplet oscillation and the population of oscillating droplets (Kaji et al., 1980; Kaji et al., 1985; Wham and Byers, 1987; Assmann, 2014; Guo et al., 2015). This is logical, given the higher electrical stresses that the applied field imposed at higher field strength. Differently, the variation in amplitude of droplet oscillation with changes in the frequency of the transient fields is not as straightforward as those obtained with changes in field strength.

In transient fields, Vivacqua et al. (2016) and Li et al. (2017) predicted with the use of numerical methods that increases in the field frequency generally result in decreases in the oscillation amplitude. They attributed this to the shorter mechanical response time of the interface to elongate than the time for the field strength to remain at around the peak value. This has been shown earlier by Kaji et al. (1985) and Assmann (2014), who conducted experimental studies on droplet oscillation behaviour in both PDC and AC fields.

Researchers, however, reported that there was a particular frequency at which the droplet deformation amplitude drastically increased. In AC fields, Kaji et al. (1985) reported this phenomenon when investigating the oscillation of a single water droplet in silicone oil at frequencies ranging from 1 to 15 Hz. In PDC fields, Scott et al. (1990) reported this phenomenon when investigating the oscillation of a single water droplet suspended in 2-ethyl-1-hexanol under the influence of PDC fields at frequencies ranging from 20 to 120 Hz. As mentioned earlier, they attributed this phenomenon to the occurrence of the so-called natural oscillation frequency.

In direct contrast with these earlier studies, Guo et al. (2015) found that the amplitude of droplet oscillation increased with increasing field frequency ranging from 20 to 70 Hz when subjecting a single water droplet in viscous white oil to AC fields. They

attributed this observation to increases in the acceleration of liquid mass within the droplet with increases in frequency, which contributed to the force opposing the capillary stress.

Inspection of the reason for this discrepancy is, however, difficult because they used different experimental methods. Assmann (2014), for example, reported his findings based on visual observations of dispersions involving a population of droplets having various sizes recorded using high-speed imaging equipment capable of recording at a frame rate up to 500 frame per second (fps). Guo et al. (2015), however, made their claim based on a set of quantitative data obtained by measuring changes in the size of a single droplet with time also using high-speed imaging equipment with a recording speed of up to 10000 fps.

Assmann (2014) found that some droplets of comparable size within the same population can exhibit markedly different oscillation amplitude. He attributed this to the different degrees of interfacial polarisation experienced by these droplets. Curiously, a closer examination of the photographs of typical droplets dispersions that he presented revealed that some droplets that showed the highest oscillation amplitudes exhibited conical ends, as if they were undergoing jetting, while there were droplets of comparable size that exhibited almost spherical shape. Because the variation in oscillation amplitudes was so significant that some droplets became unstable while the others barely deformed, it is difficult to imagine that a random encounter between migrating electrical charge and interface was the main reason for this variation. There is currently no evidence that droplets can acquire a significant external charge without directly contacting an uninsulated electrode. Besides, the general view in the literature indicates that a field strength of about 100 000 kV/cm is needed to cause direct charge emission from an electrode (Hendricks, 1973). Therefore, the idea suggesting that electrodes emit substantial charge through a dielectric liquid may need to be revisited. Furthermore, it is still unclear whether droplet oscillation exhibiting conical ends was, in fact, a jetting breakup and, thus, whether this type of oscillation was able to sustain since jetting is a manifestation of charge emission to achieve stability. Clearly, more work is required to clarify droplet oscillation behaviour in AC fields.

2.3.5 Droplet Internal Circulation in Electrostatic Fields

The existence of circulatory motions inside and outside a suspended droplet subjected to electrostatic fields was first predicted by Taylor (1966). It has been long known that the imposition of an electric field to a liquid droplet suspended in another immiscible liquid can induce electrical stresses on the droplet. Before his seminal work, however, these electric stresses were predicted to only act in the direction normal to the droplet surface (Rayleigh, 1882; O'Konski and Thacher, 1953). Consequently, subjecting electrostatic fields to a droplet was predicted to always result in prolate deformation, oriented along the direction of the field. The experimental findings of Allan and Mason (1962a), however, demonstrated that droplets can also exhibit oblate deformation, which is droplet elongation perpendicular to the field direction. Based on these results, Taylor (1966) predicted the existence of tangential electrical stress in addition to the normal electrical stresses at the interface as a result of the surface charge that interacted with the field.

He theorised that, however small the conductivity of the suspending liquids, electric charge will still be able to reach the droplet and accumulate on the surface. The electric potentials at the inside (ϕ_d) and outside (ϕ_c) of the droplet when imposed to a uniform DC field are given as, in polar coordinates,

$$\phi_d = \frac{3aE_0 \cos\theta}{2+R} \tag{2-7}$$

$$\phi_c = E_0 \cos\theta \left[r + \frac{1-R}{2+R} \frac{a^3}{r^2} \right] \tag{2-8}$$

where $R = \lambda_c/\lambda_d$ with λ_c and λ_d are the resistivities of the continuous and disperse phases, respectively, a is the droplet radius, r is the radius vector centred at $r = 0$, and E_0 is the strength of the field. The electric stresses acting on the interface, at $r = a$, have radial (T_{rr}) and tangential components ($T_{r\theta}$) as

$$T_{rr} = \frac{9\varepsilon_d E_0^2}{2(2+R)^2} [1 - S + (S(R^2+1) - 2)\cos^2\theta], \quad \text{at } r = a \tag{2-9}$$

$$T_{r\theta} = \frac{-9\varepsilon_d}{2(2+R)^2} (SR - 1)\sin\theta\cos\theta, \quad \text{at } r = a \tag{2-10}$$

where $S = \varepsilon_c/\varepsilon_d$ with ε_c and ε_d are the permittivities of the continuous and disperse phase, respectively. Taylor (1966) and Melcher and Taylor (1969) argued that for the imposed droplet to remain spherical, the tangential stresses must be balanced by the stresses associated with hydrodynamic streams from outside and inside the droplet. They provided analytical solutions of both flows at a steady state by introducing a stream function each for the outside (ψ_c) and inside (ψ_d) the droplet as

$$\psi_c = \left(X_1 \frac{a^4}{r^2} + X_2 a^2\right) \sin^2\theta \cos\theta \tag{2-11}$$

$$\psi_d = \left(X_3 \frac{r^3}{a^1} + X_4 \frac{r^5}{a^3}\right) \sin^2\theta \cos\theta \tag{2-12}$$

The four unknown constants X_1, X_2, X_3 and X_4 can be determined from the continuity conditions for velocity components on the droplet surface, at $r = a$. These conditions give $X_1 = -X_2 = X_3 = -X_4$. The maximum stream velocity U_{max} occurs at the surface, where its value is $2X_1 \sin\theta \cos\theta$. Because the maximum value of $\sin\theta \cos\theta$ is 0.5, then

$$U_{max} = X_1 = \frac{9\varepsilon_d E_0^2 a(1 - SR)}{10\mu_c(1 + M)(2 + R)^2} \tag{2-13}$$

where $M = \mu_d/\mu_c$ with μ_d and μ_c are the viscosities of the disperse and continuous phase, respectively.

Correspondingly, their analytical solutions predict toroidal circulation patterns inside and outside a suspended droplet at a neutrally buoyant state when subjected to DC electrostatic fields, as illustrated Figure 2.4. The circulation can be either from the poles toward the equator ($SR < 1$) or from the equator to the poles ($SR > 1$) depending on whether the value of U_{max} is positive or negative. The latter is the case for most SX systems because the products of the dielectric constant and electrical resistivity of the hydrometallurgical organic solvent exceed the corresponding product for the aqueous droplet. McEwan and de Jong[1] verified Taylor's prediction by adding tracer particles in and around silicone oil droplets suspended in castor and corn oil

[1] McEwan and de Jong's photos are presented in Taylor (1966) in an addendum.

mixtures in DC fields. The patterns shown by the tracer particles are similar to those depicted in Figure 2.4.

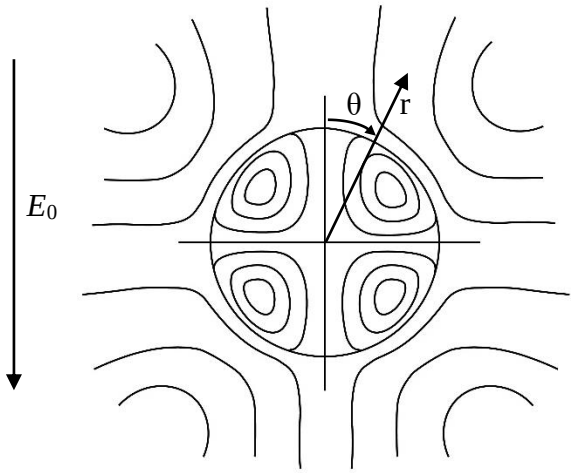

Figure 2.4. Toroidal stream patterns of liquid flows inside and outside the droplet in uniform DC electrostatic field as predicted by Taylor (1966).

Torza et al. (1971) provided an analytical solution for the droplet internal circulation in AC fields. In these fields, the field strength changes with time as

$$E = E_0 \cos \omega t \tag{2-14}$$

where E_0 is the peak field strength and ω is the angular frequency, defined as $2\pi f$ with f is the frequency of the applied field. The direction of the field periodically reverses as E alternating between a positive and negative value following the frequency of the applied field. They postulated that the magnitude of stream velocity U changes with time, proportional to $\sin(2\omega t + \alpha)$, with α being a theoretical phase angle that depends on both the liquid and field properties. Therefore, the stream direction also changes with time as the value of U alternates between a positive and negative value.

Expectedly, droplet circulation enhances mass transfer. Morrison (1977) numerically showed that electrostatically induced droplet circulation enhances the mass-transfer rate from a stationary suspended droplet, regardless of whether the circulation flows from the equator to poles or poles to the equator. Later, Elperin and Fominykh (2006) predicted the theoretical mass transfer of propanoic acid from a single stationary water droplet to benzonitrile in AC fields. They showed that the rate of mass transfer decreased with increases in frequency due to the decreasing rate of droplet circulation.

Experimental evidence to back these claims is currently lacking, probably owing to the difficulties in isolating the effect of internal circulation on droplet mass transfer. This is because droplets are not normally stationary while dispersing, and external forces can affect their internal circulation.

Chang et al. (1982) and Chang and Berg (1983) extended Taylor's analytical solutions to predict the circulation patterns for falling droplets in DC fields. They introduced a dimensionless parameter, W, in addition to Reynold number, Re, to assess the effect of electrostatic fields on droplet flow patterns for a given physical system. Specifically,

$$W = \frac{4U_{max}(1+M)}{|U_t|} \tag{2-15}$$

$$Re = \frac{\rho_c |U_t| a}{\mu_c} \tag{2-16}$$

where U_t is the terminal velocity of the moving droplet in an electrostatic field and ρ_c is the density of the continuous phase. Analogous to U_{max}, a positive W value means the induced circulation flows are from the poles toward the equator, and vice versa.

Different W and Re values give different flow patterns. Some examples of the computed flow patterns resulting from combinations of induced electrical stresses and viscous shear forces at various W and Re are shown in Figure 2.5. Droplets with positive W will have reduced terminal velocity in the presence of an electric field due to conflicting flow of gravity-induced circulation and electric circulation and, hence, the increased drag coefficient (Figure 2.5.b). Conversely, droplets with negative W will have increased terminal velocity. Small negative W will first reduce the size of any rear wake (Figure 2.5.c). As the value becomes more negative, the droplet may generate a standing eddy in front of the drop drag (Figure 2.5.d). The frontal vortex may form either a non-axisymmetric vortex sheet or induce an intermittent vortex that sheds downstream. Consequently, the predicted flow patterns for negative W may be unstable and a steady state may never appear.

Because the effect of the changes in the internal circulation patterns on the mass transfer efficiencies is not clearly apparent, Chang and Berg (1983) proposed a theoretical relationship to predict the effect of field strength on the mass transfer efficiency for a system with different Reynold numbers. Their results show that mass-transfer increases with increases in field strength. The results also show that mass-

transfer increases substantially in the region of creeping flow. This situation may be relevant to the mass transfer of very fine droplets, which are too small to exhibit oscillation and substantial acceleration. As the viscous shear forces are minimal, it does not matter whether a droplet has negative or positive W because circulating streams at all droplet sides would still occur, as in Figure 2.4. This prediction is particularly interesting because it suggests that translational droplet motions have a negative effect on mass-transfer, particularly when the mass-transfer direction is from the disperse to the continuous phase, as these motions damp the electrostatically induced internal circulating streams on one or multiple sites of the droplet.

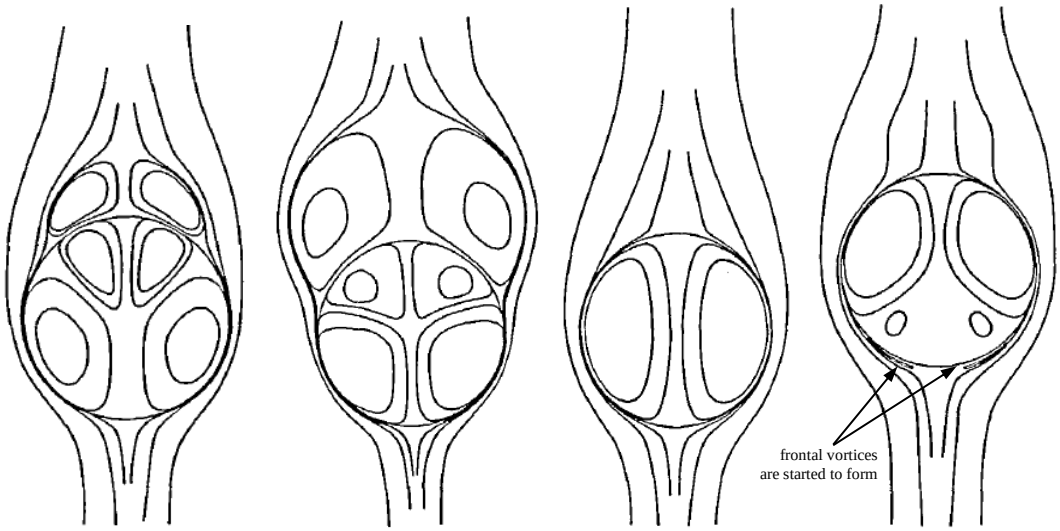

Figure 2.5. Computed flow patterns at the outside and inside of a falling droplet when subjected to DC fields between two parallel-plate electrodes for a fixed viscosity ratio $M = 2$ at $Re_0 = 60$ (a) $W = 0$, $Re = Re_0 = 60$, (b) $W = 6$, $Re = 36.68$, (c) $W = -3$, $Re = 84.24$ and (d) $W = -6$, $Re = 110.2$ (Chang and Berg, 1983). Reproduced with permission from Elsevier.

2.3.6 Behaviours of Electrical Charge on Droplets in Electrostatic Fields

Given the indications that droplets in an electrostatically induced dispersion may carry a significant net charge, it is helpful to discuss the behaviour of electrical charge within droplets when imposed to electrostatic fields. It has been established at this point that the application of electrostatic fields on neutrally charged droplets can induce a surface charge on these droplets because of polarisation. In addition to inducing elongation, there are two other significant consequences of this phenomenon on droplet behaviour. First, the induced surface charge may cause circulatory motions of liquids both inside

and outside the droplets (Taylor, 1966; Melcher and Taylor, 1969). This is discussed in more detail in the Section 2.3.7. Another significant consequence of the induced surface charge on droplets is that the daughter droplets created from the surface having either a net positive or negative charge will also carry a net charge with the same sign (Hendricks, 1973).

Lord Rayleigh (1882) formulated the criterion of stability for a conductive droplet of a radius a and charge q as

$$q^2 = 64\pi^2\varepsilon_0\gamma a^3 \tag{2-17}$$

This criterion is referred to as the Rayleigh stability criterion, and the charge limit is referred to as the Rayleigh limit.

In the case of charged droplets, several experimental studies show that the daughter droplets produced from breakup of these droplets in electrostatic fields can carry a much higher charge-to-mass ratio than the mother droplets. Schweizer and Hanson (1971), for example, showed that an *n*-octanol droplet lost about 23% of its charge while the mass loss from its tip was only 5% in both AC and DC fields. Later investigators corroborated this finding by showing that droplets of various physical properties lost about 10–40% of their charge while losing less than 5% of the mass in either AC or DC fields (Taflin et al., 1989; Duft et al., 2003; Singh et al., 2019). Using numerical methods, Elghazaly and Castle (1987) predicted that if the daughter-to-mother droplet mass ratio is less than 11.1%, the droplet will carry a charge higher than the Rayleigh limit. This will result in the daughter droplet continuing to break to seek a final stable condition (Ryce and Patriarche, 1965).

It must be noted that the experimental method performed in these charged droplet breakup studies involves evaporation of a levitating droplet in a gaseous medium with a known charge until it reaches a size that exceeds the Rayleigh stability criterion. Therefore, the only breakup mechanism observed in these studies was jetting.

It is conceivable that charged droplets required less electrostatic force to break as less induced surface charge is needed to reach the Rayleigh limit to destabilise the droplet. In the present study, it is of particular interest to determine whether droplets generated from neutrally charged droplets can carry a substantial net charge without directly

contacting an electrode directly and how this influences droplet dispersion behaviours and thus affects mass-transfer.

2.3.7 Behaviours of Small Droplets in Vigorous Electrostatic Fields

One particular interest in this study is to investigate whether there is a limit where droplets will start to behave differently with increasing intensity of the applied electrostatic field; specifically, whether droplets smaller than 100 μm in diameter in a more vigorous electrostatic field behave differently from those larger droplets in less-vigorous fields. Scott (1987a) and Scott and Sisson (1988) reported that they managed to achieve an average droplet size of less than 5 μm with their laboratory-scale ESX contactor with PDC fields at strengths up to 9.5 kV/cm. No details, however, were provided with regard to the correlation between the average droplet size, droplet size distribution, droplet motion and mass-transfer performance of the ESX contactor under the different electrostatic field conditions used. No details were provided on observations of whether these small droplets could oscillate under transient electrostatic fields.

Karyappa et al. (2016) studied the dispersion of water droplets in a viscous castor oil between two parallel-plate electrodes using DC fields at strengths ranging from 0 to 20 kV/cm. Application of the fields can reduce the droplet sizes from 300–500 μm in diameter to mainly between 5–20 μm. They reported that at high electrostatic field strengths beyond 17.5 kV/cm, wherein the average droplet diameter was 22.41 μm or less, a different breakup dynamic occurred to that observed in lower fields; i.e., droplets that contacted an electrode were observed to break via a mechanism similar to that of electrospraying from a pendant droplet attached to a charged nozzle, which emanated ultrafine droplets and pushed the charged mother droplet from the electrode with an opposite sign, analogous to that of vigorous jetting. Despite using a viscous organic phase that is not used in SX, their findings demonstrate that the behaviour of small droplets in a vigorous electrostatic fields can differ from those of the larger droplets in less-vigorous fields.

2.4 EFFECT OF ELECTROSTATIC FIELDS ON DROPLET SIZE AND SIZE DISTRIBUTION

The effectiveness of an electrostatic field in dispersing droplets varies among different types of fields. Assmann (2014) reported that PDC fields are less effective to disperse a droplet than DC fields. This was apparent from the higher electric field strength required using PDC fields to produce a dispersion with a comparable mean droplet size to that produced using DC fields. He showed that, for example, a field strength of 4.00 kV/cm was needed to produce a droplet with a Sauter mean diameter of 558 μm in DC fields, while about 5.67 kV/cm was needed to produce about the same mean size in PDC fields at a frequency of 50 Hz under comparable experimental conditions. Note that Sauter mean diameter is the diameter of a droplet having the same volume-to-surface area ratio as the entire dispersion. It is often referred to as the most relevant measure to express an average value of the size of the produced polydisperse droplet when mass transfer is a major factor in the process performance (Mugele and Evans, 1951).

In contrast to PDC fields, Assmann (2014) reported that AC fields are more effective to disperse droplets than DC fields. He showed that, for example, a dispersion with a Sauter mean diameter of 386 μm can be produced in an AC field at a field strength of 2.5 kV/cm and a frequency of 50 Hz, while a field strength of about 4.4 kV/cm was needed to produce about the same mean diameter with DC fields under comparable experimental conditions. He attributed this to the distinct waveforms that PDC and AC generated (Figure 2.3). He argued that intermittent relaxation of the electrostatic force with PDC fields when the field is pulsed off to zero voltage leads to dissipation of the imposed interfacial charges, which reduces the intensity of the imposed electrical stresses. Unlike PDC fields, AC fields impose a constant electrostatic force to the dispersed droplets as the applied voltage is cycled between positive and negative polarities, passing only fleetingly to zero voltage. He suggested that this periodic change in polarity with AC fields would result in greater migration of electrons to the liquid–liquid interface, favouring the interfacial polarisation process, than in PDC fields and, hence, more effective dispersion.

Guo et al. (2015) also showed that AC fields are more effective in dispersing a droplet than DC fields but only at frequencies higher than a particular value. They indicated

that a single water droplet immersed in a viscous white oil was appeared to be more unstable in AC fields compared with that in DC fields at the same electric field strength when the frequency of the applied AC fields was at or higher than 30 Hz. They attributed this finding to the additional forces that arise from within the droplet as a result of fluid movement owing to the periodic changes in polarity, as was previously mentioned. The increasing droplet instability with decreasing frequency of the AC fields agrees with the findings presented by Assmann (2014), but the proposed reason for these findings was different. The latter author deemed that this was owing to the shift in droplet breakup mechanism from jetting to necking.

Dispersion of droplets always shows a size distribution because droplet generation always shows some deviations. If these deviations are small and the sizes of the droplets are nearly the same, the droplet size distribution is narrow. Often, however, the larger and smaller droplets vary substantially in size, making the size distribution wide. The results of droplet size distribution measurement can be expressed in a cumulative or differential way. In the former case, the data may be presented as a smooth curve of the cumulative percentage of droplets against droplet size. In the latter, they may be presented as a histogram of the percentage of droplets against given droplet size classes by number, which is referred to as a population distribution diagram, or by volume, referred to as a volume density distribution diagram. The former gives easy access to the percentile of droplet size distribution parameters such as the median. The latter, however, has the advantage of directly showing the modal (the most frequently occurring) droplet size and therefore, is more commonly used to represent size distribution for a droplet population.

Williams and Bailey (1986) showed that the application of DC fields on water droplets suspended in silicone oil can change a dispersion with bimodal droplet size distribution into a monodisperse one. They prepared bimodal dispersions using an ultrasonic emulsifier and then subjected the droplets to 1.9 kV/cm DC fields from two uninsulated parallel-plate electrodes. The mechanism for the narrowing trend of the size distribution was postulated to be the increasing coalescence rate of smaller droplets and the breakup of larger droplets that initially existed before application of the field and those formed by the action of coalescence. The coalescence rate was enhanced owing to the induced horizontal zigzagging motion as droplets were allowed to acquire a significant net charge by directly contacting the uninsulated electrodes.

The resulted droplets then redispersed if their sizes were too large to remain stable. Furthermore, they reported that the volume density distributions of the dispersions became narrower with time, suggesting that more-frequent coalescence and redispersion are favourable to reducing polydispersity of the dispersion.

Assmann (2014) and Karyappa et al. (2016) later showed that increases in the strength of DC fields resulted in decreases in droplet polydispersity. By showing the population distribution of droplets at various size fractions as a function of field strengths ranging from 4.00 to 4.37 kV/cm, the former author showed that the narrowing trend of the droplet size distribution was largely because of the larger decreases in the volume densities of the large droplets compared with the increases in the volume densities of the small droplets that were generated. Consequently, the volume density distributions became narrower but only slightly within the tested ranges.

The latter authors studied the effect of the application of DC fields to water droplets immersed in viscous castor oil on the size distribution and behaviour of the droplets. They showed that as the strength of the field increased from 0 to 20 kV/cm, the dispersion polydispersity and the average droplet size decreased. Like the former author, they attributed this shift to decreases in the proportion of the larger droplets and increases in the proportion of the small droplets.

On the contrary, Yamaguchi, Sugaya and Katayama (1988) found that a wider droplet size distribution was produced in the presence of DC fields than in the absence of a field. Moreover, they showed that increases in field strength from 0 to 25 kV resulted in increases in both the proportions of the smaller and larger droplets, increasing the dispersion polydispersity. They attributed this to the arrangement of the electrodes used in their study that created the concurrent presence of both strong and weak fields across the column. As this relates to the design of a column, its discussion is deferred to Section 2.5.

In the case of PDC and AC fields, the study by Assmann (2014) is the only published work that reports the effect of strength and frequency of the transient fields on droplet size distribution. Note that he also performed experiments to investigate the effect of DC fields on droplet size distribution under comparable conditions to those in PDC and AC fields so the results can be directly compared. He reported that the use of PDC fields at strengths ranging from 5.00 to 5.67 kV/cm and frequencies from 20 to 60 Hz

yielded wider droplet size distribution than those in DC fields. This was because the PDC fields within his tested ranges were not effective enough to break the larger droplets and, hence, a unimodal volume density distribution was never obtained. Overall, he reported that AC fields provided narrower droplet size distributions compared with PDC and DC fields at far lower field strengths.

He studied the effect of strength and frequency of AC fields on droplet size distribution at ranges of 2.5–3.5 kV/cm and 20–60 Hz, respectively. He found that the droplet size distribution became narrower with increasing field strength at 50 Hz, but a unimodal volume density distribution was not obtained within the tested ranges. The unimodal distribution was obtained when the frequency of the field was decreased below 40 Hz at 3.5 kV/cm. He attributed this to the shift in the predominant droplet breakup mechanism from jetting at frequencies above 50 Hz to necking at frequencies below 40 Hz.

As mentioned earlier, Assmann (2014) pointed out that coalescence and redispersion occurred in his experiments with AC fields. No explanation of its influence on the droplet size distribution, however, was offered. As he also pointed out as part of his recommendation, understanding this phenomenon would be useful for developing an industrially applicable ESX column.

2.5 DESIGNS OF ELECTROSTATIC SOLVENT EXTRACTION COLUMN

This section aimed to identify a suitable design for an industrially applicable ESX column for process metallurgy. The selected design was used as the basis to select an experimental technique that can produce results relevant to the projected industrial application. Therefore, the experimental results of the present study can later be used to optimise the design.

Although no ESX column has been used at an industrial scale to date, various column designs have been proposed and studied at a laboratory scale. Most proposed designs are essentially electrostatic spray columns, where aqueous droplets are fed from the top of the column, while the organic solutions are fed from the bottom. The key difference between these columns is the configuration of the electrodes, which can be generalised into two groups. The first group uses electrified liquid distributors to produce small droplets and perforated-plate electrodes at the top and bottom of the

column. The second group uses vertical electrodes placed along the inner wall of the column.

The columns of the first group consist of multiple nozzles attached to a high voltage DC power source at the top of the column to allow the release of charged droplets to move towards an earthed perforated plate at the bottom part of the column (Stewart and Thornton, 1967; Bailes and Thornton, 1971; Bailes and Thornton, 1974; Bailes, 1977; Bailes, 1981). The design principle of such columns is illustrated in Figure 2.6. The size and speed of the droplets depend on the charge of the droplet, i.e., the higher the strength of the applied field, the greater the charge that the droplet acquires and, thus, the smaller the size of the droplet and the faster the droplet velocity towards the bottom electrode. Given that the size and motion of the droplet cannot be independently controlled because the field direction is parallel to gravity, these columns do not allow flexible control over the droplet residence time and the droplet size. Moreover, because they can only operate using static fields, there will be no induced oscillation on the dispersion. In addition to these drawbacks, these columns cannot operate with the use of insulated electrodes. Consequently, there are possibilities for short-circuits between the electrodes if the nozzle fails to produce discrete droplets (Bailes, 1977; Bailes, 1981) or if a chain of droplets forms between the electrodes (Karyappa et al., 2016).

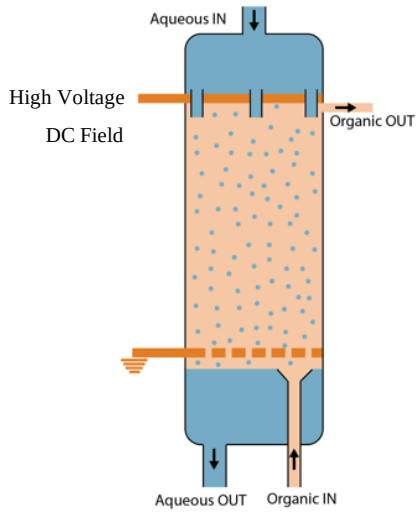

Figure 2.6. Schematic diagram of a column with charged nozzle devices (Bailes, 1977).

The columns of the second group impose electrostatic fields in the direction normal to gravity, inducing droplets to break and zigzag in the field direction, regardless of the

types of the field. This clearly allows more flexible control of the dispersion. In addition, if transient fields are used, these columns can also induce droplet oscillation.

The main column designs of this group that have been studied for SX applications to date are the serpentine-plate electrode column (Warren and Prestridge, 1979), vertical-rod electrode column (Kowalski and Ziolkowski, 1981; Yamaguchi et al., 1988; Yamaguchi et al., 1989) and parallel-plate electrode column (Martin et al., 1983; Scott and Wham, 1989; Scott et al., 1994). These designs are schematically shown in Figure 2.7.

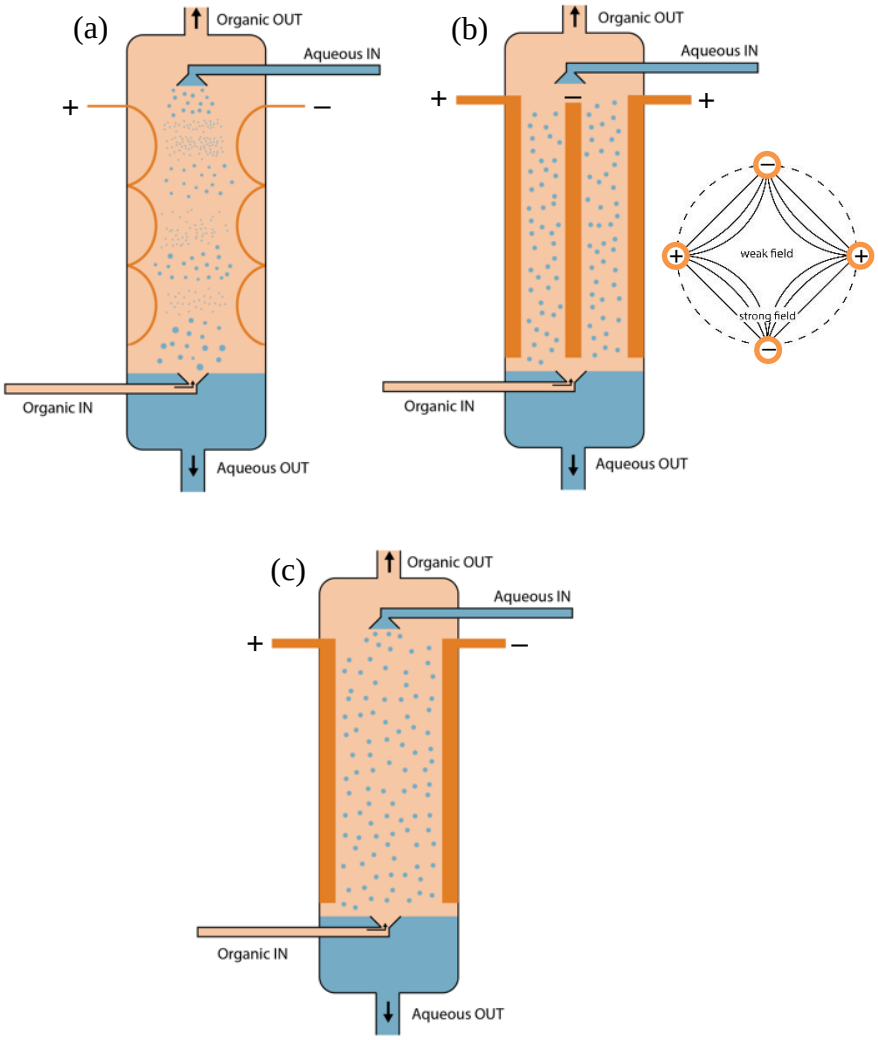

Figure 2.7. Schematic diagram of (a) serpentine-plate electrode column (Warren and Prestridge, 1979), (b) vertical-rod electrode column (Yamaguchi et al., 1988) and (c) parallel-plate electrode column.

Warren and Prestridge (1979) developed the design for the serpentine plate electrode column, as schematically shown in Figure 2.7(a). They proposed a configuration of a

series of half-circle electrodes that mirror each other on both sides of the column wall and the application of DC fields along these electrodes. Such a design allows the creation of intermittent regions of high and low electrostatic fields, resulting in droplet dispersion in the former and coalescence in the latter to minimise phase entrainment and the formation of stable emulsions. They suggested that periodic variation of field strength along the column height may induce droplet oscillation, but no evidence was presented. Overall, they provided only limited technical data on how effectively this design produces dispersion of uniform droplets with high internal turbulence. It is notable that they tested the use of AC fields and found that these fields were less effective than DC fields with this electrode configuration. The use of DC fields, however, may result in arcing between the uninsulated electrodes, particularly at high aqueous flow rates.

Kowalski and Ziolkowski (1981) developed a vertical-rod electrode column design, as schematically shown in Figure 2.7(b). They proposed using four rod electrodes that are spaced at equal intervals about the column and the application of AC fields to generate dispersion. They insulated the electrodes with polyethylene to circumvent arcing. Although they reported that up to ten times increase in mass-transfer rates of acetic acid from xylene using water droplets was achieved using the column compared with that in the absence of a field, no observation on droplet dispersion behaviours was presented.

Using a similar column design, Yamaguchi et al. (1988) reported more detailed observations on droplet dispersion behaviours but used DC fields for water-in-cyclohexane systems. They reported that the droplet size distribution became wider when the field was imposed on the droplets than that in the absence of a field. They attributed this to the arrangement of the four copper rod electrodes that created a concurrent presence of both strong and weak fields across the column; i.e., there was a zone near the wall column close to the electrodes with strong fields that induced droplets to disperse into smaller sizes, while there was also a zone around the centre of the column with much weaker fields that allowed the dispersed droplets to coalesce and stabilised at larger sizes. In addition, the presence of a weak field zone at the centre of the column may also result in droplets falling through the column undispersed. These observations demonstrate that it is important to configure the electrodes in a

way such that droplets are exposed to relatively uniform electrostatic field intensity across the column.

Martin et al. (1983) developed a column with two parallel-plate electrodes each located on either side of the inner wall, as shown in Figure 2.7(c). One major advantage of this design is that it does not allow droplets to pass through the column undispersed because the field does not vary along the column. Oddly, they used insulated electrodes to prevent arching but applied DC fields to produce the dispersion. Consequently, while the fields can affect breakup, they cannot induce lateral motion or oscillation, so the enhancement in mass-transfer rate was only up to 20% compared with in the absence of the field for the extraction of copper from a synthetic chloride solution using an organic mixture of LIX® 65N, an oxime extractant, in Escaid 100 diluent.

Later, Scott and Wham (1989) developed a column with the same electrode configuration but applied PDC fields using uninsulated electrodes to induce oscillation on the droplets. They referred to the column as an emulsion-phase contactor (EPC). By comparing the performance of EPC with a York-Schiebel column (YSC) and a Podbielniak centrifugal contactor (PCC) for the extraction of acetic acid from methyl isobutyl ketone using water, they found that EPC was 17 times more efficient than YSC and 10 times more efficient than PCC.

Scott et al. (1994) further modified the design of EPC by adding another set of parallel plate electrodes that imposed DC fields above the parallel-plate electrodes that impose PDC fields, creating two field regions located in series. The top field region imposed a stronger DC field to produce small droplets and the bottom region imposed a weaker PDC field to allow the droplets to oscillate, zigzag, coalesce and redisperse. The major drawback of their design, which they also pointed out in their work, was that arcing can occur at a high aqueous-phase flow rate because the electrodes were not insulated.

The issues in using a parallel-plate electrodes column mentioned above, such as minimal droplet agitation and risk of arcing at a high aqueous phase flow rate, can be circumvented by using AC fields to impose the electrostatic field. Steffens (2011) showed that the use of insulated parallel-plate electrodes with AC fields allowed an ESX column to operate with significantly higher fluxes and also continual dispersion of the droplets. Later, Assmann (2014) showed that, at comparable field strengths, the application of AC fields from insulated parallel-plate electrodes produced finer

droplets and narrower size distribution compared with that of DC or PDC fields with uninsulated electrodes.

There are other types of electrodes that are distinctly different from these two groups. Yoshida et al. (1986) developed an ESX contactor comprising a pair of inclined-plate electrodes, in which an aqueous film flowing on the surface of the lower earthed electrode interacts with the high-voltage DC fields imposed from the upper electrode. The interaction led droplets to pull out of the film and rise against gravity towards the upper electrode and, upon contact, fall and return to the film. Like any other columns that rely on direct charging to affect dispersion, however, this type of column is prone to arcing at a high aqueous-phase flow rate.

Differently, Steffens (2011) developed a vertical ESX column comprising numerous horizontal rod electrodes placed along the column height to impose AC fields on the droplets. This design, however, requires intricate construction and complex wiring. Despite insulating the electrodes, he found that the column was prone to arcing as the insulation was susceptible to damage. While the risk of damage can be minimised by using better insulation material, the risk will remain. The problem is, given the complexities of the column, detecting and repairing such a problem requires total dismantling, which is clearly impractical on an industrial scale. In addition, the mass-transfer performance of the column was poor: only negligible improvement was achieved when he compared the results with those from a conventional pulsed column under comparable conditions.

Based on the findings of the previous investigators, it appears that the most suitable column design for an industrial ESX column is that using a parallel-plate electrodes configuration that imposes AC fields to effect dispersion. It is notable that Steffens (2011) reported that the use of parallel-plate electrodes using AC fields for a hydrometallurgical SX system, comparable to that used by Assmann (2014), could cause formation of a swarm of ultrafine droplets that subsequently form an apparent stable emulsion. He, however, did not specify the conditions that led to this phenomenon. Understanding of the conditions that may lead to such stable emulsion formation is clearly important to the design and operation of an efficient ESX column. Hence, this was explored in the present study.

2.6 CHAPTER SUMMARY

The application of electrostatic field on conductive droplets suspended in poorly conductive liquid induces droplet polarisation, leading to the formation of charge regions that then interact with the electrode of the opposite sign. The electrical stress imposed on droplets due to the polarisation may cause them to elongate and break and move in the direction of the field. These actions are primarily a balance between the electrical stress that exerts droplet deformation and motion and capillary stress that resists droplet deformation and retains a spherical shape. In the case of the dynamics of droplet deformation, breakup and motion, viscous stress that opposes the fluid motion is also found to be a significant factor.

Emulsion-like formation and necking breakup are theoretically the two most beneficial droplet breakup mechanisms for mass transfer. The former allows the formation of a large interfacial area, and the latter leads to generation of more uniform daughter droplets. In electrostatic fields, however, droplets tend to break through jetting owing to the natural tendency for charge to accumulate at sharp points. The emulsion-like formation is still poorly understood, but researchers have shown that there are at least two ways to shift the droplet breakup mechanism from jetting to necking. The first is by imposing significant viscous stress that can dampen the formation of conical ends during droplet deformation, which requires the continuous phase to be highly viscous. This is clearly impractical for hydrometallurgical SX. The second is by regulating the dynamics of the droplet breakup by adjusting the type and properties of the fields. It is evident that the use of transient fields under a particular field condition can shift the droplet breakup mechanism from jetting to necking, even when a relatively inviscid continuous phase was used.

Between the two types of transient fields, only AC fields can affect droplet oscillation and zigzag motion without the need for the droplets to directly contact the electrodes. This allows the imposition of the fields from insulated electrodes to prevent electrical short-circuits between the two electrodes. The ability of the fields to affect oscillation is important as it allows intense turbulence mixing within and around the droplet. The zigzag motion allows control of the droplet residence time. It is also beneficial to narrow the droplet size distribution by reducing the number of smaller droplets through coalescence and improve mass-transfer by redispersing the resulting droplets if they

exceed their stability limit. Redispersion is beneficial because it provides periodic renewal of the reactant in the boundary layer. There is currently insufficient understanding of how the properties of the electrostatic fields affect droplet coalescence and redispersion and, therefore, the droplet size distribution and mass transfer in AC fields.

The results of previous studies that used various electrodes configuration to affect droplet dispersion in electrostatic fields demonstrated that imposition of a relatively uniform field is important to obtain narrow droplet size distribution with high internal turbulence. Therefore, the use of a column with parallel-plate electrodes appears to be the most promising for the application of ESX for process metallurgy. Although significant advances have been made in recent years towards understanding the droplet dispersion behaviours in AC fields, it has become clear from the present review of the literature that more investigations are needed to elucidate the behaviours of smaller droplets at higher field strengths than those previously studied. Also, more investigation is needed to determine whether the imposition of electrostatic fields that are stronger than those previously studied can allow the formation of a momentary emulsion, which may be useful to enhance mass transfer, or conversely, can lead to the formation of a relatively stable emulsion, which may hinder phase separation, or both. Thus, investigations are needed to determine whether dispersions behave differently in those stronger field conditions as they will produce smaller droplets, and these may be too small to have sufficient mass to counteract drag forces preventing them from settling. This new knowledge will contribute to optimise the design and operation of an ESX column.

CHAPTER 3
EXPERIMENTAL EQUIPMENT AND METHODS

3.1 INTRODUCTION

This chapter describes the experimental equipment, methods and materials used to achieve the objectives of the present study. The experimental investigations were aimed to elucidate the droplet dispersion behaviours when subjected to AC fields at various field conditions through a pair of insulated parallel-plate electrodes and elucidate the effect of these behaviours on the solute mass-transfer performance. The experimental method that was developed by Assmann (2014) was adopted in the present study as it allows detailed observation of droplet dispersion behaviours in electrostatic fields and collection of aqueous samples from the bottom of the experimental column. Some modifications to the previous method to improve the precision of the experiments were made and described.

3.2 EXPERIMENTAL SETUP

The experimental setup is schematically illustrated in Figure 3.1. It was developed by Assmann (2014). Its capabilities and operation are described in detail in his thesis but the description of the setup as well as some modifications to it and its operation in relation to the present study are summarised here for readers' convenience. The setup involved the use of a pair of 3-mm thick stainless-steel plate electrodes coated with ethylene tetrafluoroethylene (ETFE), which has high dielectric strength (7.88×10^4 kV/m) and chemical resistance to the solutions commonly used in hydrometallurgical SX processes. The average coating thickness was approximately 300 μm with a minimum thickness across the surface of 250 μm (Surface Technology Pty Ltd). The electrodes were connected to a variable-voltage variable-frequency AC power supply (801 RP, California Instrument) and the voltage was magnified by a voltage amplifier. The power supply was capable of generating a 15 kV signal over a frequency range of 16–500 Hz but using the current setup, arcing occured from the electrodes when a voltage higher than 6.0 kV was used. This limited the operating range.

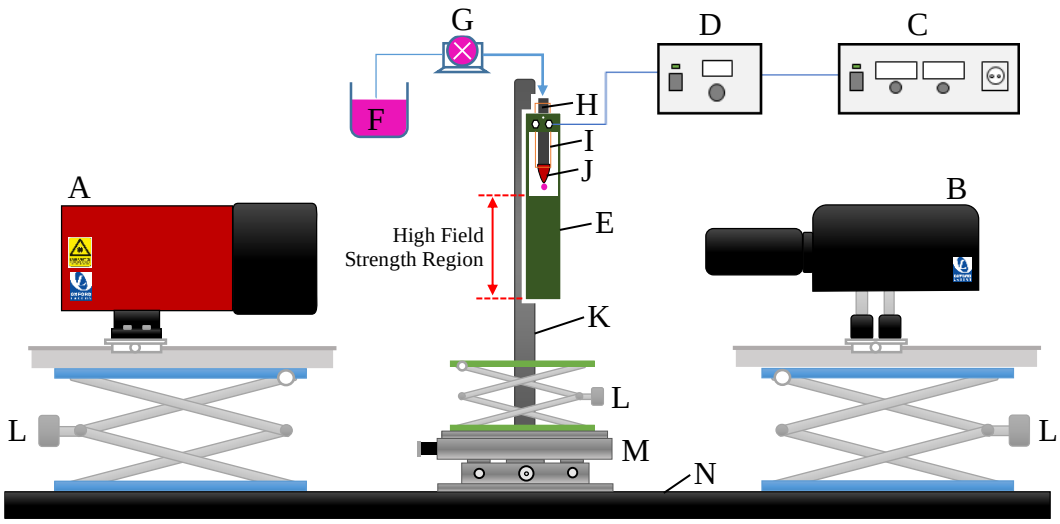

Figure 3.1. Schematic diagram of the experimental setup (A – laser with diffuser, B – high-speed camera, C – AC power supply, D – voltage amplifier, E - parallel plate electrodes, F – aqueous solution reservoir, G – peristaltic pump, H – pump tubing, I – glass enclosure, J – delivery tip, K – stand, L – support jacks, M – motorised XY platform, N – laboratory optical bench) (adopted from Assmann (2014) with some modifications).

In the present study, uniform aqueous droplets were released from a polyethylene tapered tip with an internal diameter of 0.26 mm that was positioned within the hollow area in a region with low electrostatic fields strength between the electrodes. The aqueous solution was transferred into the experimental column using a cartridge peristaltic pump (EW-07519-20, Masterflex®) with Norprene® tubing (6404-13, Masterflex) that was connected to the tapered delivery tip. The delivery tip and tubing were encased in a glass tube positioned between the two electrodes. These droplets were only substantially influenced by the electrostatic field when they entered the high electrostatic field strength region.

The distance between the electrodes was kept constant by inserting polypropylene bolts through two holes near the top of both electrodes and attaching a rubber clamp to the bolts, as shown in Figure 3.2. The glass supporting the tubing was also attached to a clamp to ensure stability of the delivery tip position. The electrodes were connected to the high-voltage AC power supply by soldering Tefzel®-coated stainless-steel wire (M22759/16 AWG22, Avial Australia) to the hole near the top of both electrodes and connecting the wires to the power supply through a pair of wire-to-wire connectors (DTHD04-1-12P, Deutsch). These connectors allowed electrode

replacement without cancelling the wire connection between the electrodes and the power supply when different electrodes were used.

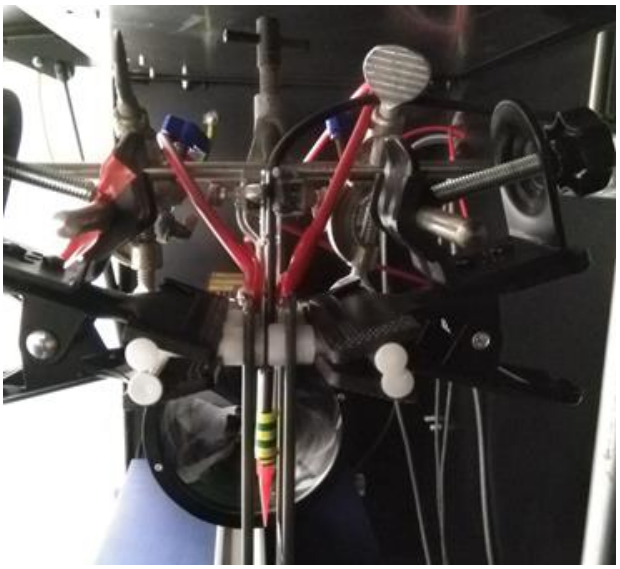

Figure 3.2. Photograph of the electrodes and delivery tip supports from the side view.

The droplet behaviours under the influence of electrostatic fields were analysed from a series of recorded images. The recording was performed using an Oxford Lasers VisiSizer D30V imaging system (IMG0021). This imaging system involves a laser that produces light for illumination of the droplets to be photographed by a high-speed camera. These images were then used to measure the droplet size and magnitude and direction of droplet velocity, and determine a qualitative description of the droplet behaviour. The main components of the imaging system were a Firefly diode laser (FF0500), which is a class IV laser, equipped with RL Diffuser, which provided pulses of infrared laser light; a laser control module, which was used to set the operating variables of the laser and to operate the laser; and an Oxford Lasers computer. The camera used the Oxford Lasers Standard Lens Option 4, which was already pre-calibrated to various levels of lens magnifications. The imaging system was supplied with two specialised computer software package; namely, Photron FASTCAM Viewer (PFV) version 3.681 to operate the camera and VisiSize version 6.206 to measure the individual droplet sizes and droplet velocities from a series of recorded images.

The positions of the laser and camera were supported by aluminium railings that were supplied with the equipment. These railings were secured onto separate laboratory support jacks by attaching steel bolts between the railing and the upper plate of the jack to fasten these two together. Once the laser and camera positions were aligned,

the support jacks that mounted them were then fixed on the laboratory optical bench (1400 mm length × 450 mm width × 25 mm height, UltraLight Series, ThorLabs) with steel bolts.

A major modification of the current setup from that in Assmann (2014) was the addition of a motorised XY positioning table (MAXY60019W1-S6, Velmex Inc) equipped with a controller (VXM-2, Velmex Inc) that was connected to a joystick to enable remote fine adjustment of the electrode positions. This allowed the adjustment to be carried out while the imaging equipment was on and the entire experimental setup was enclosed to allow safe operation of the class IV laser. This was advantageous because it enabled operation with different lens magnifications without adjusting the camera position to ensure that its focus remained at the centre of the electrodes. Hence, in the present study, the distance between the two electrodes and the position of the feed droplets when they descent between these electrodes could be easily inspected using a lower camera magnification before each experiment, improving the experimental precision. It must be noted that various manual handlings performed in the experiments, such as cleaning the electrodes, may have caused slight displacement of the electrode positions and the delivery tip position that was not visually apparent with the naked eye. Given that the distance between the electrodes was only in the order of millimetres in the present study, even a slight deviation in position can be significant. If, for example, the electrode spacing was 10 mm and some parts of the electrodes were skewed slightly towards each other, shortening the spacing by 1 mm, the electric field strength in those parts then increased by about 11 % compared with the other parts.

The electrode position adjustment was enabled by fixing the supports for the electrodes to a stand made of steel bar that was mounted on top of the motorised positioning table (Appendix A). This was achieved by attaching a mounting plate with a mounting block on top of the device. The mounting plate was made of an aluminium plate that was fabricated to have a surface dimension matching that of the top plate of the device (229 mm width × 229 mm length × 10 mm height). Since the top plate was pre-drilled, the mounting plate was then drilled in the exact same hole positions so these two can be fastened together with bolts. Because the bolt heads were sticking out of the plate surface, bumper pads were fixed on the corners of the mounting plate so supporting jacks could stand upright securely when placed on the plate. The mounting block (40

mm width × 40 mm length × 30 mm height) was made with a hole at the centre to fit the stand with a diameter of about 19 mm and four 4-mm clearance holes, one at each corner, to fasten the block on the mounting plate with stainless-steel bolts. The stand was fixed on the mounting block by drilling an 8-mm hole on one side of the block and fastening with a steel cap screw. A layer of rubber mat was placed under the device to prevent the device from moving and scratching the optical bench.

The entire experimental setup was enclosed in an aluminium box (500 mm depth × 1500 mm length × 800 mm height) to prevent radiation exposure from the emission of the class IV laser. The front side of the enclosure was fitted with hinges to act as a door. It was also fitted with toggle latches so it could be closed securely during an experimental run. As an additional safety measure, an interlock system to cut the power of the laser if these latches were undone was installed. The switches to trigger this mechanism were installed next to each latch (Appendix B). The inside of the box was painted matte black to prevent the laser emission from reflecting. Two holes were created, one on each opposite side of the enclosure upper back corners so the wiring and tubing can be put through the enclosure, and these holes were covered with a smaller enclosure to prevent the laser emission from transversing. The box was connected to an earthed wire to prevent it from acquiring charge. Photographs of the complete experimental setup are shown in Appendix C.

3.2.1 Electrodes and Experimental Columns

The electrodes used to observe the droplet dispersion behaviours and those to determine the mass-transfer performance were different. The former, which will henceforth be referred to as dispersion experiment, used electrodes with the exact dimensions as Assmann (2014) used in his experiments with AC fields to minimise variation in the experimental method and achieve a direct comparison of the results. The latter, which will henceforth be referred to as extraction experiment, used electrodes with the same dimension except that the length of the high-field region was halved, so the droplets were exposed to the electrostatic field for a shorter duration. This allowed meaningful changes in the metal extraction percentages within the tested experimental ranges because Assmann (2014) reported about 98% metal extraction at his highest field strength, which was the lowest in the present study. Diagrams showing the dimensions of these electrodes and their photographs are shown in Appendix D.

The experimental columns for the two types of experiments were also different. Although it would be better to use the same experimental column in both experiments to minimise variations, the surface of the extraction column, which was developed by Assmann (2014), was not perfectly flat, resulting in irregularities that could distort the light that passed through the column and disrupt the quality of the recording, as evident from an example presented in Appendix E.

The experimental column for the dispersion experiments was then entirely constructed of 10-mm thick flat transparent glass with 50 mm width × 50 mm length × 150 mm height internal dimensions. It was a simple rectangular column (Figure 3.3(a)) with the glass sections bonded with Loctite® 349, a modified methacrylate ester adhesive resistant to the common organic solvents used for hydrometallurgical applications. The adhesive was not resistant to acetone, but it was resistant to methylated spirits, which were used to clean the column.

A schematic diagram of the experimental column for the extraction experiments is shown in Figure 3.3(b), and its complete dimensions and photographs are shown in Appendix F. The column comprised a cylindrical section at the top of column (A), a rectangular section (C) with a transition section (B) in between. The rectangular section was formed to fit the size of the electrodes for a reason mentioned earlier. The lower part of this section was tapered (E) by means of another transition section (D) to form a funnel to facilitate the coalescence and settling of droplets. The bottom of the tapered section featured a ground glass cone (F) to connect a detachable polypropylene stopcock valve.

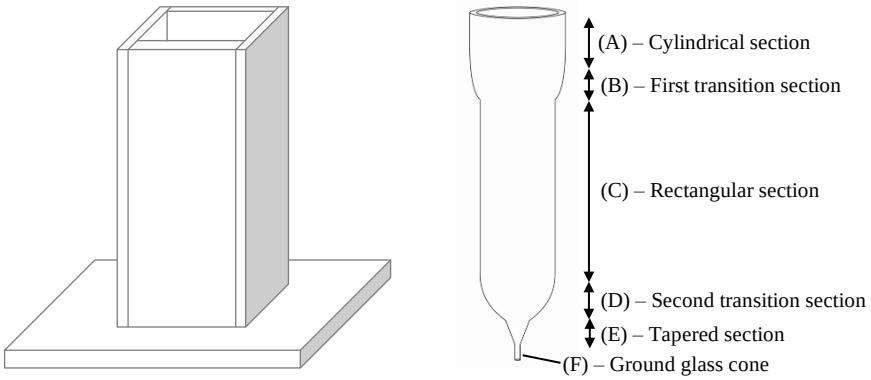

Figure 3.3. Schematic diagram of (a) the column used for dispersion experiments and (b) the column for extraction experiments, which was developed by Assmann (2014).

3.2.2 Configuration of the Imaging Equipment

The main operating variables of the camera were the lens magnification, which determined the size of the field of view, and frame rate, which determined the time intervals between the images taken. The lens magnification was set by manually adjusting the zoom dial. The standard lens option used was pre-calibrated to four levels of lens magnification, as shown Table 3.1. Notably, other levels of lens magnification, such as 1.5 and 3.0, can be used with the imaging equipment, but quantitative analysis for the images taken cannot be performed because the VisiSize software was not calibrated with these magnifications. The camera frame rate was set by adjusting its value on the PFV software.

Table 3.1. Settings for the pre-calibrated level of camera lens magnification.

Camera lens magnification	1	2	4	7
Micron/pixel ratio	30.460	15.204	7.538	4.335
Camera field of view (μm)	15 596 × 15 596	7784 × 7784	3859 × 3859	2220 × 2220

The main operating variables of the laser were the pulse duration, which determined the intensity of the background illumination, the pulse separation, which controlled the separation of two images taken in quick succession, and the laser focus, which determined the light output emitted from the diffuser. The pulse duration was set by adjusting its value on the electronic display of the laser controller by using a dongle attached to the controller. Its value was set so that the brightness shown on the images was uniform, with no pixel appearing to be darker than the other. In the present study, it was set to just above a value where a few darker pixels still existed to circumvent excessive illumination that could mask the presence of the smaller droplets. Similarly, the pulse separation was also set by adjusting its value using the dongle on the controller. Its value was set so that one pulse of light occurred near the end of the first frame and the second pulse of light was captured at the start of the second frame to allow accurate measurement of the droplet velocity. The laser focus was set by rotating the focus adjust knob at the rear of the laser. There was no marker to set its value. The adjustment was thus performed through trial and error to capture in-focus images. Once the focus was set, it was used for the various camera lens magnifications.

3.3 SAMPLING AND ANALYTICAL TECHNIQUES

3.3.1 Image Acquisition from Dispersion Experiment

Droplets experience the most uniform electrostatic field when situated at the centre of the column, equidistant from the opposing electrodes. Therefore, in the present study, the droplets observed to elucidate dispersion behaviours were those at the centre of the column. This was achieved by adjusting the camera and laser positions so that the field of view was at the centre of the column.

Two positions of the camera field of view were used in most experiments to record the droplet dispersion behaviours, as schematically illustrated in Figure 3.4. The first position was at the upper part of the high-field-strength region to observe the dispersion of feed droplets. To observe the entire dynamics of the dispersion, the field of view must capture the moment when feed droplets enter the organic phase and cover the entire space between the electrodes. This was achieved using a lens magnification of 1.5 with a laser pulse duration of 0.31 μs and locating the camera so that the upper limit of the field of view was right below the organic-phase surface. The fact that this lens magnification was not calibrated was immaterial because these experiments aimed only to elucidate the qualitative description of the dispersion behaviours.

The second position was halfway down the high-field-strength region to observe the dispersion of secondary droplets generated by the breakup of feed droplets. It was approximately the position that Assmann (2014) used to record the photographs to measure droplet sizes and droplet velocities. It was also about the location where the droplets left the high-field-strength region in the later extraction experiments. Unless otherwise stated, a lens magnification of 4.0 with a laser pulse duration of 0.82 μs was used to observe the dispersion of secondary droplets within the tested ranges. The maximum camera frame rate, which was 500 fps, was used for all droplet dispersion experiments as it was the best to observe the dynamics of the droplet dispersion and measure the droplet velocities.

Photographs of the dispersion were captured by selecting ‘Record’ on the PFV software. The camera allowed 8188 consecutive frames to be recorded at a time. The VisiSize software, however, can only analyse about 4000 frames at a time. Hence,

4000 consecutive frames were recorded in each experiment. Given that a frame rate of 500 fps was selected, the maximum experimental run time was limited to 8 s.

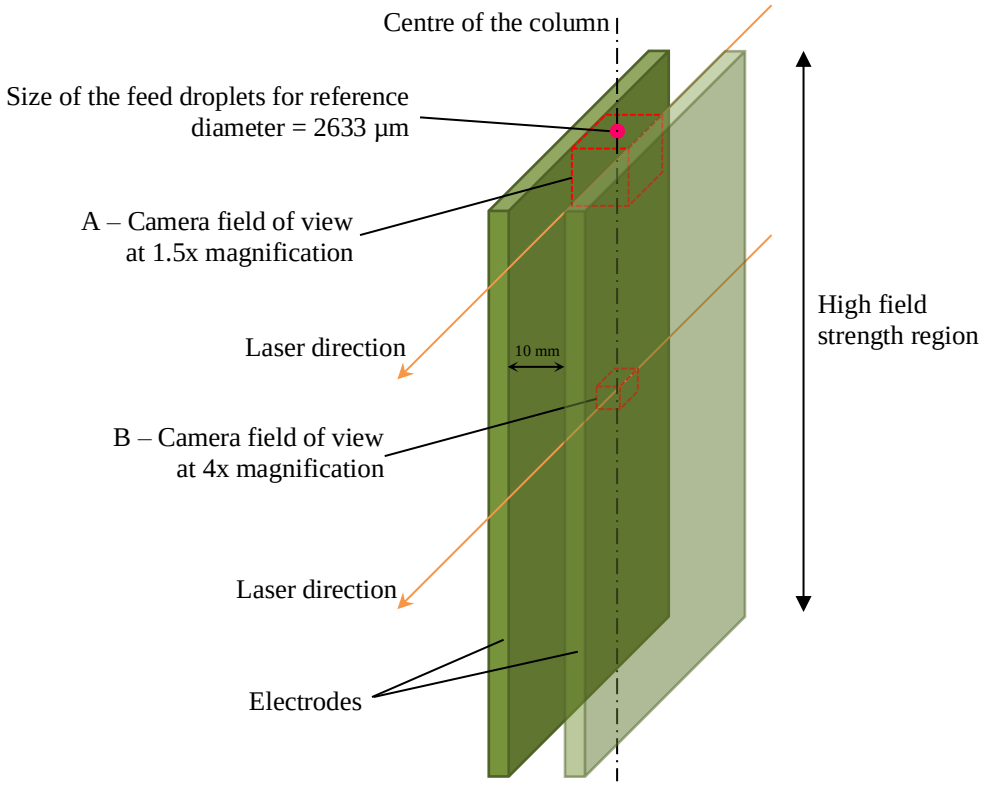

Figure 3.4. Schematic illustration of the approximate camera field of view during dispersion experiments. A – used for the observation of feed droplet dispersion; B – used to measure droplet sizes and droplet velocities.

3.3.2 Measurement of Droplet Sizes and Droplet Velocities

The imaging system applies the particle/droplet image analysis (PDIA) technique to measure the size of individual droplets. The VisiSize software processed the 8-bit digital shadow images of the droplets with a threshold grey-level set on the images to determine the intensity gradient at the edge of the droplets to measure the degree of focus. This enabled large droplets that were in focus and small droplets that were out of focus to be distinguished and accurately sized. Droplets that were out of focus more than a threshold to which the system had been calibrated were rejected from size analysis. The calibration was performed by loading the calibration data that were supplied by the lens manufacturer for the specific lens magnification used. As mentioned earlier, a lens magnification of 4.0 was used to measure droplet sizes and droplet velocities. The droplet sizes that can be measured and reliably corrected for using this lens magnification ranged from 23.26 to 3859.54 µm. Previous researchers

verified the PDIA technique accuracy using a VisiSize software to determine the size of individual droplets within a population of droplets with diameters as small as 25 µm (Wigley et al., 2000; Kashdan et al., 2007).

Given the nature of the study that used an electrostatic field, which induced frequent droplet deformations, many of the observed droplets were non-spherical. The software determines the diameter of the droplet, d, by calculating the equivalent circular area as

$$d = C\sqrt{\frac{4A}{\pi}} \tag{3-1}$$

where C is the microns/pixel calibration of the lens and A is the pixel area that covered the droplet. The sphericity of the droplet is defined as $(d/d_p)^2$ where d_p is the equivalent circular perimeter defined as

$$d_p = C\left(\frac{P}{\pi}\right) \tag{3-2}$$

where P is the pixel perimeter. The value of sphericity ranges from 0 to 1, with 1 being a perfect sphere.

The VisiSize software expresses the mean particle size in various forms, including the arithmetic mean diameter, surface mean diameter, volume mean diameter and Sauter mean diameter. In the present study, the Sauter mean, d_{32} was used to express the mean size of a droplet population, as it is the most relevant measure when mass transfer is a major factor in the process performance (Mugele and Evans, 1951). It is the diameter of a droplet having the same volume-to-surface area ratio as the entire dispersion, defined as

$$d_{32} = \frac{\sum_i d_i^3}{\sum_i d_i^2} \tag{3-3}$$

In addition to focus rejection, other parameters could be set to constrain the quantitative analysis on the individual droplet when processing images to improve the accuracy of the analysis. This was carried out by enabling or disabling parameters listed on the Rejections and Velocity panels on the VisiSize software.

The Rejections panel comprised the following parameters: focus rejection, depth-of-field (DOF) correction, shape rejection, background intensity rejection, border contact rejection, edge contact correction and repetition rejection. The focus rejection option allows out-of-focus droplets to be rejected from the analysis. The DOF correction allows the software to account for the smaller droplets that may not be measured within the camera field of view by considering that larger droplets can be measured over a greater depth. The calibration for this was included within the calibration for each pre-calibrated lens magnification. The shape rejection allows for droplets with sphericity that is less than a specified value to be rejected. The background intensity rejection allows frames to be rejected if their average background level is outside a specified range. The border contact rejection allows droplets to be rejected if they are contacting the border of the field of view. The edge contact correction allows the software to account for larger droplets that may be rejected owing to border contact rejection by considering that they are more likely to contact the border than smaller droplets. The repetition rejection option allows droplets that appear in the same position on the field of view in five consecutive images to be rejected. The settings of the Rejection panels used in the present study when using a camera lens magnification of 4.0 are shown in Figure 3.5(a).

The settings of the Velocity panels used in the present study when using a camera lens magnification of 4.0 are shown in Figure 3.5(b). The Image Pairs mode is the normal mode of operation for velocimetry and, hence, was used. Velocity measurement is achieved in this mode by measuring droplet displacements between a pair of consecutive images. The other two modes were not suitable for the present imaging equipment model. The Double Exposed Images mode requires the laser to emit two pulses of light in each camera frame, resulting in double-exposed images where each droplet casts two shadows in the same image, while the Interframe mode requires a very high frame rate so that a given droplet can be tracked from frame to frame. The direction option specifies the general direction of the droplet motion, which was clearly downward in the present study owing to gravity. The maximum angle deviation option limits the angle of the droplet motion. Because the droplet may translate directly perpendicular to that of gravity, no limit was selected for this parameter. The maximum search radius controls how far the software will search for the same droplet between two consecutive images. The droplets are deemed the same if the ratios of the

maximum area, maximum halo area and maximum shape factor between two droplets in two consecutive images are at or below the specified limits. The pulse separation settings automatically matched the value set on the laser controller.

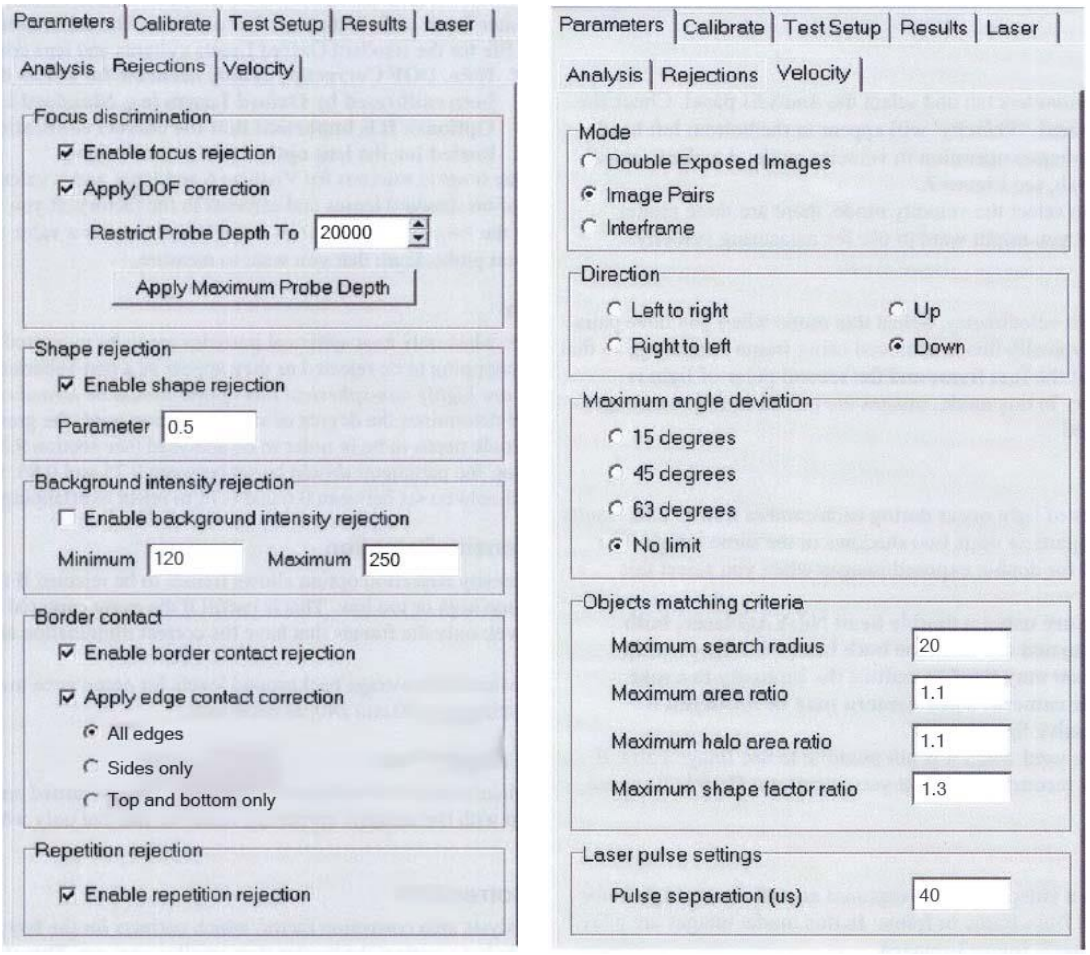

(a) (b)

Figure 3.5. Displays of the (a) rejections and (b) velocity panel.

The VisiSize software allows setting the number of divisions between the minimum and maximum diameters to a value ranging from 1 to 140 to construct the droplet size distribution. The higher the number, the smaller the range of each size fraction generated by the software. Note that the software divides the droplet size fraction in a logarithmic scale and there was no option to change the scale. Also note that the software reports sample analysis summary for the entire droplet population (Appendix G) and analysis for individual droplet data (Appendix H) as separate files. Given that the results of the analysis for a droplet population accounted for the various correction factors mentioned earlier, reconstructing the droplet size distribution data using the generated individual droplet data, which showed only the data for in-focus droplets,

would result in additional errors and inconsistencies with the other software generated data, such as the Sauter mean diameters. Hence, it was deemed best to use the droplet size distribution data, as generated by the software, without reprocessing.

A suitable data representation for the droplet size distribution data was determined to be in the form of histograms because each generated data point accounted for the frequency of number or volume of droplets in a size fraction. Constraints to determine the number of divisions were the following: if the number was too low, the resolution in the data was low; and if the number is too high, there were some size fractions that showed drastic changes in trend, disrupting the general trend of the size distribution, particularly at the larger size fractions where the number of samples was more limited. It was found that 35 was the most suitable number of divisions. An example of a histogram constructed to represent the volume density distribution of a dispersion in the present study is shown in Figure 3.6.

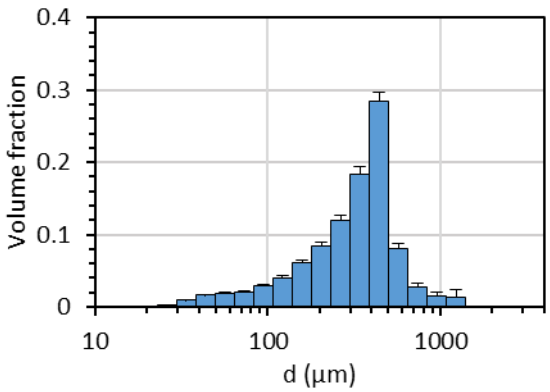

Figure 3.6. An example of the volume density distribution representation for a droplet dispersion that was used in the present study. Error bars represent standard error from a number of independent experimental replicates.

Differently, processing of droplet velocity data was more flexible as the data were generated solely based on the in-focus droplets shown in the analysis of the individual droplet data. The VisiSize software reports individual droplet velocity by a value for the magnitude and an angle for the direction. The reported direction and angle of the droplet velocity used the configuration shown in Figure 3.7.

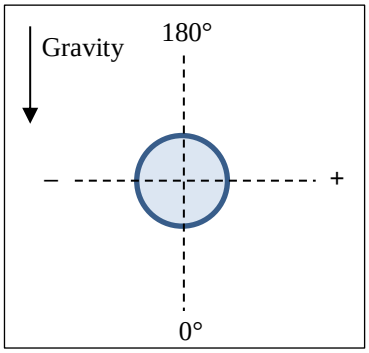

Figure 3.7. The configuration of the direction and angle of droplet velocity reported by the VisiSize software (redrawn from Assmann (2014)).

3.3.3 Aqueous Sample Acquisition from Extraction Experiments

In the present study, the percentage of metal ion extraction achieved in an experiment was used to determine the mass transfer performance in the experimental condition. The extraction data were generated by acquiring samples of the aqueous phase, which were then assayed for their elemental concentrations.

The column setup to acquire aqueous samples from the extraction experiments is shown schematically in Figure 3.8. The experiment was performed by pumping the feed droplets through the delivery tip and allowing the droplets to disperse under the influence of the applied electrostatic field and settle at the tapered droplet section after passing through the high-field-strength region. When a sufficient volume of sample had been transferred, the pump was then quickly turned off. After the last dispersed droplet passed through the high-field-strength region, the AC power supply was also turned off. The pool of collected droplets at the bottom of the column was then carefully drained by manually rotating the knob of the stopcock valve into a syringe that had its mouth connected to a polyvinylidene fluoride syringe (PVDF) filter with a 45 µm pore size (Fisherbrand). The two glass beakers shown in the setup were used to support the syringe to avoid spillage. When a sufficient sample volume was collected, it was then passed through the hydrophilic syringe filter to separate any entrained organic phase. The sample was then diluted and sent for assay.

Because the imaging equipment was not required in these experiments, the setup was not enclosed and hence, a direct visual inspection could be performed during experiments. This was important to ensure that there was no droplet dangling on the

mouth of the delivery tip after both the pump and AC power supply were turned off, which may accidentally fall through the organic phase and contaminate the sample.

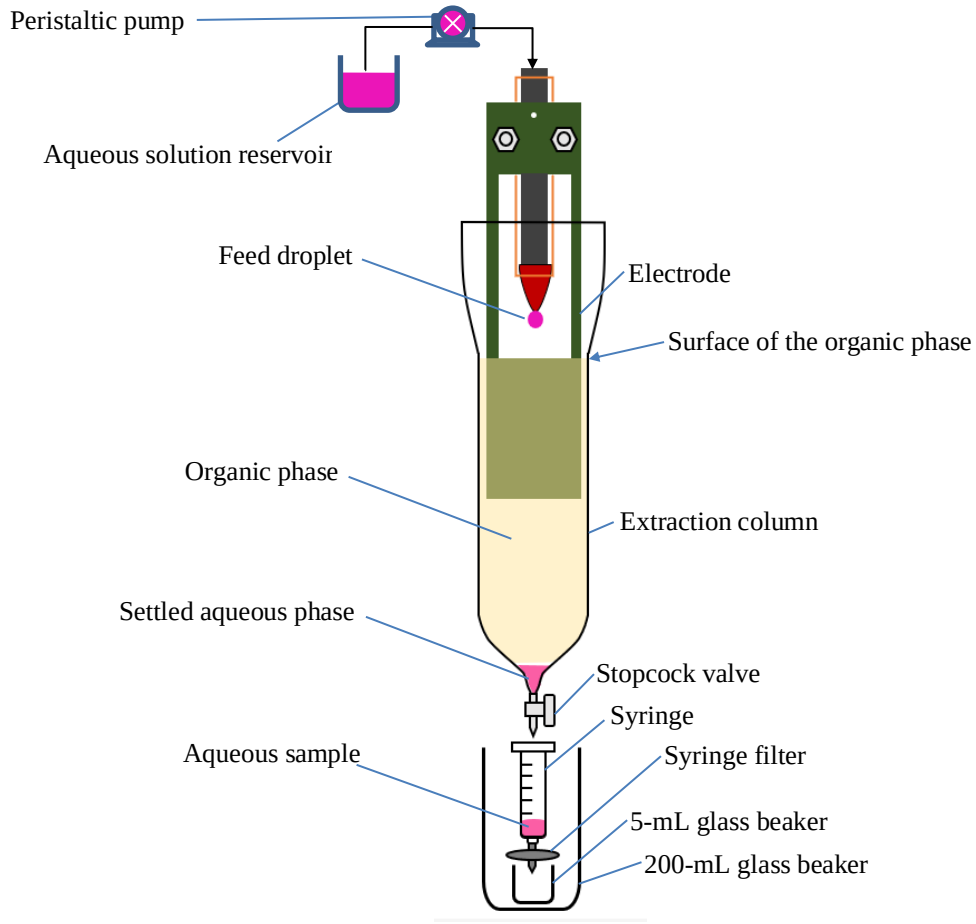

Figure 3.8. Column setup to acquire aqueous samples from extraction experiments.

As Assmann (2014) mentioned previously, additional mass-transfer may occur between the pool of raffinate at the bottom of the column and the surrounding organic phase. This mass-transfer was assumed to be negligible compared with that when the droplets descended through the organic phase. In the present study, the experimental run time was significantly shortened to further minimise the effect of this mass transfer. Only 0.25 mL of sample was collected in each experiment rather than the 20 mL that was collected in the previous study. Hence, the time for the sample to remain in the column was shorter and the surface area of the raffinate pool was smaller than in the previous study. In most cases, an experimental run time of 2.5 min was used when a feed flow rate of 0.25 mL/min was used to accommodate losses from the draining to filtering steps.

3.3.4 Assay of Metal Ion Concentrations

The metal ion concentrations in all aqueous phases were analysed using inductively coupled plasma optical emission spectroscopy (5100 ICP-OES, Agilent) following the procedures recommended by the manufacturer. Aqueous samples of the feed solutions or those obtained from experiments were diluted between 20 to 200 times with 1% nitric acid solution in either a 5-mL or 10-mL volumetric flask before analysis so there would be sufficient volume for analysis and the metal ion concentrations were approximately fall within its calibration range (0.5–5.0 mg/L).

3.3.5 Measurement of pH

All pH measurements were carried out using a benchtop pH meter (SevenCompact™, Mettler-Toledo) equipped with a Mettler-Toledo InLab® Expert pH probe. The probe simultaneously measured the temperature when measuring the pH to allow correct temperature compensation.

3.4 MATERIALS

There are two group of aqueous and organic solutions for the experiments performed in this chapter. The first group of aqueous and organic solutions were identical to those Assmann (2014) used to allow direct comparison. This group comprised an aqueous solution containing cobalt sulfate and an organic solution containing acidic extractant with an active component of bis(2,4,4-trimethylpentyl)phosphinic acid, CYANEX® 272. The second group comprised an aqueous solution containing copper sulfate and an organic solution containing chelating extractant with an active component 2-hyroxy-5-nonylacetophenone oxime, LIX® 84-I, which is known to be an SX system with a relatively slow kinetics (Dehkordi, 2002; Li et al., 2019). Because the first group of solutions was used for the work reported in Chapter 4, 5 and 6, it was deemed appropriate to describe the reagents, the composition of the test solutions and the procedures to prepare these solutions here to avoid multiple repetitions.

3.4.1 Reagents

The following analytical reagent (AR) grade reagents were used for the work described in this thesis: cobalt(II) sulfate heptahydrate (99% $CoSO_4 \cdot 7H_2O$, ChemSupply

Australia), copper(II) sulfate pentahydrate (99% $CuSO_4 \cdot 7H_2O$, Alfa Aesar), sodium sulphate anhydrous (99% Na_2SO_4, Ajax Finechem), sodium hydroxide (98% NaOH, Rowe Scientific), acetic acid (99.7% CH_3COOH, Fisher Scientific), nitric acid (70% HNO_3, Ajax Finechem). The following reagents were used to prepare the organic solutions and were of industrial grade: CYANEX 272 (Cytec Australia), LIX 84I (BASF) and ShellSol 2046 (Viva Energy Australia). In addition, the following reagents were also used: single-element cobalt standard for ICP-OES (1000 mg/L in 5% nitric acid, Agilent), single-element copper standard for ICP-OES (1000 mg/L in 5% nitric acid, Agilent), industrial-grade methylated spirits (Diggers Australia). All reagents were used as supplied.

3.4.2 Test Solutions and Their Preparations

The first group of solutions, which will henceforth be referred to as the $CoSO_4$ – CYANEX 272 system, comprised an aqueous solution containing 300 mg/L of Co^{2+} (as sulfate) and 0.2 mol/L of Na^+ (as sulfate) in an acetic acid/acetate buffer with a pH of 5.5, and the organic solutions consisted of 10% CYANEX 272 by volume in ShellSol 2046. The pH buffer was added to maintain the pH relatively constant throughout mixing as the cobalt extraction reaction with CYANEX 272 releases hydrogen ions.

The aqueous solutions were prepared by dissolving the required amounts of $CoSO_4 \cdot 7H_2O$ crystals in a volumetric flask with the buffer solution, which was prepared in a separate glass beaker. The buffer solution was prepared by dissolving the required amounts of NaOH and CH_3COOH in a minimum amount of deionised water. The calculations for the composition of the buffer solution are shown in Appendix I. The solution was vigorously mixed to ensure that the NaOH was completely dissolved. The solution was then allowed to cool to room temperature and subsequently added into a volumetric flask to dissolve the $CoSO_4 \cdot 7H_2O$ crystals. The solution was mixed with a magnetic stirrer and after the crystals were completely dissolved, the stirrer was removed from the flask and deionised water was added to fill to the mark. The pH of the solution was then measured to ensure that it was 5.5. The organic solutions were prepared by transferring the required volume of CYANEX 272 and ShellSol 2046 into a volumetric flask.

The second group, which will henceforth be referred to as the $CuSO_4$ – LIX 84-I system, comprised an aqueous solution containing 1000 mg/L Cu^{2+} (as sulfate) in an acetic acid/sodium acetate buffer with a pH of 4.5 and an organic solution containing 5% LIX 84-I by volume in ShellSol 2046 diluent. The aqueous and organic solutions of this group were prepared in the same manner as the first group of aqueous and organic solutions. The calculations for the composition of the buffer solution for the $CuSO_4$ – LIX 84-I system are shown in Appendix I.

3.5 LIMITATIONS OF THE EXPERIMENTAL EQUIPMENT

Limitations of the experimental equipment have been discussed by Assmann (2014) in his thesis, but it was deemed important to discuss these limitations in this chapter in relation to the present experimental conditions. Some new limitations are identified in the present study and discussed here.

The present imaging equipment is only able to observe a limited range of droplet sizes. This is because, for a section that can be observed at a particular lens magnification, the relative size of the droplets cannot differ too significantly as droplets that are too large or too small within the field of view would not be able to be sized. This, in turn, limits the range of the applied voltage that can be investigated as it must produce a droplet dispersion that fits the observable size ranges.

The imaging equipment can also only observe a limited number of droplets in a frame. This is because an excessive number of droplets, particularly ultrafine ones, would reduce the software ability to distinguish between different droplets. Increases in the number of droplets increased the instances of droplets overlapping each other and consequently, they were either inaccurately sized or not sized owing to shape rejection. Figure 3.9 shows an example of the software inability to distinguish individual droplets accurately from an image of a dispersion with an excessive number of droplets. Consequently, the imaging equipment cannot operate at electrostatic field conditions that produce such a dispersion, thus limiting the ranges of applied voltage that can be investigated. The instance of droplets overlapping each other was unavoidable, so the ranges of the electrostatic field conditions were chosen to minimise excessive formation of ultrafine droplets. Within the tested experimental ranges, at least 2000 droplets were able to be characterised in each experiment.

For the same reason, it was found in the present study that the use of a high flow rate can result in an excessive number of droplets, leading to a large proportion of droplets that overlap each other. Thus, the present experimental setup was only able to operate with a relatively low flow rate, e.g., 0.25 mL/min, when visual analysis of the dispersion was required.

Investigations of the effect of electrode spacing on the droplet dispersion behaviours cannot be performed using the current experimental setup. This was because substantially increasing the electrode spacing beyond 10 mm was not possible due to the limited capability of the high-voltage AC power supply, whereas decreasing the spacing below 10 mm was restricted by the required space to allow the pump tubing and delivery tip to be hung above the high-field-strength region between the electrodes. In addition, a fairly large distance between the electrodes relative to the droplet size was needed to minimise non-uniformity in the electrostatic field strength as well as hydrodynamics due to the presence of electrodes.

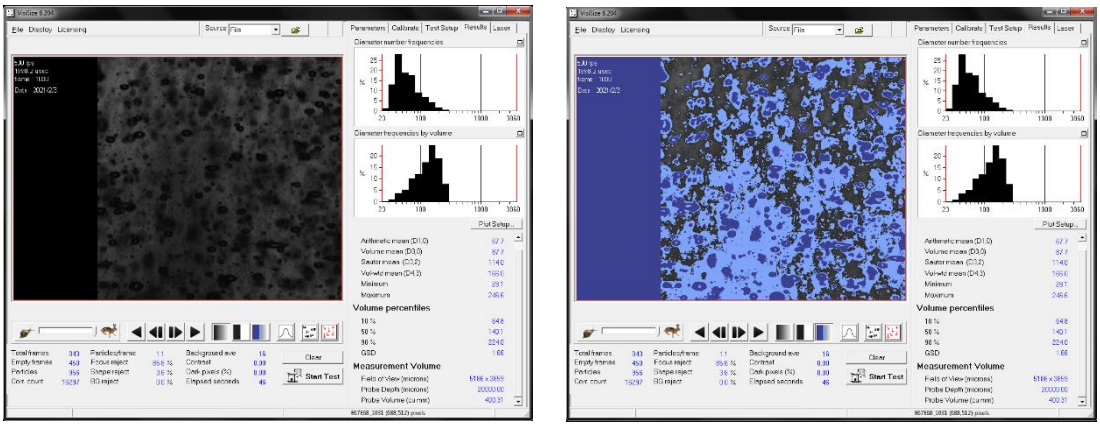

(a) (b)

Figure 3.9. An example of (a) a grey-scale image of a dispersion with an excessive number of droplets taken by the imaging system and when (b) the image was analysed by the VisiSize software.

3.6 CHAPTER SUMMARY

Two types of experiments were devised to achieve the objectives of the present study; namely, dispersion and extraction experiments. The dispersion experiment involved using a high-speed imaging system to record droplet dispersion under the influence of electrostatic fields. The recording was then be used to determine the droplet behaviour and measure the droplet sizes and magnitude and direction of the droplet velocities.

The extraction experiment involved collecting an aqueous sample from a dispersion experiment to allow measurement of the percentage of metal ion extraction, which was then used to determine the mass-transfer performance at that electrostatic field condition. A different set of experimental column and electrodes was used in these extraction experiments to allow quick sample acquisition to minimise additional mass transfer that was not from the influence of the applied electrostatic fields.

CHAPTER 4
EFFECT OF ALTERNATING CURRENT FIELDS ON DROPLET BREAKUP, MOTION AND OSCILLATION

4.1 INTRODUCTION

Assmann (2014) found that the application of a high-voltage and low-frequency AC field was the most suitable for ESX. He showed that such a field condition led to the production of small droplets with a high amplitude of zigzag motion and oscillation. He observed these behaviours for droplet dispersions with Sauter mean diameters ranging between 243 and 386 μm at field strengths ranging from 2.5 to 3.5 kV/cm and frequencies from 20 to 60 Hz.

In this chapter, the breakup, motion and oscillation behaviours of droplets smaller than those previously studied by Assmann (2014) under the influence of more-vigorous electrostatic fields were investigated. In the context of the present study, these behaviours refer to how the droplet acts with the changes in the electrostatic field condition. The aims of these investigations were to determine the behaviours of droplets that are smaller than 100 μm in diameter and determine the conditions that allow the formation of momentary emulsion. Before discussing the former, the mechanisms of the droplet formation are discussed to investigate the latter. New observations on droplet formation, motion and oscillation are reported. In studying the droplet motion, the magnitude and direction of the individual droplet velocity were measured.

4.2 EXPERIMENTAL METHODOLOGY

4.2.1 Materials

The $CoSO_4$ – CYANEX 272 system was used for the work described in this chapter. Preparation of the test solutions and the reagents used to prepare them are described in Chapter 3.4.

4.2.2 Experimental Procedures

The experimental set-up developed by Assmann (2014), described in Chapter 3.2, with the dispersion column was used in this part of the study. The experiments were carried out at ambient temperatures (25 ± 2 °C). In each experiment, 200 mL of the organic solution was used. The aqueous-phase flow rate was kept constant at 0.25 mL/min in all experiments, unless otherwise stated.

The general procedure to observe the droplet dispersion behaviours between the two parallel plate electrodes is described in Chapter 3.3.1. The observation was facilitated by recording videos of the dispersion at a rate of 500 fps and replaying the recording at reduced speeds using the PFV software. The dispersion of feed droplets was observed from the top end of the high-field-strength region using a camera lens magnification of 1.5, whereas the dispersion of the secondary droplets was observed from halfway down the high-field-strength region using a lens magnification of 4.0 and, in few cases, 7.0. The droplet size and velocities were obtained by analysing the recorded images using the VisiSize software.

The generation of high-strength electrostatic fields was achieved by using a variable-voltage variable-frequency AC power supply and a voltage amplifier that was connected to the electrodes through high-voltage electrical wires. Before performing any experiment, the spacing of the electrodes and position of the feed droplets between the electrodes when entering the high-field-strength region was inspected by recording the descent of the feed droplets in the absence of a field using a lens magnification of 1.0 to ensure that they were kept constant. The detailed procedures to perform this inspection, as well as the overall dispersion experiment, are described in Appendix J.

Each experiment was replicated five times to achieve a representative profile, i.e., each data point for droplet size and droplet velocity in this chapter is an average of five experimental runs. In each run, 4000 consecutive images of the dispersion under the influence of the applied electrostatic field were recorded.

4.2.3 Experimental Data Analysis

The droplet size and droplet size distribution were analysed from the recording using the VisiSize software version 6.206, which applies the PDIA technique. The general

procedure to analyse the droplet size and velocities using the software is described in Chapter 3.3.2.

The qualitative description of the droplet behaviour was determined through visual observation of the recording using Photron FASTCAM Viewer (PFV) software version 3.681 at reduced speeds ranging from 1 to 30 fps in most cases. Screenshots from the recording were captured to show these behaviours when necessary.

Quantitative analysis of the effect of electrostatic fields on droplet elongation was attempted by manually comparing the lengths of the droplet in the major (horizontal) axis from a frame wherein the droplet exhibited maximum elongation and another frame wherein it exhibited a spherical shape using the PFV software. This could be carried out because the pixel-to-micron ratios for the lens magnifications of 4.0 and 7.0, which were used in the experiments to observe droplet elongation, were known and the software was equipped with a manual measurement tool to determine the pixel distance between two points. The droplets were deemed to be spherical when the lengths of both the major and minor (vertical) axes were equal. Note that the VisiSize software cannot measure droplet elongation because it was unable to recognising a droplet was the same in different frames if its shape was markedly changed.

4.3 RESULTS AND DISCUSSION

4.3.1 Preliminary Experiments to Determine Experimental Ranges

The range of applied AC field strength was determined by a series of preliminary dispersion experiments, which were performed in duplicate, by visually observing changes in the dispersion characteristics as the field strength increased beyond 3.5 kV/cm at a constant frequency of 50 Hz. This frequency was selected as the default, given that it is the frequency of the mains power supply in Australia. Visual analysis of the dispersions revealed that when the field strength increased beyond 4.00 kV/cm at a feed flow rate of 0.5 mL/min, which flow rate was used by Assmann (2014), the dispersion may generate a cloud of ultrafine droplets that led to the formation of an emulsion that was not readily demulsified even after the field was turned off. The emulsion formation prevented the measurement of the droplet size as the cloud of the

ultrafine droplets blocked the laser illumination and hindered the software from detecting the size and motion of most of the droplets in the dispersion.

The apparent stability of the emulsion appeared to be caused by droplets that were too small to exhibit significant velocity in the gravity direction to settle, as evident from the photographs presented in Figure 4.1. This was consistent with the explanation proposed by Steffens (2011). Figure 4.1(a) shows that a significant proportion of daughter droplets generated by the first feed droplet remained at the top of the high-field-strength region before the next droplet entered. Consequently, the dispersion became more crowded as more droplets entered the column, to the point that it entirely blocked the laser illumination (Figure 4.1(c)). When the field was turned off and another droplet entered the column, a significant portion of the droplets was able to settle quickly, suggesting that the emulsion was not stable and could be broken by simple physical means (Figure 4.1(d)). Because the emulsion formation was not permanent, it will henceforth be referred to as semi-permanent emulsion (SPE) for brevity and clarity.

It was found that the SPE formation could be broken down by either heating it at around 40 °C for a few minutes, depending on the severity of the emulsion formation, or by filtering it with a phase separation paper. It must be noted, however, that later, aqueous samples needed to be taken during the mass transfer experiments and performing either of those treatments before taking these samples would have led to extraneous mass transfer, leading to erroneous analysis. Although heating the organic phase to 40 °C could break the SPE formation, operating at that temperature could still lead to the SPE formation under comparable conditions and it was not readily demulsified.

In practice, the emulsion formation can lead to a phase-disengagement issue. Such a phase-disengagement issue is already known with mechanically agitated contactors due to excessive agitation, and the findings of the present study demonstrate that the issue also applies to ESX contactors. One aspect of interest in the present study is to determine how to lower the proclivity for the emulsion to form and the smallest mean droplet size at which the ESX technique can operate before the emulsion forms. The latter is discussed in Chapter 5.

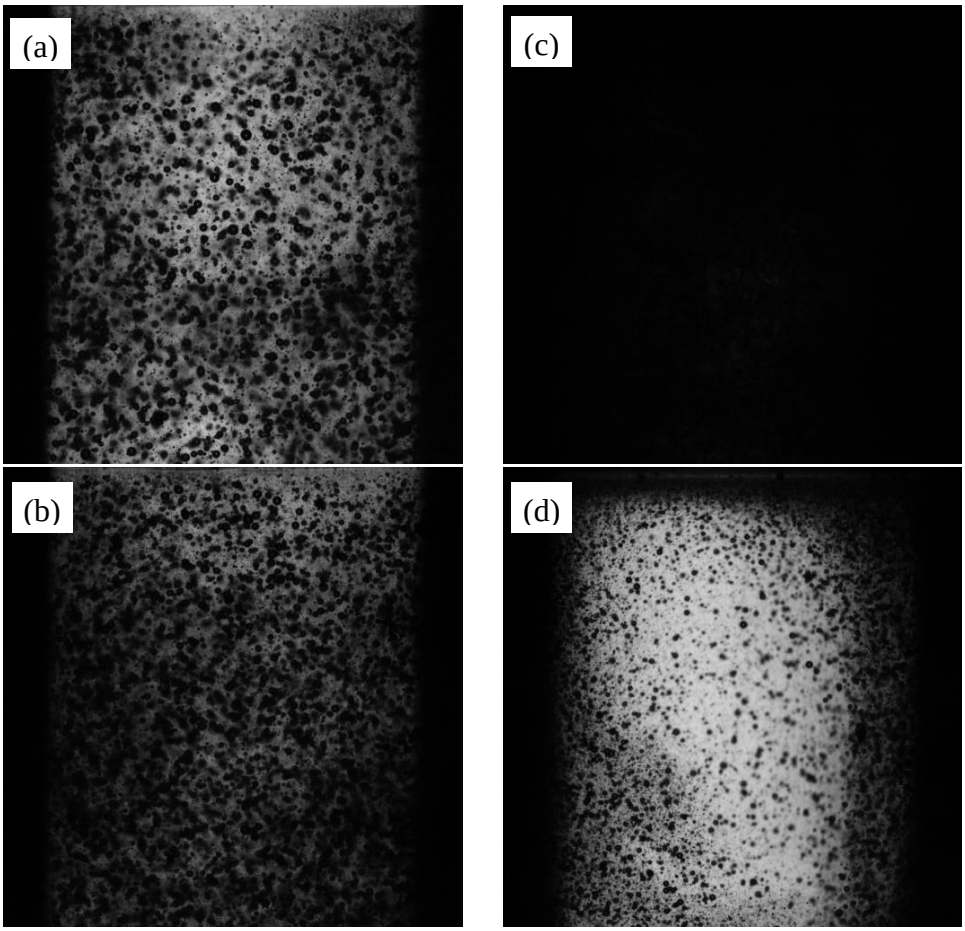

Figure 4.1. Photographs taken at the top of the high-field-strength region with a camera lens magnification of 1.5 in 5.0 kV/cm AC field at a frequency of 50 Hz. They display the situation after the (a) first, (b) second, and (c) fifth droplet entered, and (d) after the field turned off and the sixth droplet entered.

It was thought that the emulsion formation and the issue with droplet analysis if the emulsion formed could be circumvented by reducing the droplet population density in the generated dispersion. This could be achieved by reducing the feed flow rate and by increasing the gap between the electrodes. Because the latter cannot be performed using the current experimental setup, given the limit of the voltage that the equipment could supply, attempts to use lower feed flow rates were carried out. The proclivity for the emulsion to form at 4.25 kV/cm decreased when the flow rate decreased from 0.50 to 0.25 mL/min. When the field strength increased further to 4.50 kV/cm, however, the dispersion of even a single droplet led to the SPE formation, as shown in Figure 4.2. Hence, the investigation of droplet behaviours at field strengths beyond 4.25 kV/cm was not pursued and the aqueous flow rate was kept constant at 0.25 mL/min in subsequent experiments as there was no benefit to operating at a lower flow rate.

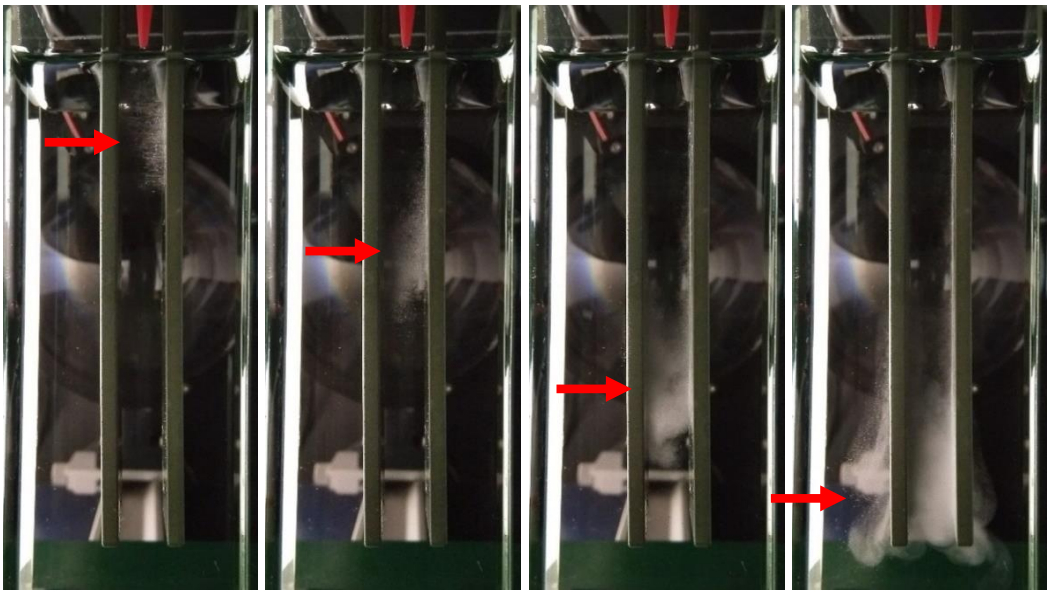

Figure 4.2. Development of emulsion formation from a single feed droplet as it descended between the electrodes at a field strength of 4.5 kV/cm and frequency of 50 Hz.

Regarding the range of field frequency, it was found that the voltage reading shown on the power supply significantly fluctuated when the frequency decreased below 30 Hz at field strengths ranging from 3.50 and 4.25 kV/cm. The phenomenon of voltage fluctuation is not uncommon for sinusoidal power supplies (Tennakoon et al., 2004; Masoum and Fuchs, 2015). It was observed that the reading deviation increased from ± 0.01 kV for the target reading at 70 Hz to ± 0.05 kV at 50 Hz, i.e., the field strength randomly fluctuated between 3.99 and 4.01 kV when the frequency was set at 70 Hz, and between 3.95 and 4.05 kV when set at 50 Hz if the targeted reading of the AC field strength was 4.00 kV. The deviation was relatively stable at ± 0.05 kV when the frequency was decreased to 30 Hz, but then increased significantly to about ± 0.11 when the frequency decreased further to 20 Hz. Given the marked erratic nature of the supplied voltage below 30 Hz, experiments were thus performed at frequencies ranging from 30 to 70 Hz and field strengths ranging from 3.50 to 4.25 kV/cm.

Given the limited ranges of field strength and frequencies that could be investigated in the present study, it was important to first ensure that dispersions that contained droplets mainly below 100 µm in diameter can be produced to achieve the objectives. Dispersion experiments were then performed under the most-vigorous field conditions that could be used before SPE forms, which was at a field strength of 4.25 kV/cm and a frequency of 50 Hz. The results show that the average droplet diameter of the

dispersion was about 54 μm and more than 80% of the droplets were smaller than 100 μm. These results confirmed that the experimental ranges were still suitable to achieve the objectives of the present study.

4.3.2 Droplet Breakup Mechanisms in Alternating Current Fields

The behaviours of droplet dispersion within the studied experimental ranges differed significantly depending on the size of the droplets in the dispersion. It was observed that when the feed droplets entered the organic phase and were exposed to the strong electrostatic fields (E_0 = 3.50–4.25 kV/cm, f = 50 Hz), they elongated and broke apart to form a population of large droplets (primary droplets) that then dispersed vigorously in an apparently random manner until the majority of the droplets reached a particular size. Subsequently, these smaller droplets (secondary droplets) continued to disperse as they translated through the field, but this occurred less vigorously in a more predictable manner. This observation is consistent with that observed by Assmann (2014). Based on these observations, the droplet dispersion behaviours in AC fields can be classified into three regimes that occur in sequence; namely, feed droplet dispersion, primary droplet dispersion and secondary droplet dispersion. High-speed photographs of the typical droplet dispersion in each regime from a single feed droplet as it descended through the field are shown in Figure 4.3.

Figure 4.3(a) shows the sequence of events leading to the breakup of the feed droplet. When the feed droplet was exposed to the applied field, it elongated to a point where both of its ends touched the electrode. It then underwent breakup via jetting, resulting in thinning of the middle portion of the droplet as the liquid streamed out of opposite ends. Most of the liquid was observed to clump on the surface of the electrodes, probably owing to the hydrodynamic forces towards the electrodes during ejection, which hindered the liquid from moving. Thinning of the middle portion of the droplet eventually led to a necking breakup, which marked the end of the feed droplet dispersion.

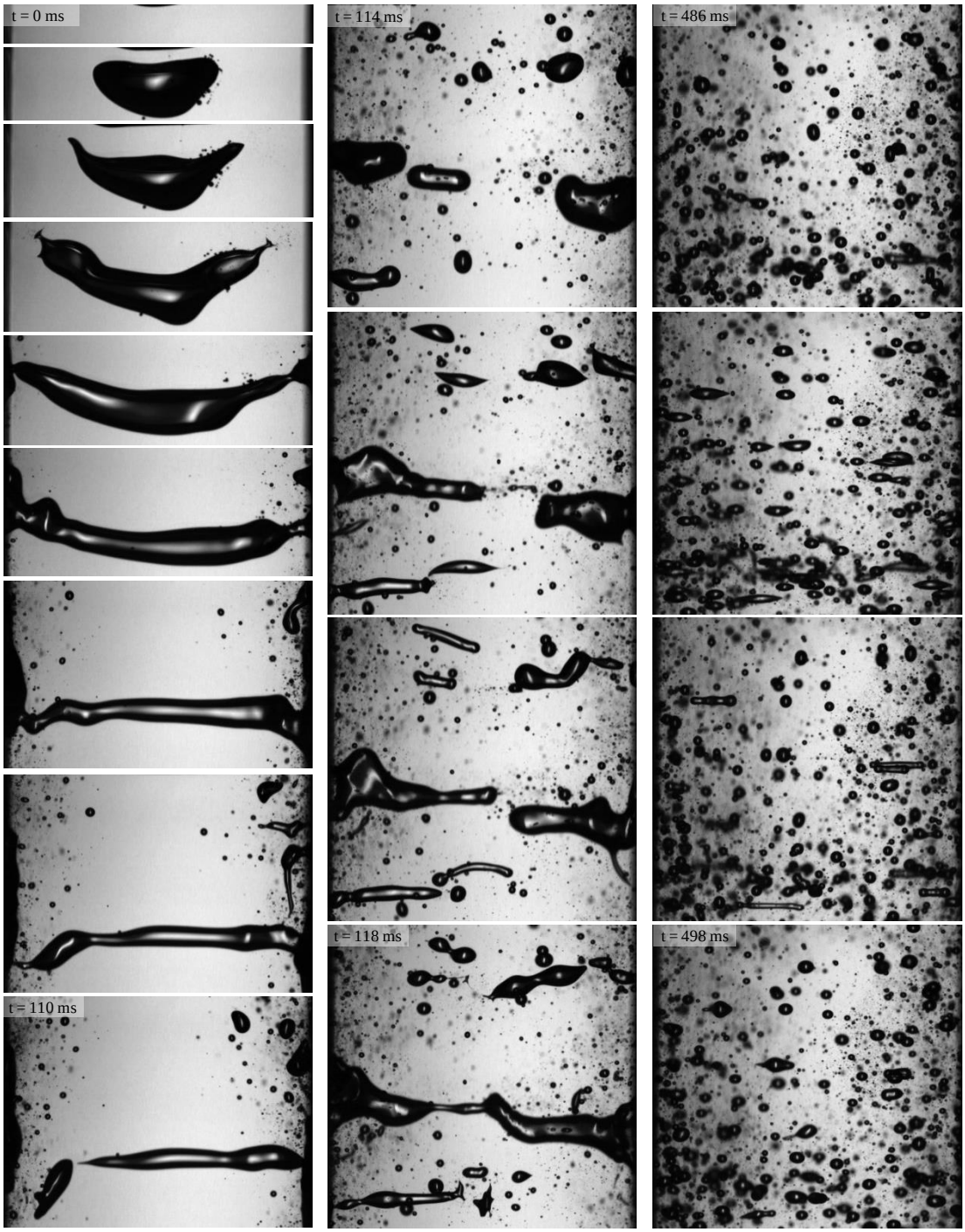

Figure 4.3. Dispersion behaviours of an aqueous feed droplet as it descended through 4.0 kV/cm AC field at a frequency of 50 Hz. Based on the size of the droplets, the dispersions can be classified to three regimes that occur in sequence: (a) feed droplet dispersion, (b) primary droplet dispersion and (c) secondary droplet dispersion. Timestamps relative to when the droplet entered the organic phase are given in some frames for reference.

Figure 4.3(b) shows that after the feed droplet completely broke apart, the formed clumps on both electrodes were propelled towards the opposite electrodes as the forces

that were pushing these clumps toward the stiff, flat electrodes were reflected. They then elongated and broke apart while translating towards the opposite electrode, forming many daughter droplets that continued to break apparently until they reached a particular size (Figure 4.3(c)). This was evident by the decrease in the maximum droplet diameter (d_{max}) in the dispersion when plotted against E_0, as shown in Figure 4.4. This aligns with the general view in the literature that droplets would break when their size is greater than the critical value at a given field strength in electrostatic fields.

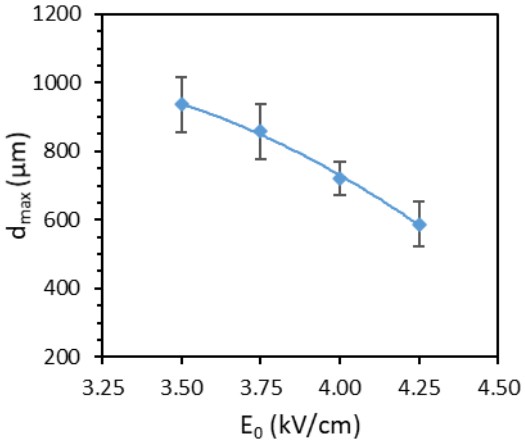

Figure 4.4. Plots of the maximum droplet diameter as a function of field strength at a frequency of 50 Hz. The data shown are means and standard errors from five replicates.

Several breakup mechanisms were observed during the dispersion of primary droplets. These included previously known breakup mechanisms in AC fields; namely, jetting (Figure 4.5(a)), necking (Figure 4.5(b)), irregular breakup (Figure 4.5(c)), and combination breakup (Figure 4.5(d)) as well as a previously known mechanism that had only been observed in DC and PDC fields; namely, emulsion-like formation (Figure 4.5e).

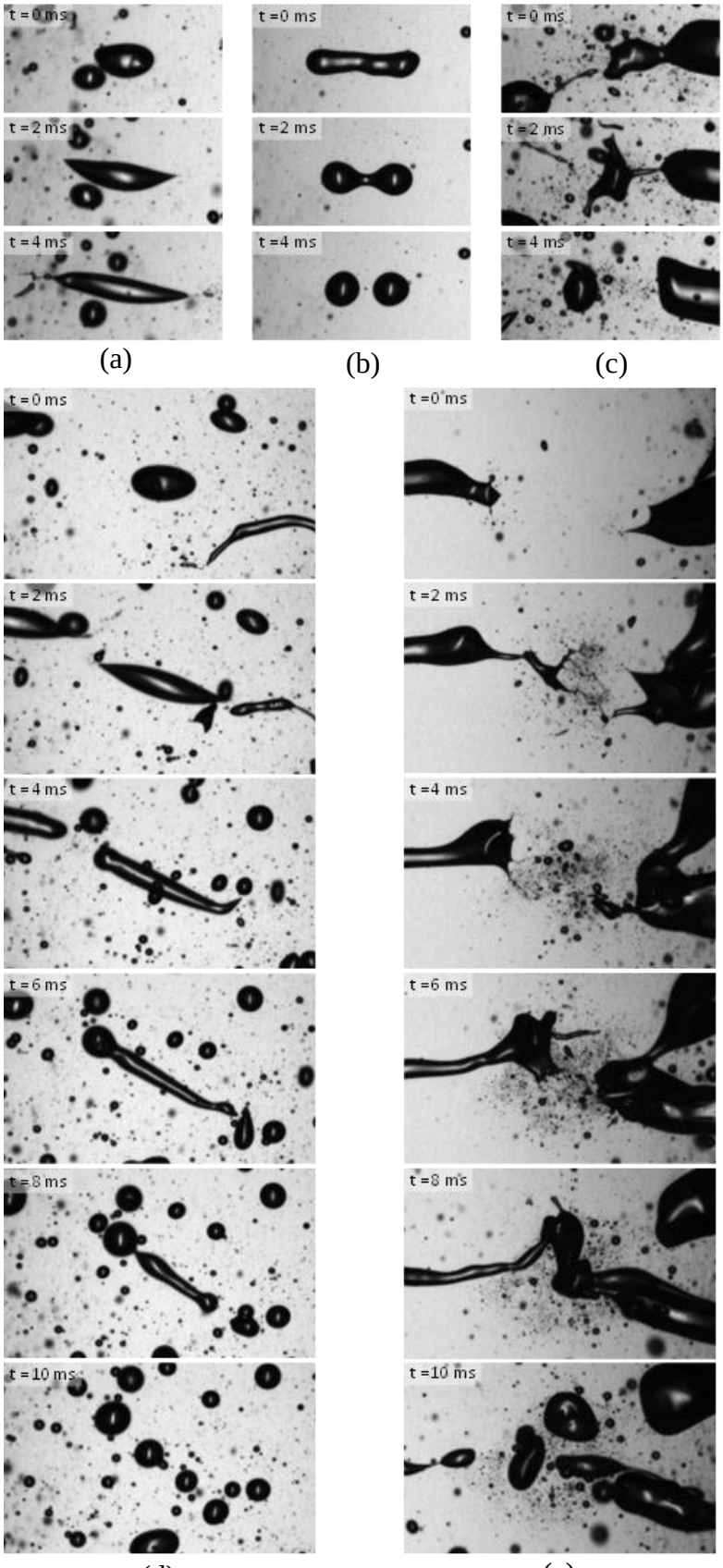

Figure 4.5. Examples of (a) jetting, (b) necking, (c) irregular breakup, (d) combination breakup and (e) emulsion-like-formation induced by AC fields. The scale is the same in these images.

Despite the aspherical and irregular shapes of the dispersing primary droplets, as can be seen from Figure 4.3(b), these breakup mechanisms can be identified based on their distinct characteristics. Jetting is characterised by cone formation on one or both ends of an elongating droplet and emission of ultrafine droplets from these conical ends. Necking is characterised by thinning in the middle portion of the droplet that leads to either detachment of round spheroidal lobes from one or both ends, leaving the middle part of the droplet intact or total separation of the droplet into two or more smaller droplets. Irregular breakup is characterised by the formation of multiple protrusions on the droplet surface in various directions. Combination breakup involves the occurrence of two or more breakup mechanisms on the same droplet, such as jetting and necking or irregular breakup and necking. Emulsion-like formation is characterised by the violent burst of relatively small droplets as if they exploded when situated between two larger droplets, forming a cloud of ultrafine droplets similar to an emulsion. The majority of these ultrafine droplets were observed to eventually coalesce to form larger droplets, but a considerable number of these droplets spread around the column before having the chance to coalesce.

Despite being smaller than the apparent critical droplet size, secondary droplets were observed to undergo breakup. This clearly deviates from the classical theory of droplet breakup in electrostatic fields. The discussion on the onset of breakup for secondary droplets is deferred to the following section to maintain the focus of the current discussion on the droplet breakup dynamics.

Unlike the dispersion of primary droplets, only necking, jetting and a combination of jetting and necking were observed during the secondary droplet dispersion. The typical dynamics of such a combination breakup mechanism are shown in Figure 4.6. The breakup was often initiated by coalescence of two secondary droplets (D1 and D2), resulting in an unstable droplet, which then underwent redispersion. If any of the daughter droplets was still unstable, the process repeated until all daughter droplets reached stability.

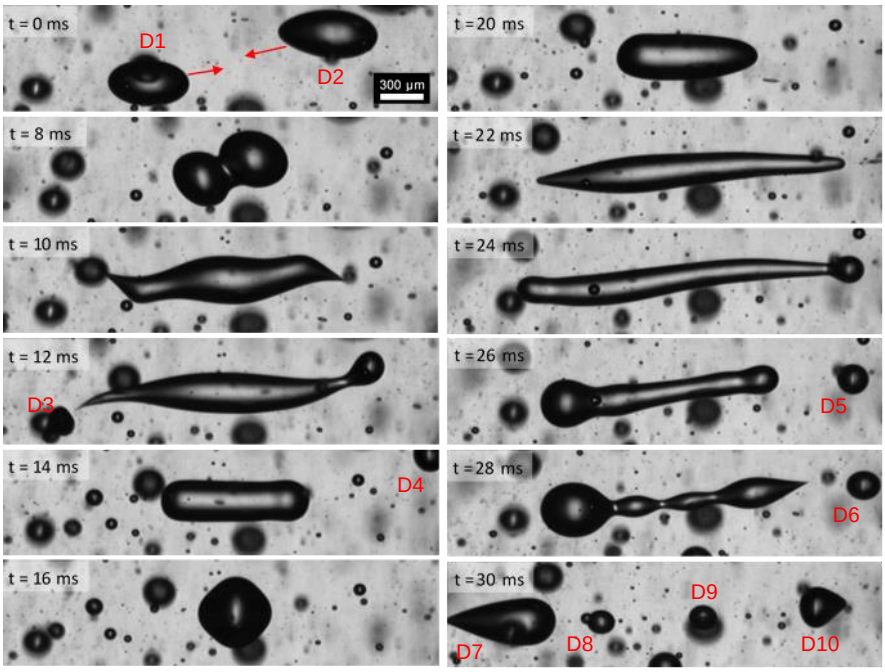

Figure 4.6. Example of dispersion behaviours of a droplet formed through coalescence of two stable secondary droplets (D1 + D2). Each frame is cropped to follow the droplet as it descended through the field. D3–D10 were the produced daughter droplets. Experimental condition: E_0 = 3.5 kV/cm, f = 50 Hz.

The breakup during the redispersion process was consistent with both orientational and interfacial polarisation. The former resulted in the orientation of the permanent dipole moment of each polar species within droplets in the field direction, while the latter led to the accumulation of charge of opposite signs at their opposite ends. These resulted in droplet elongation as these ends acted as poles and were attracted to the electrode with unlike sign.

It has been established that for an elongated aqueous droplet immersed in nonconductive organic liquid with a similar viscosity, pointed ends would form at the poles when the droplet is subjected to static fields (Richardson et al., 1989; Dubash and Mestel, 2007; Karyappa et al., 2014). Comparatively, when the field intensity increased from zero to a peak value, either positive or negative, within the voltage cycle of the AC fields, the formation of pointed ends was observed in the present study. This led to jetting, which manifests as charge emission in the form of fine droplets that carry a higher charge-to-mass ratio than the mother droplet since charge tends to collect at the poles (Taflin et al., 1989; Dubash and Mestel, 2007). The uncharged droplets may still preserve their net neutrality after jetting as an opposite charge may be emitted from the poles (Mora, 2007). When the field intensity decreased from

maximum to zero, the shape of the droplet ends changed from conical to roundish owing to deceleration of the polar species. This action hindered further jetting and often resulted in the formation of lobes at the ends and necks at the middle portions of the droplets leading to necking breakup (Maruyama et al., 2003).

The formation of the lobes and necks was probably a result of inertial effects, which caused some portions of the mass at the droplet ends to remain accelerating while the field strength reached zero. Consequently, they remained at the droplet ends forming lobes, while the rest of the mass was already accelerating towards the opposite direction, resulting in the formation of necks when the field polarity reversed.

Both irregular breakup and emulsion-like formation were only observed during dispersion of the primary droplets. The irregular breakup was analogous to that of a combination breakup wherein thinning occurred, leading to formation of the lobe, but the lobe was so unstable that it formed multiple protrusions with conical ends that often ejected ultrafine droplets. The instability of the lobe possibly occurred because it carried charge above the Rayleigh limit.

Researchers have experimentally shown that a single charged droplet would lose a significant amount of charge (10–40%) but only a small fraction of mass (< 5%) during jetting (Schweizer and Hanson, 1971; Taflin et al., 1989; Duft et al., 2003; Singh et al., 2019). There has been no similar study that measures the charge loss from necking due to the limitation of the experimental technique required to accurately measure the difference in charge and mass before after breakup. It involves evaporation requiring the droplet to be immersed in gaseous media, in which necking is not favourable. If, however, the same phenomenon is applied to predict the charge of a daughter droplet that detached from a mother droplet as a large lump of mass rather than a stream of fine masses, which is reasonable because charge tends to accumulate at the poles, then the daughter droplet can be unstable. Elghazaly and Castle (1987) made such a prediction numerically and showed that if the mass ratio between the daughter and the original droplet is greater than 11.1%, then the daughter droplet must have a charge exceeding the Rayleigh limit and exhibiting instabilities. It appears that the occurrence of irregular breakup in the present study aligns with their theoretical prediction.

The emulsion-like formation observed in the present study appeared to be similar to that reported by Assmann (2014). The presence of two large droplets appears to be

important to induce emulsion-like formation in the present study because in the absence of large droplets, such as those during the regime of secondary droplet dispersion, this breakup mechanism was not observed. Unlike in DC and PDC fields, where the large droplets can be directly charged by contacting a bare electrode, the droplets in the present study cannot obtain such a significant charge from the electrode to induce such a vigorous breakup. Thus, the onset of the emulsion-like formation in the present study can probably be attributed to the formation of highly unstable lobes from one of the large droplets that carried charge excessively above the Rayleigh limit as apparent from the protrusions on the lobes before even detaching from the mother droplet. The presence of a large droplet at each opposite side of the unstable lobe probably provided local field intensification, enhancing the lobe instability and resulting in its sudden violent burst.

4.3.3 Onset of Breakup for Secondary Droplets in Alternating Current Fields

Recall that the breakup of uncharged droplets is a result of an imbalance between the destabilising electrical stress due to the imposition of an electrostatic field and the stabilising capillary stress due to the surface tension (Allan and Mason, 1962a; Torza et al., 1971; Karyappa et al., 2014). The droplets in the present study carried no net charge as the electrodes were insulated and the feed droplets were transported from the solution reservoir using a rubber tube and plastic tip that were protected by a glass housing. Therefore, these uncharged droplets should theoretically break only when their size exceeds the critical droplet size at a given field condition. This has been experimentally evident from several single droplet dispersion studies in both DC (Allan and Mason, 1962a; Ha and Yang, 2000; Karyappa et al., 2014) and AC fields (Torza et al., 1971; Guo et al., 2015; Yan et al., 2015). This was also apparent in the present study from the decreasing maximum droplet diameter with increasing field strength, as shown in Figure 4.4. Visual analysis of the recorded dispersions, however, revealed that most of the droplets underwent breakup despite being significantly smaller than the maximum droplet size, which clearly indicates that they were much smaller than the critical droplet size.

Figure 4.7 shows an example of how two stable secondary droplets (D11 and D12) coalesced, and the resultant droplet (D14) became unstable as soon as it formed and

underwent breakup despite being smaller than the critical droplet size, as apparent from the presence of a significantly larger droplet that did not undergo breakup (D13). One possible explanation for the phenomenon is that the droplet formed after coalescence carried a total charge exceeding the Rayleigh limit.

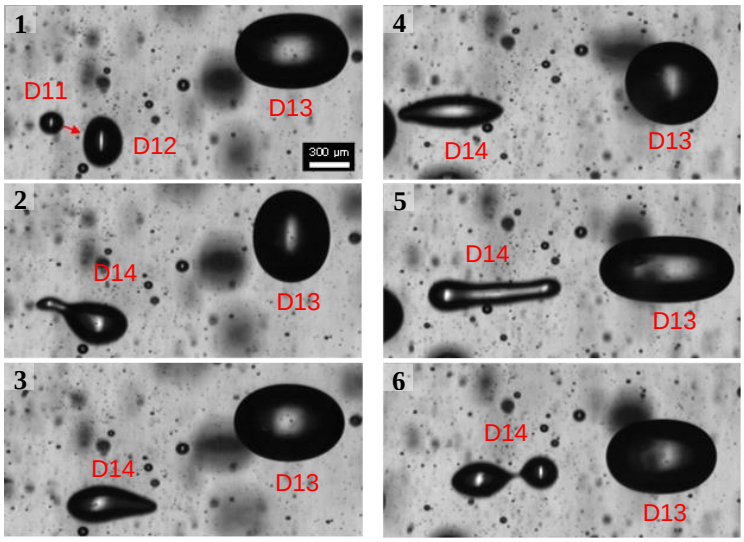

Figure 4.7. Example of a droplet (D14) breakup while its size was smaller than the critical droplet size, as apparent from the presence of a larger stable oscillating droplet (D13). The unstable droplet was formed through the coalescence of two stable oscillating droplets (D11 and D12). The maximum droplet diameter measured in this experiment (E_0 = 3.5 kV/cm; f = 70 Hz) was 1028 µm.

The instability of a droplet resulting from the coalescence of two stable droplets that each carried a total charge below the Rayleigh limit can be explained by the relationship between charge and droplet radius in the classical Rayleigh stability criterion. Saranin (1999) provided a mathematical description of the phenomenon. Assuming that two droplets satisfy the Rayleigh stability criterion

$$Q_i \equiv \frac{q_i^2}{64\pi\varepsilon_0\gamma a_i^3} < 1\,, \quad i = 1,2 \tag{4-1}$$

where Q is the Rayleigh parameter, q is the droplet charge, ε_0 is the permittivity of free space, γ is the interfacial tension and a is the droplet radius, the Rayleigh parameter for the droplet formed can then be formulated as

$$Q = \frac{(q_1+q_2)^2}{64\pi\varepsilon_0\gamma(a_1^3+a_2^3)} = Q_1\frac{(1-q_2/q_1)^2}{1-(a_2/a_1)^3}\,. \tag{4-2}$$

Accordingly, the stability condition for the initial drops and the instability condition of the resulting droplet set the following system of inequalities

$$Q_1 \frac{(1 - q_2/q_1)^2}{1 - (a_2/a_1)^3} \geq 1\,, \qquad \frac{Q_1 (q_2/q_1)^2}{(a_2/a_1)^3} < 1\,, \qquad Q_1 < 1\,. \tag{4-3}$$

If the two droplets have identical droplet potential $(q_2/q_1) = (a_2/a_1)$, then

$$\frac{Q_1^2\,(1 + a_2/a_1)}{1 - a_2/a_1 - (a_2/a_1)^2} \geq 1, \qquad Q_1^2 > \frac{a_2}{a_1}, \qquad Q_1^2 < 1\,. \tag{4-4}$$

Hence, by plotting Q_1^2 as a function of a_2/a_1, Saranin (1999) not only demonstrated that two stable charged droplets can coalesce and form a droplet with Rayleigh instability, but also predicted the parameter region wherein the resulting droplet is unstable. Indeed, when the charge of the droplets formed was well below the Rayleigh limit, these droplets remained stable after coalescence. Many such instances were observed in the present study.

Clearly, for the resulting droplet to exhibit instability while being smaller than the critical droplet size, the coalescing droplets must carry a significant charge near the Rayleigh limit. Because direct charging was not possible, given that both the electrodes were insulated, one possible explanation for the existence of droplets with a high charge-mass ratio to a point near its stability limit is the breakup of their mother droplets generated daughter droplets with imbalance charge proportion. For example, lobes detached from the opposite ends of their mother droplet may carry a higher charge-to-mass ratio than the mother droplet and the other daughter droplets formed at the middle portion because charge tends to accumulate at the poles owing to interfacial polarisation. This was apparent in the present study from the occurrence of irregular breakup and emulsion-like formation.

The daughter droplets formed from these lobes may carry a higher proportion of one charge than the other resulting in the existence of a net charge, either positive or negative, on the droplet surface. The possibility for an uncharged droplet to produce daughter droplets with a net charge in electrostatic fields has been analytically verified by Shchukin and Grigor'ev (2000) using the principle of minimum potential energy. It should be pointed out that although they are not given charge through external means (uncharged by definition), conducting droplets naturally carry some intrinsic charge.

Figure 4.8 shows a schematic illustration of how an uncharged droplet can generate daughter droplets with a net charge.

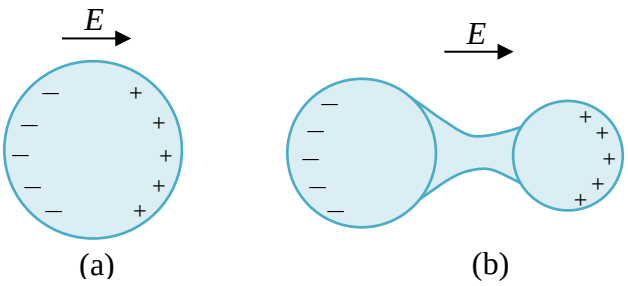

Figure 4.8. Schematic illustration of the breakup of (a) an uncharged droplet into (b) two daughter droplets with a net charge and unlike sign.

In the present study, the existence of net charge was evident from the occurrence of strong repulsion between neighbouring droplets when situated in close proximity, as shown in Figure 4.9. This repulsion can only be attributed to Coloumbic force between droplets that carried a net charge of the same sign. Also shown in these photographs, the interaction between droplets can lead to breakup even without direct contact between them. This has not been reported before in the literature. Moreover, since there was no significant charge transfer among them, these photographs show that neighbouring droplets can locally amplify the field strength. This reinforces the argument for the onset of emulsion-like formation, wherein the presence of large droplets can amplify droplet instability to induce explosive breakup of the droplet.

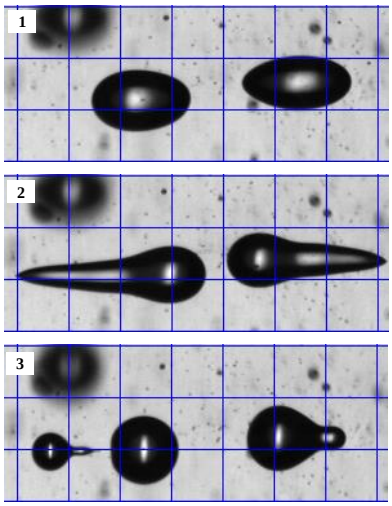

Figure 4.9. Example of a Coloumbic repulsion between neighbouring droplets that led to breakup via the combination breakup mechanism. Grid = 300 µm.

4.3.4 Effect of AC Fields on the Droplet Breakup Mechanism

Visual observations of the dispersion of both the primary and secondary droplets revealed that the combination breakup involving jetting and necking was the dominant mode of breakup mechanism in all tested ranges. This was different to that reported by Assmann (2014), who observed that in AC fields at strengths ranging from 2.5 to 3.5 kV/cm, this breakup mechanism was only prevalent at frequencies below 50 Hz at the highest tested field strength. Given the nature of the breakup mechanism, the occurrence of necking during dispersion was closely associated with jetting, i.e., while the frequency of necking increased with increasing field strength and decreasing frequency, the frequency of jetting also increased. Individual jetting and necking breakup were observed, but there was no discernible gap in the increases or decreases in either breakup mechanism with variation in the field conditions. Hence, different to that observed in the lower field strengths, it was found that it was difficult to make one mechanism to be more dominant than another using AC fields under the tested ranges.

Notable changes in the dynamics of the combination breakup were observed when the field frequency was varied. Decreases in the frequency lead to a longer duration for the droplets to exhibit pointed ends. This was due to the longer duration for the droplets to experience electrical stress around the maximum value as the polarity changed more slowly at the lower frequencies, which led to higher proclivity for necking to occur. This, however, apparently also led to more ultrafine droplets being ejected during the jetting breakup.

As mentioned earlier, the irregular and emulsion-like formation occurred only during dispersion of the primary droplets. Visual analysis of the dispersions revealed that the frequency of these two mechanisms increased with increasing field strength. This can be attributed to the higher electrical stress imposed on droplets at the higher field strengths, leading to higher proclivity for these droplets to become unstable and violently break. There was no discernible difference in the proclivity of these two mechanisms with variation in the field frequency.

The results of the present study thus show that the conditions that favour the formation of momentary emulsion via the emulsion-like formation mechanism were identified during primary droplet dispersion but it did not seem possible to sustain the occurrence of this breakup mechanism during the secondary droplet dispersion. Coalescence of

the ultrafine droplets after they formed was also found to be incomplete, with a marked proportion of these droplets spread around the column, contributing to the increase in the population of ultrafine droplets in the dispersion. Moreover, given that the dispersion of primary droplets lasted < 0.3 s, it is reasonable to deem that the occurrence of emulsion-like formation was relatively insignificant to mass transfer compared with the dispersion of secondary droplets. Hence, further investigation into the emulsion-like formation was not pursued.

4.3.5 Effect of Alternating Current Fields on Droplet Motion

Droplets were observed to exhibit zigzag motion when subjected to AC fields with strengths ranging from 3.50 to 4.25 kV/cm and frequencies ranging from 30 to 70 Hz. Specifically, droplets were observed to translate horizontally between the electrodes, and the direction periodically reversed at a rate that was in apparent synchrony with the frequency of the field as, for example, shown in Figure 4.10. This figure also shows that droplets of comparable size (D23 and D24) can exhibit not only a significant difference in the distance but also the direction in which they translated. These were a clear indication that droplet zigzagging resulted from the interaction between the electrodes and a droplet that carried a net charge (Steffens, 2011; Assmann, 2014). Note that when a droplet carries a net charge, assuming that the electrostatic field is relatively uniform, the electrostatic force in one direction will be higher than in the opposite direction, leading to the net displacement in one direction rather than axisymmetric elongation at a stationary position. These observations also reinforce the earlier observation that the amount of charge that each droplet carried may vary and are consistent with observations of previous investigators who studied droplet motion under the influence of AC fields at lower field strengths when treating larger droplets (Steffens, 2011; Assmann, 2014).

Some droplets were observed to exhibit horizontal motions owing to repulsion between droplets, as previously mentioned (see Figure 4.9). When two droplets are situated in close proximity, they may exhibit sudden enhanced acceleration to move away from each other, notwithstanding their original trajectory or the field direction.

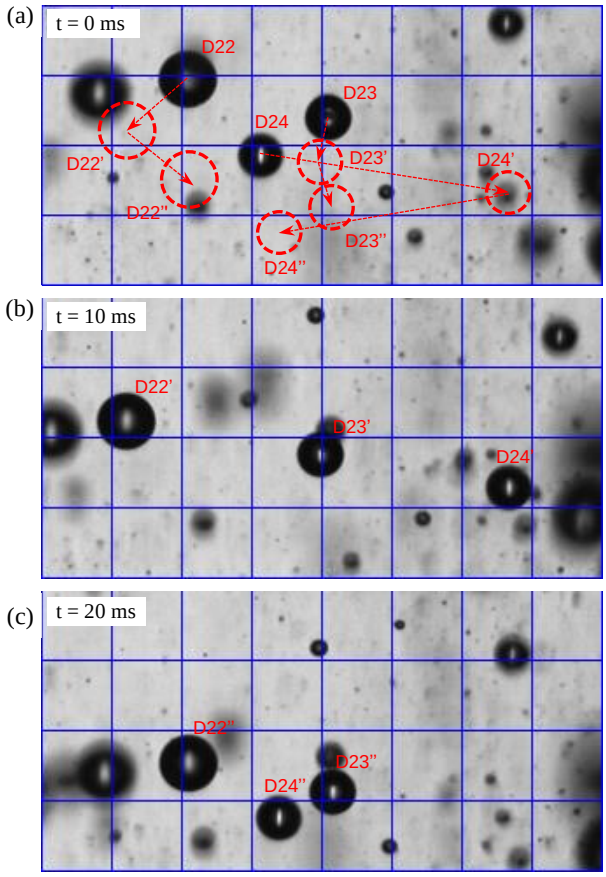

Figure 4.10. Examples of (a) droplet zigzag motions in AC fields. The red circles indicate the droplet positions after the next 10 and 20 ms as shown in (b) and (c), respectively. Experimental condition: E_0= 3.5 kV/cm, f= 50 Hz. Grid = 300 µm.

The occurrence of droplet breakup can also lead to horizontal motions as, for example, shown in Figure 4.11, which was the continuation of the combination breakup shown in Figure 4.6. These motions can be attributed to the attractive electrostatic force between electrodes and lobes that carried a net charge with the opposite sign. After detachment, the daughter droplets formed from these lobes (D7 and D10) zigzagged between the electrodes in directions opposing each other, showing that each carried a net charge with the opposite sign. The other daughter droplets formed at the middle (D8 and D9), however, exhibited minimal horizontal motion. These observations reinforce the argument that charge within droplets tended to accumulate at the poles and the lobes carried a majority of charge from the original droplet.

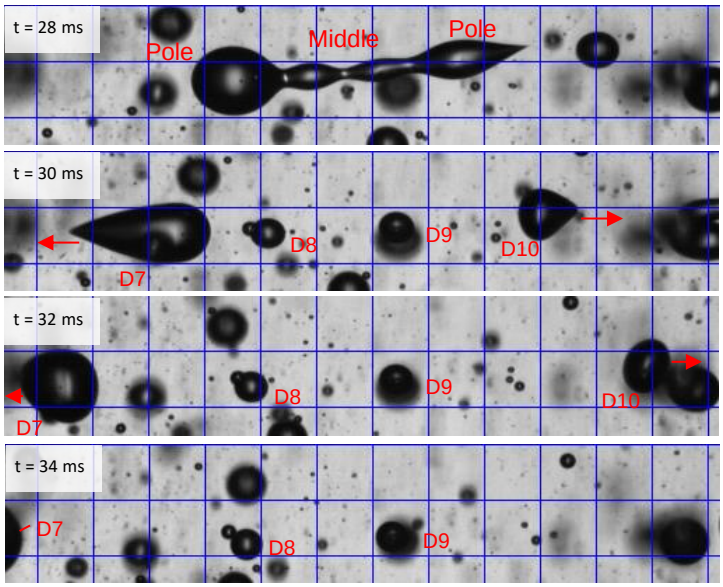

Figure 4.11. Examples of two daughter droplets formed at the poles (D7 and D10) that exhibited acceleration towards opposite directions, while the daughter droplets formed at the middle (D8 and D9) exhibited minimal zigzag motions and oscillations. Experimental condition: E_0 = 3.5 kV/cm, f = 50 Hz. Grid = 300 µm.

The degree of turbulence within the dispersion increased with the amplitude of droplet zigzagging, the proportion of droplets that exhibited zigzagging, the frequency of droplet repulsion and the frequency of droplet breakup, which was often a result of droplet coalescence. Given the unavailability of an analytical instrument to differentiate between different types of droplet motion within the present study, the degree of turbulence was estimated by the average linear velocity of the droplet in any direction. Following the convention assumed by Assmann (2014) for consistency, this velocity is henceforth referred to as droplet speed.

It is reasonable to assume that increases in the droplet horizontal motion increase the frequency of interactions between droplets because they increase the probability for droplets to collide. The occurrence of these interactions promotes more interactions to occur as droplet interactions also enhance the horizontal motion. The amplitude of droplet horizontal motion can be calculated from the measured droplet speed and the angle of the droplet motion relative to the horizontal axis that is perpendicular to the gravity direction. Again, following the convention of Assmann (2014), the horizontal component of the speed is henceforth referred to as horizontal velocity for brevity.

Figure 4.12 (a–c) shows the effect of the field strength of the applied AC fields ranging from 3.50–4.25 kV/cm at a constant frequency of 50 Hz on the droplet motion for four

droplet size fractions from < 50 to 300 µm. Note that the smallest droplet diameter that could be characterised was 23 µm, and there were too few droplets with sizes beyond 300 µm that were sampled to draw a representative profile. Figure 4.12(a) shows that the average droplet speed increased when the field strength increased from 3.50 to 4.25 kV/cm. Similarly, Figure 4.12(b) shows that the average horizontal velocity increased when the field strength increased from 3.50 to 4.25 kV/cm, and the slope of the trend was almost the same as that of the droplet speed (0.27 for speed compared with 0.31 for horizontal velocity). These almost parallel trends indicate that the increase in droplet speed was mainly due to the increase in the droplet horizontal velocity.

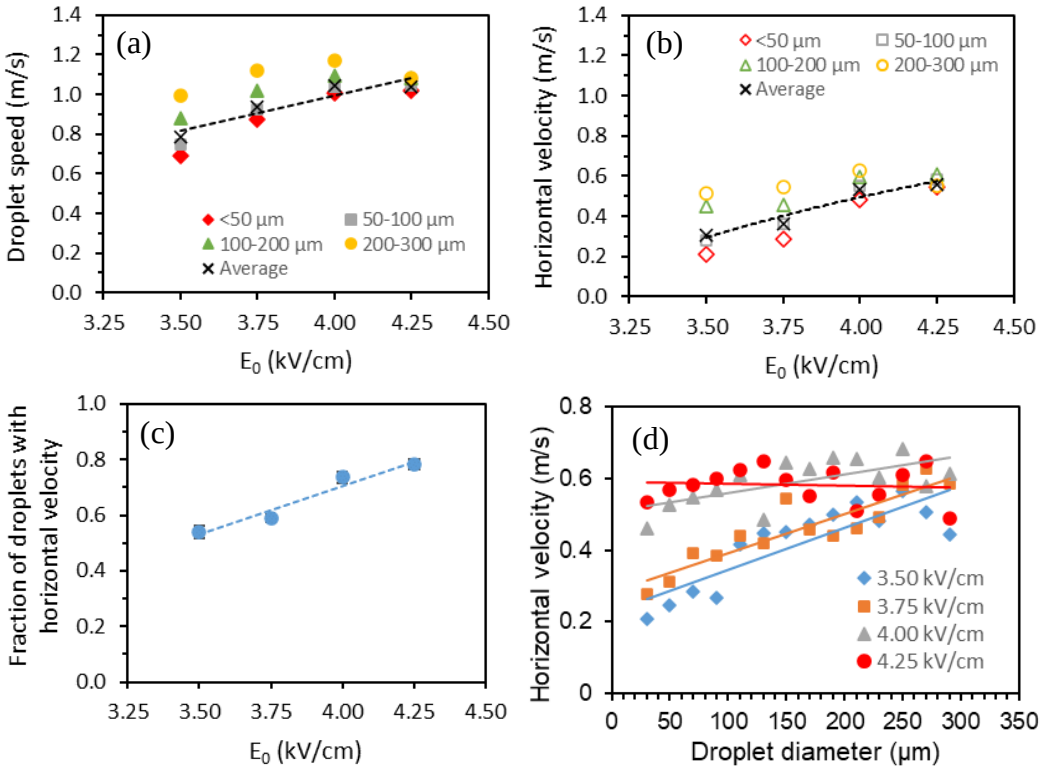

Figure 4.12. Effect field strength of AC fields at a frequency of 50 Hz on the (a) average droplet speed, (b) horizontal velocity, and (c) fraction of droplets exhibiting horizontal velocity. (d) Plots of horizontal velocity as a function of droplet diameter at various field strengths.

The observed increases in the droplet speed and horizontal velocity with field strength are consistent with those reported by Assmann (2014) at lower field strengths when observing the agitation of larger droplets. These results suggest that the application of AC fields to effect agitation on droplets remained effective at the higher field strengths when the droplets were smaller than those previously studied.

Assmann (2014) argued that increases in droplet horizontal velocity with increasing field strength is a result of increases in the amount of incidental charges, leading to greater interfacial polarisation. Differently, the present author proposes that the increasing droplet horizontal velocity is owing to the increased number of droplets with net charge through more frequent droplet breakup with increasing field strength coupled with the higher electrostatic force imposed on these droplets. The increased number of droplets with net charge was evident from the increased proportion of droplets exhibiting horizontal velocity with field strength, as shown in Figure 4.12(c).

Figure 4.12(d) shows that horizontal velocity of the droplets smaller than 100 μm in diameter increased with increasing droplet size like those of the larger droplets, except at 4.25 kV/cm wherein the velocities of droplets larger than 100 μm tended to decrease with size. As can also be seen from Figure 4.12(b), the gap in the droplet horizontal velocity between droplets with a diameter less than 100 μm and the larger droplets markedly decreased with increasing field strength to a point where the difference became insignificant at 4.25 kV/cm. This was not observed by Assmann (2014) at lower field strengths. The decreasing gap appeared to be largely owing to the more significant increase in the smaller droplet horizontal velocity with field strength compared with those of the larger droplets. This can be attributed to the higher probability for the smaller droplets having a high charge-to-mass ratio to exhibit significant zigzagging and the lower drag force hindering them from moving through the continuous phase.

The effect of the frequency of AC fields on droplet motion was investigated at two different field strengths, 3.50 and 4.00 kV/cm. The upper field strength was selected to be 4.00 rather than 4.25 kV/cm because the experiments at frequencies below 50 Hz at 4.25 kV/cm led to the SPE formation. The results, depicted in Figure 4.13, show that both the droplet speed and horizontal velocity increased with decreasing frequency. This was logical, given that the droplets were allowed to accelerate for a longer period at the lower frequencies. The apparent parallel between the trends of droplet speed and droplet horizontal velocity indicate that increases in the droplet speed mainly resulted from the increases in the horizontal velocity. These observations are consistent with the findings of the previous investigators in less-vigorous electrostatic fields (Steffens, 2011; Assmann, 2014).

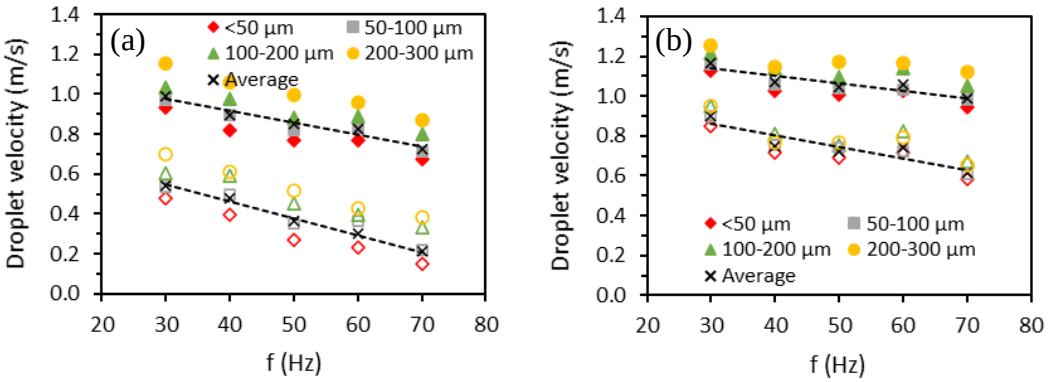

Figure 4.13. Effect of frequency of AC fields on the average droplet speed (closed markers) and horizontal velocity (open markers) at (a) 3.5 kV/cm and (b) 4.0 kV/cm.

Figure 4.14 shows that horizontal velocity of the droplets smaller than 100 µm in diameter increased with increasing droplet size like those of the larger droplets, but the slope decreased with increasing field strength. This was consistent with the earlier observation when investigating the effect of field strength on droplet horizontal velocity (Figure 4.12). The results of the present study suggest that the application of a higher field strength than those previously studied is particularly more effective in inducing agitation on smaller droplets than those at the lower field strengths.

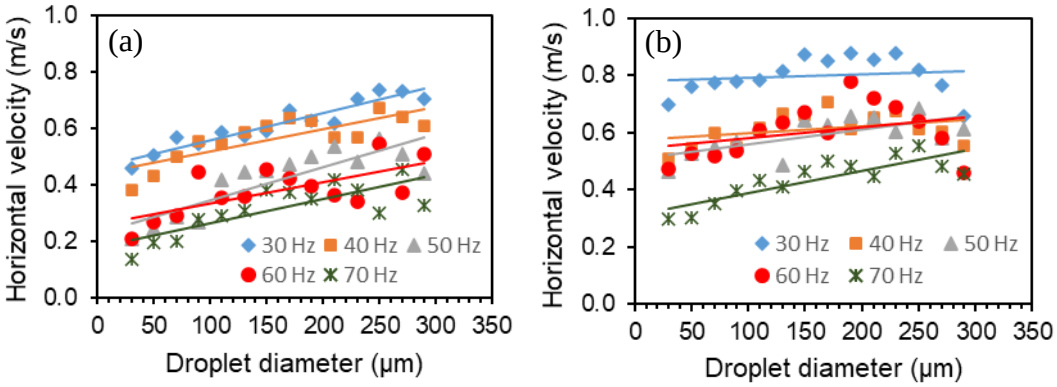

Figure 4.14. Plots of droplet horizontal velocity as a function of droplet diameter at various field frequencies at (a) 3.5 kV/cm and (b) 4.0 kV/cm fields.

4.3.6 Effect of Alternating Current Fields on Droplet Oscillation

Most droplets were observed to oscillate when subjected to AC fields at strengths ranging from 3.50 to 4.25 kV/cm at frequencies ranging from 20 to 70 Hz. To correlate the effect of droplet oscillation on mass transfer, the behaviours of droplets that were larger than 100 µm also needs to be discussed. Typically, droplets oscillated axisymmetrically about a spherical shape with rounded ends formed at peak elongation

(Figure 4.15(a)). Even under the same experimental conditions, however, some droplets exhibited higher amplitudes of oscillation than most droplets of comparable size (Figure 4.15(b)), and some elongated so extensively that they formed conical ends at peak elongation (Figure 4.15(c)). Moreover, some of the droplets with the higher oscillation amplitudes formed an oblate spheroid during oscillation, which behaviour clearly deviates from the general view in the literature on droplet deformation in electrostatic fields.

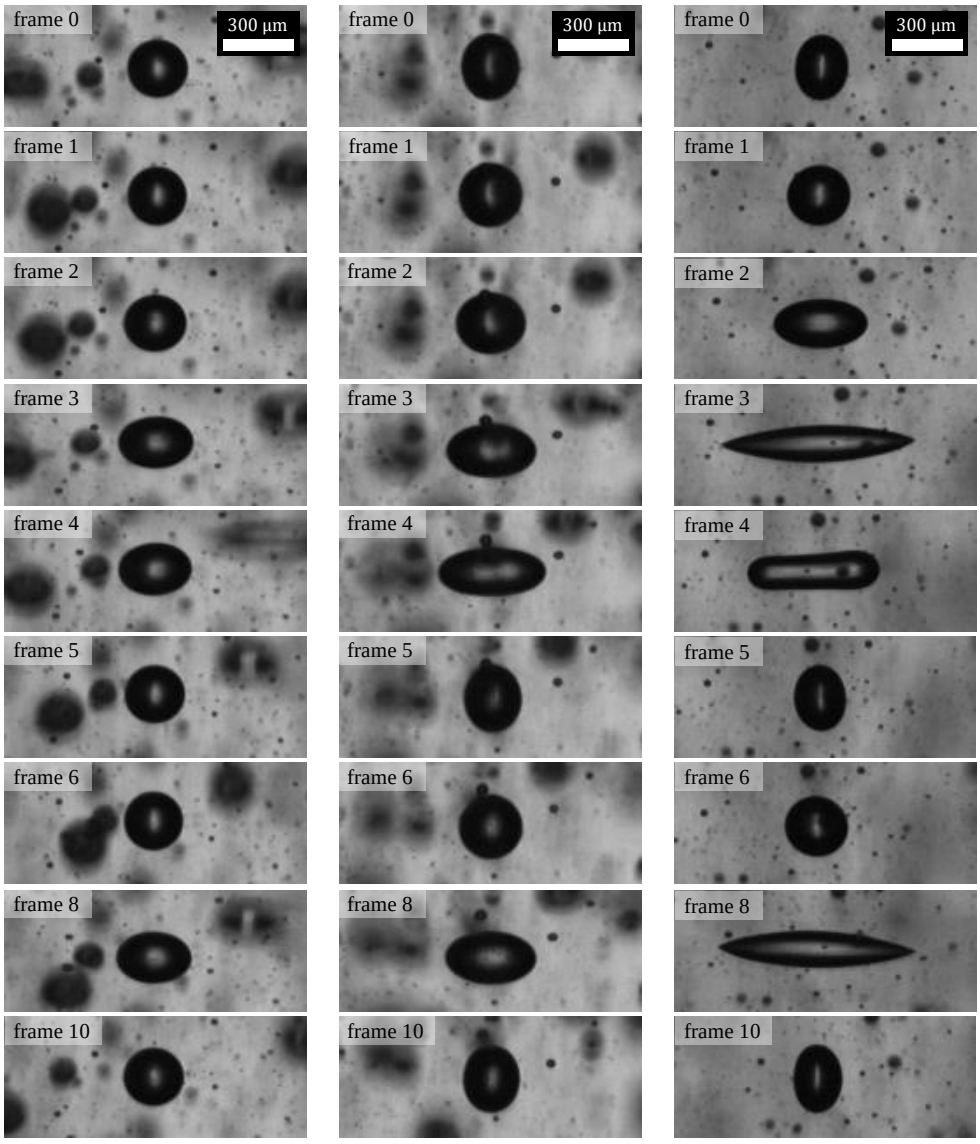

Figure 4.15. Examples of (a) a typical droplet oscillation and (b) oscillation that exhibited a higher amplitude than the droplets of comparable size during one full voltage cycle up to a point where (c) conical ends formed. These photographs were taken during the same experiment in 4.0 kV/cm AC fields at 50 Hz.

The droplet oscillation frequency was found to be invariably proportionate to the frequency of the field, notwithstanding the applied field strength and droplet size and oscillation amplitude. Droplets, for example, were observed to consistently complete two cycles of oscillation in 10 consecutive frames, which is equivalent to the required time to complete one cycle of an AC field at 50 Hz when recording at 500 fps. Note that the voltage in AC fields forms a sinusoidal cycle from zero to a positive maxima and then to a negative maxima by fleetingly passing the zero point. Thus, consistent with the general view in the literature, these observations suggest that all droplet oscillation in the applied AC fields was mainly influenced by the periodic cycling of the field strength.

Because droplets of comparable size have approximately the same amount of polar species, the difference in the oscillation amplitude at a given field condition can be attributed to the variation in the amount of charge that each droplet held. Specifically, the larger the amount of charge, the higher its oscillation amplitude. The increased elongation can be explained by the increase in the droplet charge-to-mass ratio that resulted in higher electrical stress due to the applied electric field, which value is proportional to the electric charge per area of the drop and electric field strength (Löwe et al., 2020).

There appeared to be an onset value of charge for a droplet at a given size to start exhibiting cone formation, analogous to that for the droplet to undergo breakup. This was based on the observation that the droplet remained oscillating while exhibiting instability (but no progeny droplets were ejected) unless disturbed by neighbouring droplets, differentiating the behaviour from jetting breakup. Hence, for brevity, the oscillation of droplets at noticeably higher amplitudes than most droplets of similar size is henceforth referred to as unstable oscillation. Correspondingly, droplets were deemed to have stable oscillation when the amplitude of their oscillation was similar to the majority of droplets of similar size.

Similar to the mechanism of secondary droplet breakup, most unstable oscillation appeared to be a result of droplet coalescence but between a relatively large droplet and ultrafine droplets. Ultrafine droplets can only form through jetting, irregular breakup or emulsion-like formation, and they result in these droplets carrying a high charge-to-mass ratio. Thus, it was logical that, in the present study, the proportion of

droplets exhibiting unstable oscillation increased with increasing field strength as more ultrafine droplets were generated in these conditions. The amplitude of unstable oscillation, however, varied greatly even under the same experimental condition. Consequently, examination of the effect of the field condition on the amplitude of unstable oscillation was practically impossible.

On the contrary, the variation in the amplitude of stable oscillation with changes in the applied field condition was found to be patterned. Given that the majority of droplets exhibited stable oscillation, its amplitude was used to determine the effect of field strength and frequency on droplet oscillation. Attempts to quantify the stable oscillation were carried out by carefully selecting frames from experiments at various field conditions that show several stable oscillating droplets with comparable sizes. Notably, the results should not be treated as definitive, given the lack of proper tools to gather a sufficient pool of data, but simply as markers to support the visual observations on droplet oscillation. The amplitude of droplet oscillation was defined as the ratio of droplet radius at maximum elongation (a_M) and spherical state (a_0). The radius was manually measured using the PFV software, which is equipped with measuring tools based on the length of pixels between two points. The droplets were deemed to be spherical when the lengths of the major and minor axes were equal.

The results, presented in Figure 4.16, show that the droplet oscillation amplitude increased with increases in field strength (3.50–4.00 kV/cm) and decreases in frequency (30–70 Hz). The results also show that the amplitude decreased with decreasing droplet size, which aligns with the theory formulated by the electrical capillary number (Equation (2-5)). The increasing amplitude of oscillation with increasing field strength clearly shows that the elongation was a direct consequence of the induced electrical stress on the droplet. The increasing oscillation amplitude with decreasing field frequency, however, shows the significant influence of hydrodynamic factors that opposed the induced electrical stress (Assmann, 2014).

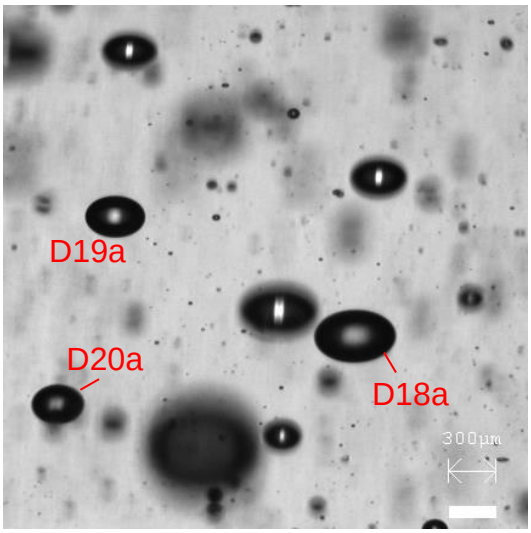

(a)

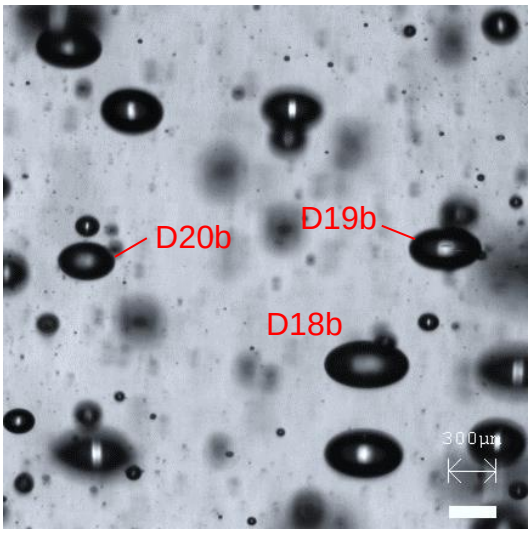

(b)

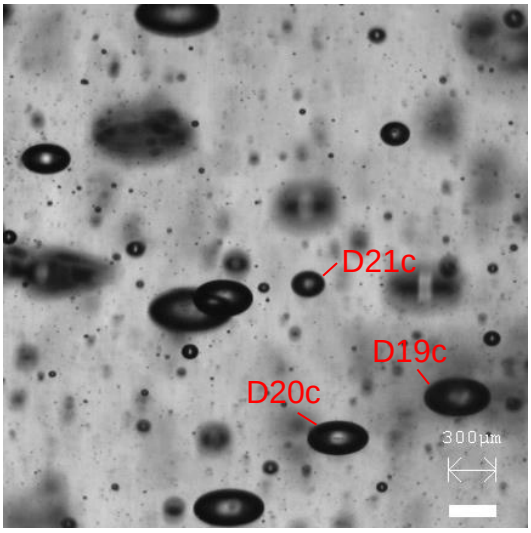

(c)

Droplet	a_0 (μm)	a_M (μm)	a_M/a_0
D18a	185	253	1.37
D19a	147	185	1.26
D20a	136	162	1.19
D18b	177	260	1.47
D19b	155	223	1.44
D20b	136	174	1.28
D19c	147	208	1.41
D20c	136	189	1.39
D21c	91	106	1.17

(d)

Figure 4.16. Typical droplet dispersions showing the maximum elongation of droplets during stable oscillation at various AC field conditions: (a) E_0= 3.5 kV/cm, f= 70 Hz; (b) E_0= 3.5 kV/cm, f= 30 Hz; (c) E_0= 4.0 kV/cm, f= 70 Hz. The table (d) shows the droplet radius at the spherical state (a_0) and at maximum elongation (a_M) as well as the amplitude of the droplet elongation (a_M/a_0).

The presence of hydrodynamic hindrances in the forms of capillary and viscous stresses can cause a hysteresis effect, wherein droplets need some time to reach their maximum elongation after an electrical stress being imposed exceeded the opposing stresses (Gong et al., 2015). This is apparent from Figure 4.15(a), which shows that the droplet remained undeformed for at least 2 ms after it reached a spherical shape. Hence, the smaller oscillation amplitude at the higher frequencies can be attributed to the shorter duration wherein the droplet experiences elongation.

The oblate deformation during oscillation cannot be explained using the classical theory of droplet deformation in electrostatic fields, which predicts that a conducting droplet in a nonconducting liquid will exhibit prolate deformation when the electric stress is higher than the capillary stress (Allan and Mason, 1962a; Taylor, 1966; Melcher and Taylor, 1969; Torza et al., 1971). It can probably be explained by the existence of a significant inertial force when the droplets retract back to their undeformed state. Correspondingly, the degree of oblate deformation increased with increases in the oscillation amplitude, and the propensity for oblate deformation to form decreased with decreases in the droplet size. These results are consistent with visual observation of the dispersions. The oblate deformation is essentially a lateral oscillation and, theoretically, it should increase the degree of turbulence within the droplet as the frequency of oscillation was practically doubled.

4.3.7 Oscillation of the Smallest Observable Droplets

The oscillation of droplets smaller than 100 μm in diameter, particularly those smaller than 50 μm, was difficult to observe using the camera lens magnification of 4.0. Therefore, the highest camera lens magnification, which was 7.0, was used in this analysis. Observation of the oscillation of these small droplets was made from a dispersion experiment performed in duplicate at a field strength of 4.0 kV/cm and a frequency of 30 Hz, which was found to induce the greatest amplitude of stable oscillation within the tested ranges.

It was observed that droplets smaller than 100 μm in diameter also exhibited stable and unstable oscillation and, generally, the smaller droplets exhibited smaller oscillation amplitude. The smallest droplet diameter that the imaging equipment could measure using the highest lens magnification was found to be 23 μm. Droplet D22 in Figure 4.17 was one of those smallest droplets. With a careful visual examination, it can be seen that it oscillated about a spherical shape. To the best of the present author's knowledge, this is the first observation on the oscillation of droplets as small as 23 μm under the influence of electrostatic fields. The slightly larger droplets (D23 and D24) shown in the photographs showed more apparent oscillation. Although not as clearly observable, the smaller droplet (D25) also showed oscillation. This was observed by magnifying these photographs multiple times and comparing the droplet pixel lengths in these two photographs using the PFV software. This observation suggests that the

application of AC fields within the tested ranges can induce oscillation to droplets with a diameter even smaller than 23 µm. It is notable that these small droplets were also observed to exhibit significant motion.

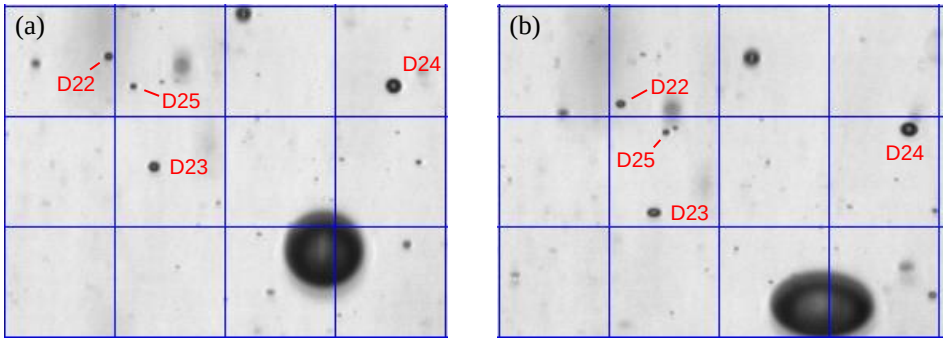

Figure 4.17. Photographs of small droplets at (a) their undeformed and (b) elongated state during their oscillation cycle in 4.0 kV/cm AC field at a frequency of 30 Hz. The diameter of the droplets: D22 = 23 µm; D23 = 26 µm; D24 = 43 µm; D25 = <23 µm. Grid = 300 µm.

4.4 CHAPTER SUMMARY

In this chapter, the effect of AC fields on droplet breakup, motion and oscillation for a hydrometallurgical SX system was investigated at field strengths higher than those previously studied, wherein the droplets were mainly smaller than 100 µm. It was found that with the application of the stronger fields conditions, a semi-permanent emulsion could form. The proclivity for the emulsion to form increased with increasing field strength and decreasing frequency. It appeared that this was due to the generated droplets being too small to exhibit significant mass to counteract the drag force to settle. In the present case, the emulsion formed when the strength of the AC field was higher than 4.25 kV/cm at a frequency of 50 Hz, or when the field frequency was below 50 Hz at a field strength of 4.25 kV/cm.

Visual analysis of the dispersions showed that five breakup mechanisms were responsible for the formation of droplets; namely, jetting, necking, irregular and combination breakup mechanism and a mechanism that was previously known to occur only when uninsulated electrodes were used; namely, emulsion-like formation. The emulsion-like formation was initially predicted to allow the formation of a momentary emulsion. It was, however, found that under the vigorous field conditions, which entailed vigorous agitation, the breakup mechanism contributed to the increase

in the population of ultrafine droplets because a significant proportion of the formed ultrafine droplets were quickly pushed away and spread around the column before having the chance to coalesce. In addition, this behaviour was only observed during the initial phase of the dispersion lasting for less 0.3 s, wherein a significant proportion of the droplets were still large. Hence, it was deemed that it could not be controlled within the tested experimental ranges to allow high mass-transfer rates and fast phase disengagement.

The combination breakup mechanism involving jetting and necking was found to be the predominant breakup mechanism in all tested ranges. Consequently, field conditions that increase the frequency of necking also led to increases in the jetting frequency. Unlike that in the lower field strengths, it appeared that the strategy to narrow droplet size distribution at the higher field strengths could not be achieved by controlling the droplet breakup mechanism.

The interaction between droplets that leads to either collision or repulsion can result in a breakup. The collision can lead to coalescence and the resulting droplet may be unstable and undergo breakup. This was responsible for most breakups that occurred in the column. The repulsion can result in abrupt propulsion of mass within the droplet from one side to the opposite leading to the breakup. This has not been reported before in the literature.

Some droplets were observed to exhibit zigzagging or oscillation or both owing to the periodic cycling of the applied AC fields. The amplitude of the zigzagging and oscillation increased with increasing field strength and decreasing frequency. The former increased the electrical stress imposed on the droplets, while the latter increased the period wherein the droplet experienced electrical stress near the maximum value before reverting back to zero. The horizontal velocity of droplets smaller than 100 μm in diameter was generally smaller than the larger droplets, but the gap between them decreased with increasing field strength to the point that it was practically negligible at 4.25 kV/cm. This was different to those observed previously at the lower field strengths. The amplitude of droplet oscillation under a given electrostatic field condition increased with increasing droplet size. This also applied to droplets smaller than 100 μm in diameter. The smallest observable droplets with the current imaging

equipment, which had a diameter of 23 μm, were found to exhibit significant motion and oscillation within the tested ranges.

CHAPTER 5
EFFECT OF ALTERNATING CURRENT FIELDS ON DROPLET SIZE AND SIZE DISTRIBUTION

5.1 INTRODUCTION

This chapter describes the study on the effect of strength and frequency of a more vigorous AC fields than those previously studied on droplet size and size distribution. The study aimed to understand the relationship between the droplet breakup, motion and oscillation behaviours under the influence of the fields on the droplet size characteristics of the dispersion. Information on the droplet size characteristics is important to determine the effect of the behaviours of droplets smaller than 100 μm on mass transfer as it relates to the interfacial contact area of the dispersions. This is also important to provide an insight on how to produce a dispersion of droplets that are mainly smaller than 100 μm in diameter with a narrow droplet size distribution.

The study also aimed to determine the smallest droplet size that could be produced before a semi-permanent emulsion formed and hindered the phase separation process. The outcomes of this study are valuable for optimising and designing an industrially applicable ESX column.

5.2 EXPERIMENTAL METHODOLOGY

5.2.1 Materials and Experimental Procedures

The materials and experimental procedures used in this part of the study are the same as those in Chapter 4, except that the recording was only performed for dispersion of the secondary droplets from halfway down the high-field-strength region using a lens magnification of 4.0. This camera lens magnification was found to be the most suitable for the ranges of droplet size generated within the tested experimental ranges.

5.2.2 Experimental Data Analysis

The droplet size measurement was performed by processing the recorded images of the dispersions using VisiSize software version 6.206. The measurement followed the

general procedures described in Chapter 3.3.2. The droplet size of the dispersion is expressed by the Sauter mean diameter, which is a relevant measure when the surface area is important. The droplet size distribution is expressed in terms of volume density distribution, which was normalised so that the sum of all size classes equals unity through the division of volume per class by the total volume of the sample. A suitable data representation for the droplet size distribution data was determined to be in the form of histograms because each generated data point accounted for the volume of droplets over a range of droplet size in each size class, and the software divided the size classes in a logarithmic scale. The most suitable number of divisions of the size classes was found to be 35.

Attempts to generate population density distributions of the dispersions were performed in the same manner, but the distributions were too thinly spread over the largest size fractions and overlapped each other over the smallest size fractions due to the disproportionate abundance of small droplets compared with the large droplets. Consequently, the trends were not clearly apparent. Examples of how the generated population density distribution and volume density distribution diagrams show the variation in the trends are depicted in Figure 5.1. Note that the error bars represent the standard errors of the means for each data set.

Preliminary experiments revealed that some variations occurred in the droplet size distributions for a given set of experimental conditions. Hence, five experimental runs were recorded for each set of experimental conditions, i.e., each data point in this chapter is a mean of five experimental runs.

To allow a clearer analysis of the droplet size distribution, the volume distributions of the droplets were distributed over six selected size fractions (< 50 μm, 50–100 μm, 100–200 μm, 200–300 μm, 300–400 μm and > 400 μm). Each data point was obtained by plotting the cumulative volume fraction of the droplets as a function of diameter and performing simple regression from two points on the plots that were generated by software (e.g., the cumulative fraction at 100 μm was obtained from the data points at 82.78 and 106.95 μm). For tidiness and clarity of the graphs, error bars are not included in these graphs.

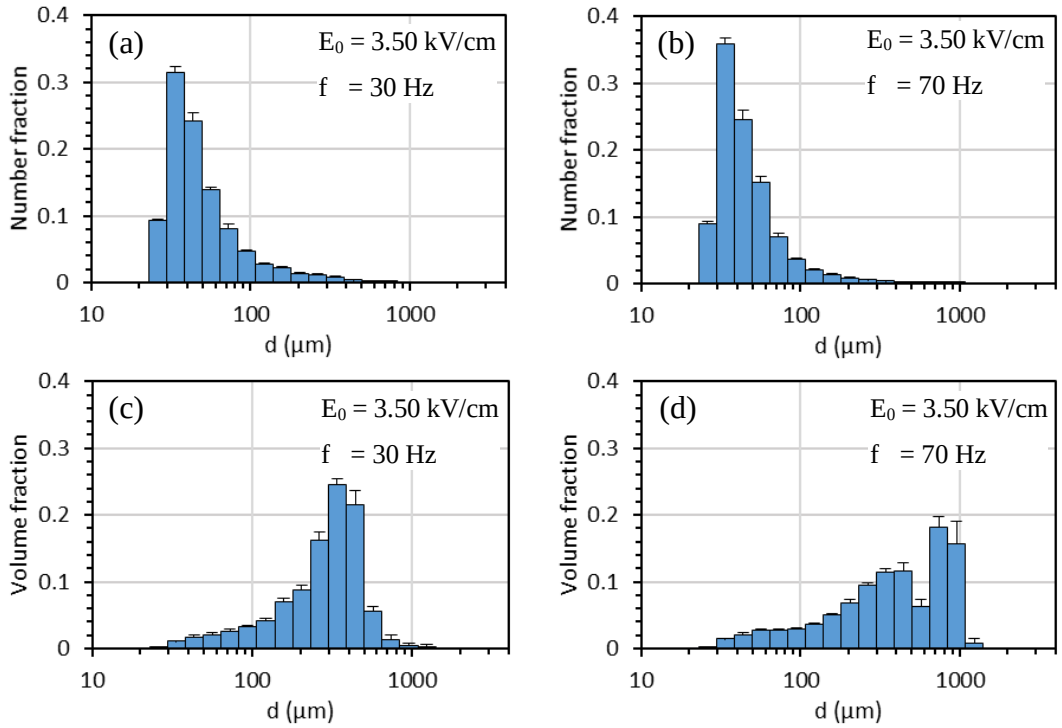

Figure 5.1. Examples of (a–b) population density distribution diagrams for the 35 size classes generated by the VisiSize software from experiments at two different field frequencies using the same field strength, and (c–d) the corresponding volume density distribution diagrams generated from the same experiments.

5.3 RESULTS AND DISCUSSION

5.3.1 Effect of Field Strength on Droplet Size and Size Distribution

The effect of field strength ranging from 3.50 to 4.25 kV/cm on droplet size and size distribution of the electrostatically produced dispersions was investigated using a frequency of 50 Hz as the default. Plots of the Sauter mean diameter as a function of field strength, as depicted in Figure 5.2, show that increases in the field strength within these ranges resulted in decreases in droplet size. The Sauter mean diameter decreased almost linearly from 220 µm at 3.50 kV/cm to 114 µm at 4.25 kV/cm. These values correspond to decreases in the average droplet size of the dispersion from 59 to 54 µm. The trend in the Sauter mean diameter was consistent with that reported by Assmann (2014) for the same liquid–liquid system when using lower AC field strengths ranging from 2.50 to 3.50 kV/cm at the same field frequency, which is also depicted in the figure for comparison. Clearly, this trend can be attributed to the increasing magnitude of electrical stress that was imposed on droplets.

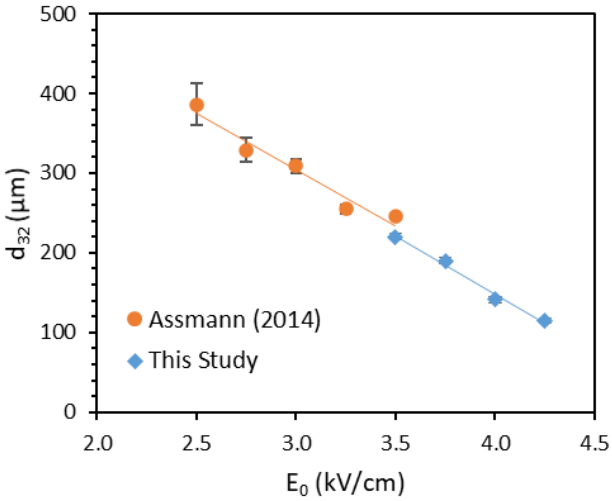

Figure 5.2. Sauter mean diameter of the dispersion as a function of field strength at a constant frequency of 50 Hz. The data shown from Assmann (2014) are means and standard errors of the means from ten replicates, while the data shown from this study are from five replicates.

The application of AC fields within the tested ranges of field strength resulted in dispersions with a unimodal droplet size distribution, as shown in Figure 5.3. The peaks of the histograms shift towards the smaller droplet diameter with increasing field strength. Changes in field strength also resulted in conspicuous variations in the generated droplet size distributions, but whether these variations led to narrower or wider distributions was not clearly apparent. Therefore, a dimensionless parameter known as relative span, S, was introduced to quantitatively determine the effect of field strength on the droplet size distribution. This parameter is expressed as

$$S = \frac{D_{90} - D_{10}}{D_{50}}, \tag{5-1}$$

where D_{90}, D_{50} and D_{10} represent the diameters at which the cumulative volume of droplets having that size or smaller are 90, 50 and 10% of the total volume, respectively. A lower relative span value indicates a narrower droplet size distribution.

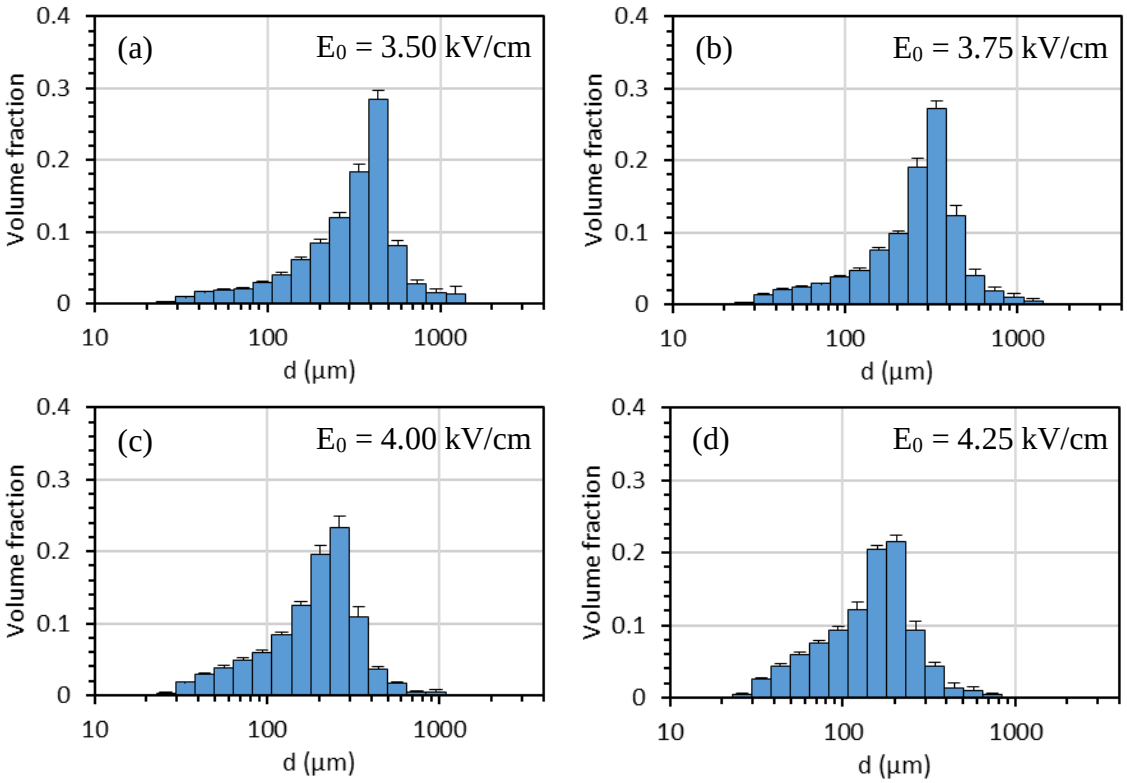

Figure 5.3. Volume density distribution of the dispersion at (a) 3.50 kV/cm, (b) 3.75 kV/cm, (c) 4.00 kV/cm and (d) 4.25 kV/cm using a constant field frequency of 50 Hz.

Plots of the relative span as a function of field strength, depicted in Figure 5.4, show that the droplet size distributions were relatively unchanged with increasing field strengths within the tested ranges. This provided further proof that there is no apparent relationship between the prevalence of a particular droplet breakup mechanism and field strength in AC fields, as was also observed by Assmann (2014) at lower field strengths. He, however, found that an increase in field strength from 2.50 to 3.50 kV/cm changed the droplet size distribution curve from bimodal to unimodal, owing to a significant reduction in the number of large droplets with a diameter above 500 µm, while the number of small droplets with a diameter below 200 µm was relatively unchanged. This was not the case at the higher field strengths.

Figure 5.5 shows the volume density distributions of the six selected size fractions for the generated dispersions as a function of field strength. When the field strength increased from 3.50 to 3.75 kV/cm, the proportion of droplets in the largest size fraction (> 400 µm) decreased, but the proportion of droplets in all of the smaller size fractions, including those in the smallest size fraction (< 50 µm), increased. As the

field strength increased further from 3.75 to 4.00 kV/cm and then to 4.25 kV/cm, the proportion of the top size fractions progressively decreased, but the proportion of the bottom size fractions also increased. Overall, the droplet size distributions remained unchanged with increasing field strength at the tested ranges. It thus appears that when the applied AC field is strong enough to generate a unimodal droplet size distribution, any further increase in field strength will not significantly affect the size distribution.

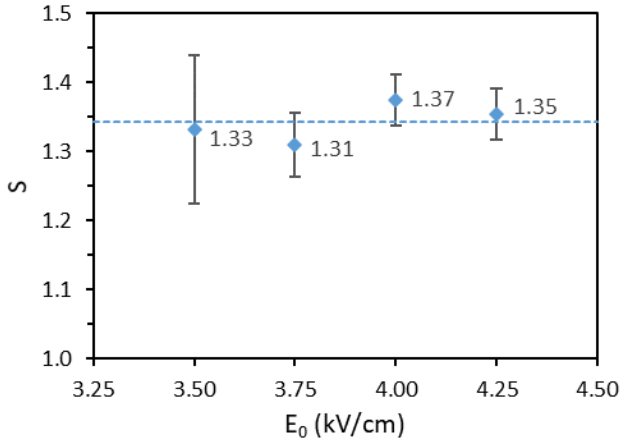

Figure 5.4. Effect of field strength on the relative span of the dispersions at a field frequency of 50 Hz.

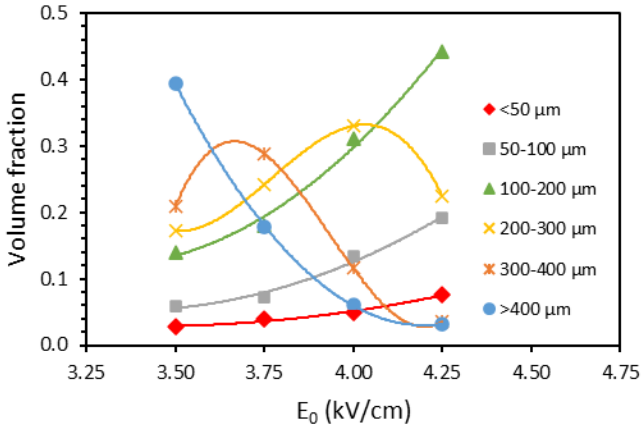

Figure 5.5. Effect of field strength on the volume density distribution of the selected size fractions at a field frequency of 50 Hz.

5.3.2 Effect of Field Frequency on Droplet Size and Size Distribution

The effect of field frequency ranging from 30 to 70 Hz on droplet size and size distribution of the produced dispersion was investigated at 3.50 and 4.00 kV/cm. As mentioned in Chapter 4.3.5, a field strength of 4.00 kV/cm was selected as the upper level rather than 4.25 kV/cm because a semi-permanent emulsion formed when a field

frequency below 50 Hz was used in the latter fields, preventing the droplet size measurement for the full frequency ranges. Figure 5.6 shows that the Sauter mean diameters decreased with decreasing field frequency. The trends of the Sauter mean diameter as a function of frequency at the two selected field strengths are nearly identical, indicating that the effect of frequency on droplet size was consistent within these ranges. Moreover, the apparent parallel between these two plots suggests that there was no significant interaction effect between field strength and frequency on the droplet size.

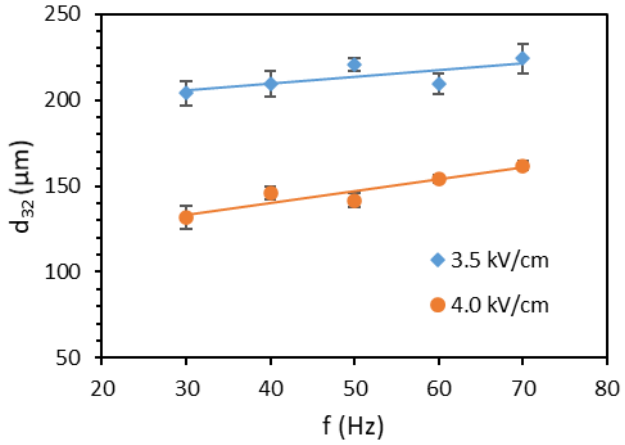

Figure 5.6. Effect of field frequency on the Sauter mean diameters of the dispersions at 3.5 and 4.0 kV/cm.

It appeared that the decreasing trend of the Sauter mean diameters with decreases in frequency was related to the increasing proclivity for droplets to undergo breakup, as evident from the decreasing proportion of the largest sized droplets shown in Figure 5.7. This can probably be attributed to the increasing amplitude of droplet elongation with decreasing frequency. The visual evidence for this is presented in Chapter 4.3.6.

The relationship between droplet elongation and its instability under the influence of an electrostatic field has long been predicted by Taylor (1964). He found that droplets consistently undergo breakup when they deformed beyond a limiting elongation amplitude, which is defined by an aspect ratio between the length of the major and the minor axis of 1.9. Later studies found a similar relationship and the values of the limiting aspect ratio were similar (Garton and Krasucki, 1964; Brazier-Smith, 1971). Given that the amplitude of elongation increases with increasing droplet size, the effect of field frequency on droplet instability is greater for the larger droplets, which aligns with the present observation. Berg et al. (2002) provided experimental evidence on

decreasing droplet stability with a decreasing field frequency when subjecting a single water droplet suspended in crude oil between a pair of parallel-plate electrodes with AC fields. They reported that the required field strength to induce breakup decreased with decreasing frequency ranging from 2000 to 2 Hz for a given size droplet, although no explanation was given for this observation.

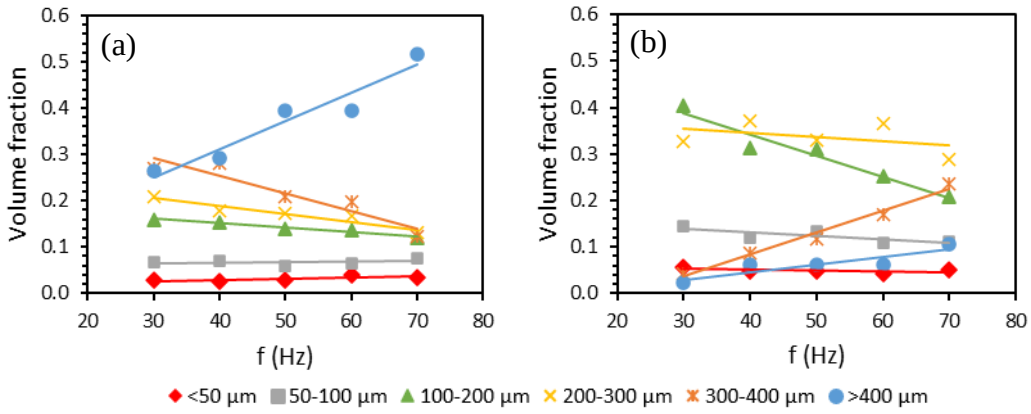

Figure 5.7. Effect of field frequency on the volume density distributions of the selected size fractions at a field strength of (a) 3.50 and (b) 4.00 kV/cm.

Assmann (2014), however, found a different relationship between the Sauter mean diameters and field frequency in AC fields. He reported that the Sauter mean diameter of his experimental dispersion increased from 243 to 273 µm when the frequency decreased from 50 to 20 Hz in 3.50 kV/cm AC fields, and it remained unchanged when the frequency increased from 50 to 60 Hz. He attributed the former to the higher amplitude of droplet elongation and the latter to hydrodynamic hindrance. Similar droplet behaviours were observed in the present study, but the outcomes of these behaviours were different. These differing outcomes are peculiar because the same aqueous and organic solutions and similar experimental methods were used. No notable difference in the methods can be identified to cause such a discrepancy and hence, no explanation can be offered for the discrepancy.

The relative spans and the droplet size distributions of the dispersions at the tested frequencies in the 3.50 and 4.00 kV/cm fields, as depicted in Figure 5.8, show that the droplet size distribution became narrower with decreasing frequency. The trend of the size distribution in the 3.50 kV/cm fields agrees with that reported by Assmann (2014). Conspicuously, at frequencies higher than 50 Hz, the droplet size distribution became

significantly narrower when the field strength increased, which at first seemed to differ from what was reported in Chapter 5.3.1.

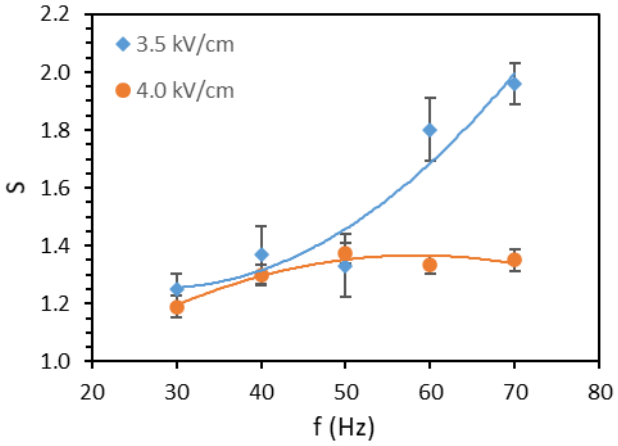

Figure 5.8. Effect of field frequency on the relative span of the dispersions at a field frequency of 50 Hz.

The volume density distributions at the various tested field frequencies in 3.50 and 4.00 kV/cm fields are shown in Figure 5.9 and Figure 5.10, respectively. The droplet size distributions obtained at field frequencies beyond 50 Hz in the 3.50 kV/cm fields were bimodal, while the earlier observations suggested that the effect of field strength on droplet size distribution is minimal only in the regimes where the droplet size distributions are unimodal.

Additional dispersion tests were performed in 4.25 kV/cm AC fields at 60 and 70 Hz to reinforce this observation. It was found that the relative span values of the dispersions obtained in the 4.25 kV/cm fields (1.35 at 60 Hz and 1.40 at 70 Hz) were essentially the same as those obtained from the 4.00 kV/cm fields (1.33 at 60 Hz and 1.35 at 70 Hz) at the same field frequency. Hence, the significant decreases in the relative span values at a field frequency of 60 and 70 Hz in the 3.50 kV/cm fields were consistent with the earlier observations. Noticeably, the decreases in the relative span value when the field frequency decreased from 70 to 50 Hz in the 3.50 kV/cm field suggest that, similar to that of field strength, the effect of field frequency is more significant in the regimes where the droplet size distributions are multimodal.

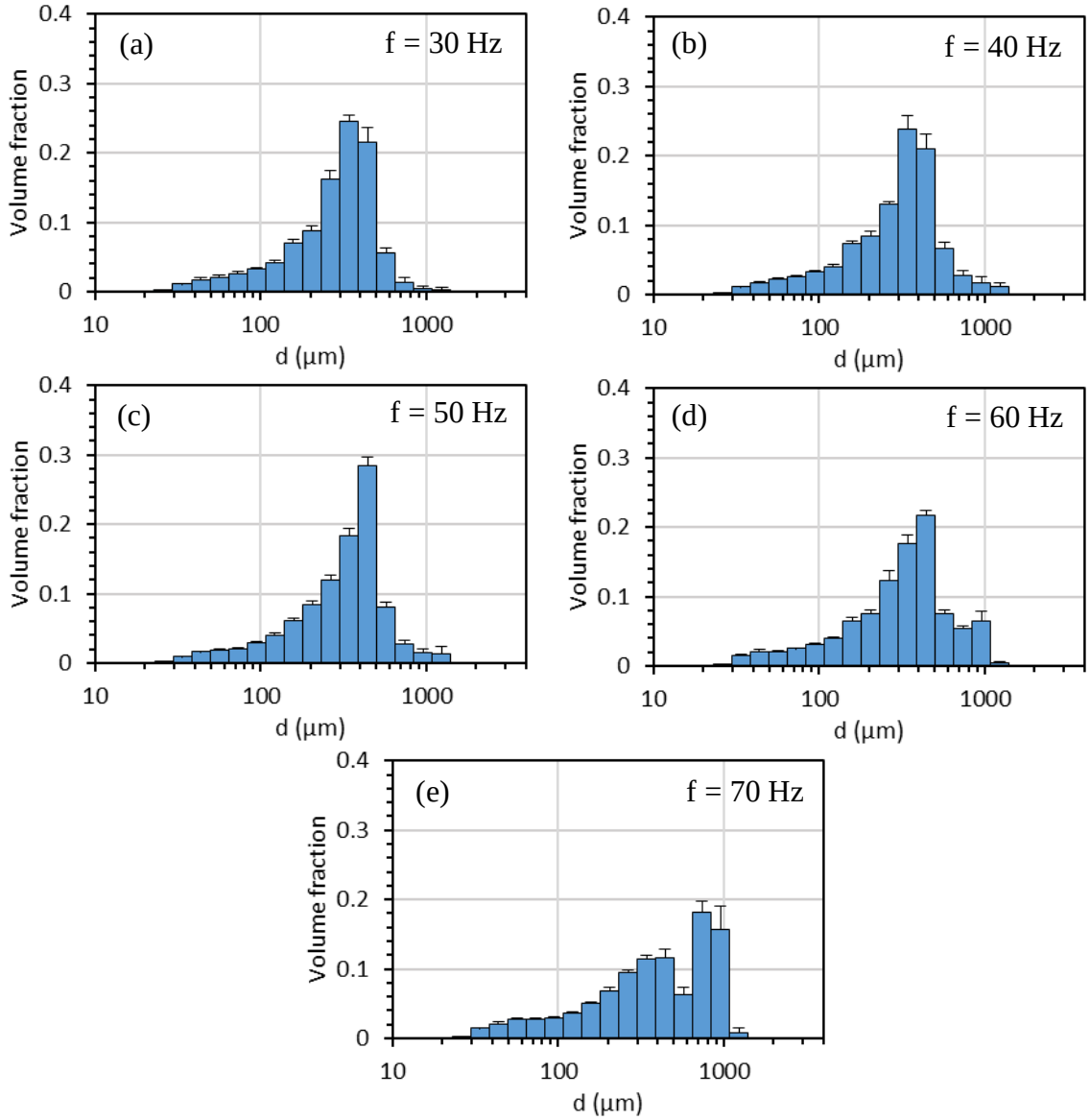

Figure 5.9. Volume density distributions of dispersions in 3.50 kV/cm AC fields at a frequency of (a) 30 Hz, (b) 40 Hz, (c) 50 Hz, (d) 60 Hz and (e) 70 Hz.

Based on the volume density distributions curves shown in Figure 5.7, it appeared that the decreases in the relative span value with decreasing frequency resulted from the decreasing proportion of the largest-sized droplets, while the proportion of the smallest-sized droplets remained relatively unchanged. Consequently, the droplets at the lower frequencies became more concentrated in the middle size fractions, ranging from 100–400 μm (Figure 5.7(a)) for the case of 3.50 kV/cm fields, and from 50–300 μm (Figure 5.7(b)) for the 4.00 kV/cm fields, resulting in the narrower droplet size distribution.

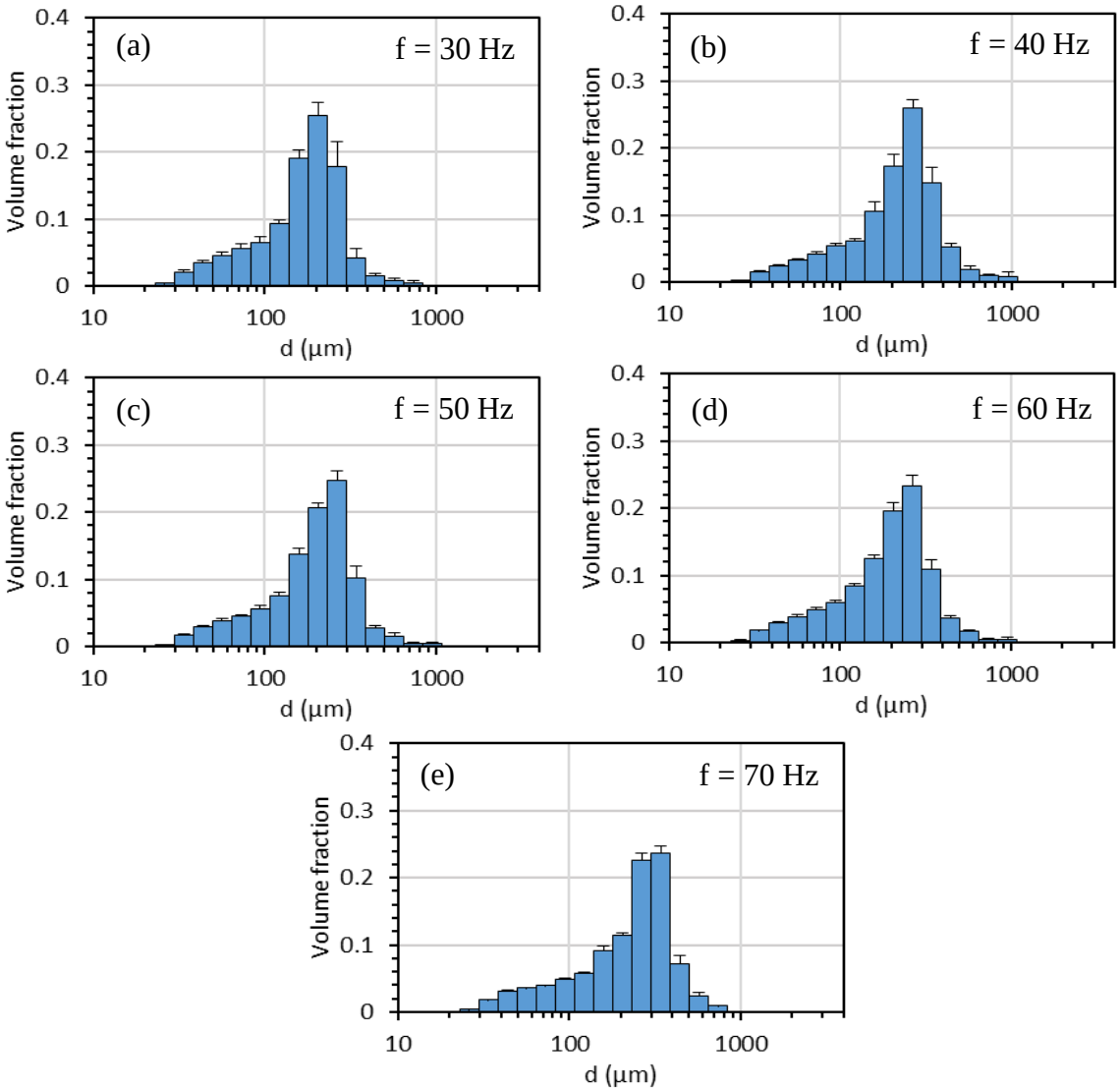

Figure 5.10. Volume density distributions of dispersions in 4.00 kV/cm AC fields at a frequency of (a) 30 Hz, (b) 40 Hz, (c) 50 Hz, (d) 60 Hz and (e) 70 Hz.

Given that there was no indication that variation in the field frequency affected the prevalence of a particular breakup mechanism, the proportion of the smallest sized droplets that remained relatively unchanged with decreasing frequency, despite the increased probability for droplets to break, can be attributed to the effect of field frequency on droplet coalescence. Recall that decreases in frequency markedly increased the amplitude of droplet horizontal motion, increasing the probability of coalescence between droplets (Chapter 4.3.5). Because the droplet breakup is largely a function of field strength and droplet size, the coalescence between small droplets at a given field strength is more likely to form stable droplets. Conversely, the coalescence between the larger droplets is more likely to form unstable droplets. Hence, the overall effect of the frequent coalescence and redispersion was an increase

in the proportion of droplets in the middle size fractions while the proportions of droplets in the top and bottom size fractions decreased. In the present study, the proportion of the small droplets remained relatively unchanged (rather than decreased) probably because the increased frequency of breakup at the lower frequencies generated more small droplets than at the higher frequencies and, consequently, the advantage of more frequent coalescence in decreasing the number of small droplets was cancelled out.

The results presented above show that when the probability of breakup increased without being accompanied by a sufficient increase in the amplitude of droplet horizontal motion, the droplet size distribution remained relatively unchanged, as was observed while investigating the effect of field strength on the droplet size distribution. When the increased breakup probability was accompanied by increases in the amplitude of horizontal motion, the results were narrower droplet size distributions, as observed while investigating the effect of field frequency on the droplet size distribution. These results demonstrate that controlling the probability of coalescence during dispersion is important to control the droplet size distribution in AC fields when the droplets are mainly below 100 μm in diameter.

5.3.3 Droplet Size Characteristics Near the Onset of Semi-Permanent Emulsion Formation

The smallest Sauter mean diameter measured before the field condition was so intense that a semi-permanent emulsion formed was 114 μm, obtained at a field strength of 4.25 kV/cm and a frequency of 50 Hz. Applying either a higher field strength or a lower frequency was found to lead to SPE formation. To ascertain these findings, further examinations into the smallest Sauter mean diameters before the emulsion formed were carried out by conducting experiments in 4.50 kV/cm AC fields at a frequency of 50 Hz and in 4.25 kV/cm AC fields at a frequency of 40 Hz, but the droplet size measurements were performed at a different position. The camera and laser positions were set midway between the middle and the top of the high-field-strength region, about 25 mm below the latter. This position was selected because the first few droplets that entered the column still had significant vertical velocity and their characteristics could still be measured before a significant cloud of ultrafine droplets was formed and blocked the laser illumination in the whole high-field-strength region.

Each of these two additional experiments was duplicated, and the results are summarised in Table 5.1. These results align with the earlier observation that the smallest Sauter mean that can be achieved before the emulsion formed was about 114 µm.

Table 5.1. Sauter mean diameters at conditions before a semi-permanent emulsion formed in the column.

E_0 (kV/cm)	f (Hz)	Camera Position	d_{32} (µm)
4.25	50	Middle*	114.4
4.50	50	Top**	115.5
4.25	40	Top	111.9

*) 50 mm from the top of the high-field-strength region
**) 25 mm from the top of the high-field-strength region

Th relative span values of the dispersions obtained from these three experimental conditions were similar, ranging from 1.25 to 1.35, while the generated cumulative population distributions of the dispersions were practically the same, as shown in Figure 5.11. The figure shows that about 92% of the droplet population had diameters below 100 µm, and about 64% of the population had diameters below 50 µm. The average droplet diameters obtained were also similar, ranging from 52.65 (E_0 = 4.50 kV/cm, f = 50 Hz) to 54.50 µm (E_0 = 4.25 kV/cm, f = 50 Hz). These consistent droplet size characteristics reinforce the visual observation that the SPE was caused by the generation of droplets that are too small to settle and disengage from the organic phase.

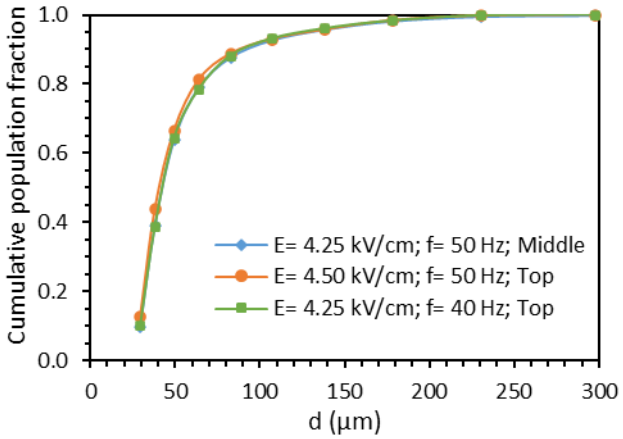

Figure 5.11. Cumulative population fraction of droplets at conditions before emulsion would form.

5.4 CHAPTER SUMMARY

In this chapter, the effect of field strength and frequency on droplet size and droplet size distribution were investigated. The effect of field strength on droplet size was found to be more significant than field frequency as it directly controls the maximum magnitude of the electrical stress imposed on droplets. The field frequency affects the droplet size largely due to its effect on the amplitude of droplet elongation, which affects the droplet stability.

In the present study, it was found that the effect of field strength and frequency on the droplet size distribution appeared to be closely related to the probability of droplets breaking and coalescing. The droplet breakup played a more significant role in regimes where the droplet size distributions were multimodal, while droplet coalescence was found to be more significant in regimes where they were unimodal. In regimes where they were multimodal, increases in strength and decreases in the frequency of the field, which increase the breakup probability, favoured the formation of narrower droplet size distributions. In regimes where they were unimodal, however, increases in field strength had a negligible effect. Differently, decreases in the field frequency still favoured a narrower droplet size distribution, whether the droplet size distributions were in a regime where they were unimodal or multimodal, but the changes were found to be more significant in the latter regime. These results suggest that controlling the probability of coalescence during dispersion is important to control the droplet size distribution in AC fields when the droplets are mainly smaller than 100 μm in diameter.

The experimental results show that the semi-permanent emulsion formation was related to the size of the droplets that prevented them from settling. The smallest Sauter mean of the dispersion that can be achieved before an emulsion formed was about 114 μm, which corresponds to an average droplet diameter of about 54 μm.

CHAPTER 6
EFFECT OF ALTERNATING CURRENT FIELDS ON MASS TRANSFER

6.1 INTRODUCTION

This chapter aimed to elucidate the effect of changes in droplet behaviours and dispersion characteristics with variation in the field conditions, as reported in the previous chapters, on mass transfer. The dispersions involved a population of droplets mainly with a diameter below 100 µm. The results can be used to determine whether the mass-transfer performance of an ESX column differs when dispersing smaller droplets in more vigorous AC fields than those previously studied by Assmann (2014). This is important to advance the development of ESX because in theory, its major advantage is that it can be operated with smaller droplets than those previously investigated.

In addition to the cobalt(II) and CYANEX 272 system, the use of ESX to enhance the mass transfer of a copper(II) with LIX 84-I system, which is known to have a slower extraction kinetics, was tested. The results can be used to help evaluate the performance of the proposed ESX technique in overcoming the slow extraction kinetics of the system.

6.2 EXPERIMENTAL METHODOLOGY

6.2.1 Materials

The $CoSO_4$ – CYANEX 272 and $CuSO_4$ – LIX 84-I systems were used for the work described in this chapter. The preparation of the test solutions and the reagents used to prepare them are described in Chapter 3.4.

6.2.2 Experimental Procedures

The experimental set-up developed by Assmann (2014), described in Chapter 3.2, with the extraction column was used in this part of the study. The experiments were all carried out at ambient temperatures (25 ± 2 °C). In each experiment, 80 mL of the

organic solution was used. The aqueous phase flow rate was kept constant at 0.25 mL/min in all experiments unless otherwise stated.

The general procedure to perform the extraction experiments is described in Chapter 3.3.3. Because the imaging equipment was not required in these experiments, the setup was not enclosed and hence, a direct visual inspection was performed during experiments. This was important to ensure that there was no droplet dangling on the mouth of the delivery tip after both the pump and AC power supply were turned off, which may accidentally fall through the organic phase and contaminate the sample.

As in the dispersion experiments, the spacing of the electrodes and position of the feed droplets between the electrodes when entering the high-field-strength region was inspected before performing any experiment by recording the descent of the feed droplets in the absence of a field using a lens magnification of 1.0. This was to ensure that the spacing of the electrodes and the positioning of the feed droplets were kept constant. The detailed procedures to perform the inspection and the extraction experiment are described in Appendix K.

Each experiment was triplicated unless stated otherwise. The experiment was performed for about 2.5 min and, from each, 0.25 mL of the aqueous sample was collected. The sample was filtered using a hydrophilic PVDF syringe filter (Fisherbrand) with 0.45 µm pore size to separate any organic entrained in the sample and diluted with 1% nitric acid solution before being sent for assay.

The droplets' apparent residence time in the high-field-strength regions was measured by recording the experiments using a phone camera (Nokia 6.1) equipped with Zeiss optics that can record high-resolution images at a speed of 30 fps. The apparent residence time here refers to the time when the majority of droplets left the high-field-strength region after they entered the column. This was determined by playing back the recording at a reduced speed. Note that the measurement was only meant to provide an approximate value for perspective, rather than a precise value for a detailed analysis.

6.2.3 Experimental Data Analysis

The mass transfer in each experimental condition was determined by the extraction percentage of metal ions in the aqueous feed and raffinate solutions. The extraction percentage was calculated by mass balance using the following equation

$$\%Extraction = \frac{C_i - C_f}{C_i} \times 100\,, \tag{6-1}$$

where C_i is the initial metal ion concentration (mg/L) and C_f is the final metal ion concentration (mg/L) in the aqueous phase. The procedure to determine the metal ion concentrations in the aqueous solutions is described in Chapter 3.3.4. The standard deviations obtained from analysis of the triplicated experiments in all experimental sets were all below 5%, and mostly below 2%, proving the reproducibility of the experimental method. The mean value of the metal ions extraction from experiments in the presence of electrostatic fields was plotted, along with error bars that represent the standard deviation of the mean from each set of experimental conditions.

6.3 RESULTS AND DISCUSSION

6.3.1 Effect of Field Strength on Mass Transfer

The effect of the strength of AC fields on mass transfer was studied at field strengths ranging from 3.50 to 4.00 kV/cm and a constant frequency of 50 Hz. The dispersions produced in these field strengths were found to have an average droplet diameter ranging from 59 to 56 μm. A set of experiments was performed with no electrostatic field applied as a standard for comparison purposes. The results of the experiments are shown in Figure 6.1. Clearly, the application of AC fields significantly enhanced the mass transfer, and increases in the strength of the field increased the mass transfer enhancement. The cobalt extraction increased from 42.29% in the absence of a field to 86.11% when the 3.50 kV/cm AC field was applied. When the field strength increased from 3.50 to 3.88 kV/cm, the cobalt extraction increased almost linearly to 98.84%. The extraction percentage was then plateaued when the field strength increased further as only small amounts of the cobalt ions remained in the droplets.

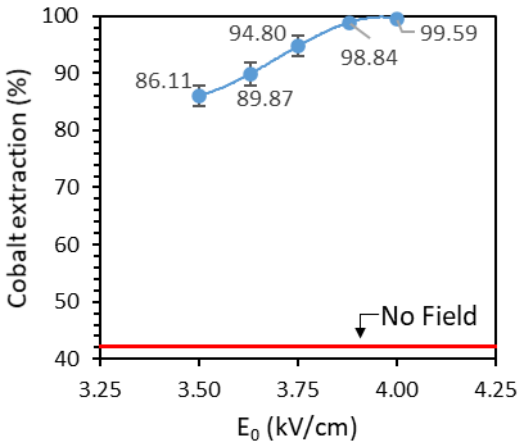

Figure 6.1. Effect of field strength on cobalt extraction at a field frequency of 50 Hz. The error bars represent the standard deviations of the mean.

The dispersion characteristics at 3.50 and 3.75 kV/cm were used to assess the effect of the changes in the droplet dispersion behaviours on mass transfer as the field strength increased because the trend of the cobalt extraction was linear in this range. Data on the dispersion characteristics obtained from the results in Chapter 4 and 5 are summarised in Table 6.1. The Sauter mean diameter decreased from 216.92 to 190.16 µm when the field strength increased from 3.50 to 3.75 kV/cm; this increased the specific interfacial area of the dispersion, defined as the ratio of surface area and the volume of the droplets, from 27.24 to 31.60. The droplet speed and horizontal velocity increased by 20% and 18%, respectively, to 0.94 and 0.36 m/s at 3.75 kV/cm. In addition, the visual observation performed in Chapter 4.3.6 showed that the droplet oscillation amplitude and proportion of droplets exhibiting unstable oscillation increased with increasing field strength. The only important dispersion characteristic that remained essentially unchanged with the increasing field strength was the droplet size distribution, as indicated by the relative span values. These show that the increased cobalt extraction was a compounding effect of the increased interfacial contact area and droplet agitation, which was influenced by the droplet speed, horizontal velocity and oscillation amplitude.

It is helpful to note that there was no discernible difference between the droplet dispersion characteristics and droplet size distribution when the extraction column was used and when the dispersion column was used. This was apparent from the visual observations of the extraction experiments with the naked eye and from a few preliminary experiments using high-speed equipment to compare the droplet clarity

when the images were taken from the extraction and dispersion column under the same experimental condition.

The results show that the effects of the decreased droplet size and increased droplet speed, horizontal velocity and oscillation amplitude on mass transfer are consistent with the theory of mass transfer. The results are also consistent with those reported earlier by Assmann (2014) in the lower field strengths ranging from 2.5 to 3.5 kV/cm. The individual contribution of each of these changes in the dispersion characteristics to enhance the mass transfer was, however, difficult to quantify based on these results.

Table 6.1. Changes in dispersion characteristics as the field strength increased from 3.50 to 4.00 kV/cm at a frequency of 50 Hz.

Variable	**3.50 kV/cm**	**3.75 kV/cm**	**%Change**
Mass transfer (%)	86.08	94.80	+10%
Sauter mean diameter (μm)	216.92	190.16	−14%
Specific interfacial area (mm^{-1})	27.24	31.60	+16%
Droplet speed (m/s)	0.78	0.94	+20%
Horizontal velocity (m/s)	0.31	0.36	+18%
Relative span	1.33	1.31	−3%

Visual observations of the experiments at the 4.00 kV/cm indicated that almost quantitative extraction of cobalt (99.59%) was achieved in less than 10 s of mixing. The apparent residence time was measured by observing the time when the majority of droplets left the high-field-strength region after they entered the column. This observation shows that the ESX technique can affect fast mass transfer in SX even when operating with droplets with a diameter mainly below 100 μm.

6.3.2 Effect of Field Frequency on Mass Transfer

The effect of the frequency of AC fields, ranging from 30 to 70 Hz, on mass transfer was studied at two different field strengths, 3.50 and 3.75 kV/cm. The upper field strength was 3.75 kV/cm because the cobalt extraction at 4.00 kV/cm was already almost complete, so a meaningful trend could not be observed at 4.00 kV/cm. The results, depicted in Figure 6.2, show that decreases in field frequency enhanced the mass transfer at both field strengths. The cobalt extraction increased significantly from 73.20% at 70 Hz to 95.33% at 30 Hz in the 3.50 kV/cm fields. Likewise, the cobalt

extraction increased significantly from 86.84 to 98.00% when the frequency decreased from 70 Hz to 30 Hz in the 3.75 kV/cm fields.

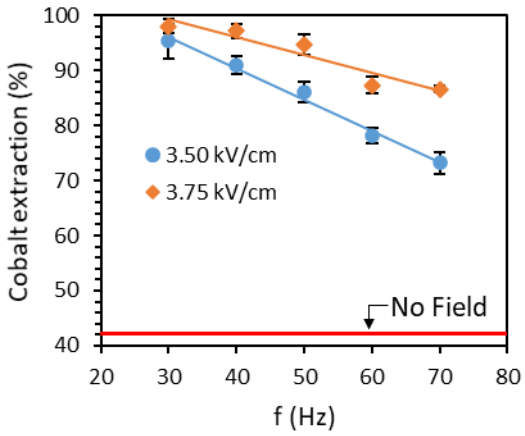

Figure 6.2. Effect of field frequency on cobalt extraction at a field strength of 3.50 and 3.75 kV/cm.

Unlike when the field strength was varied, the Sauter mean diameters changed only slightly with the variation in field frequency (Figure 5.8). This allows the assessment of the effect of factors other than the interfacial area on the mass transfer. The dispersion characteristics data, presented in Table 6.2, show that decreasing the field frequency from 70 to 60 Hz in 3.50 kV/cm fields led to a 6% increase in the cobalt extraction, from 73.20 to 78.13%, followed by a 7% increase in specific interfacial area, 15% increase in droplet speed, 38% increase in horizontal velocity and 8% decrease in relative span. When the frequency decreased further from 60 to 40 Hz, the cobalt extraction increased more significantly from 78.13 to 90.99%, but this was not followed by an increase in the specific interfacial area because the Sauter mean diameter was essentially unchanged. The droplet speed increased, but this can be mainly ascribed to the increase in the droplet horizontal velocity. The horizontal velocity increased by 86%, and the relative span decreased by 31%. These values clearly show that the increase in mass transfer with field frequency was largely associated with the changes in the droplet horizontal velocity and droplet size distribution.

The increased droplet horizontal velocity could enhance the mass transfer by increasing the translational motion of the droplet, the droplet residence time in the column, and the frequency of droplet coalescence and redispersion. Intuitively, increases in droplet motion in any direction would increase the mass transfer. This is

true in the absence of a field as these motions increase droplet internal circulation. The application of electrostatic fields, however, induces circulation inside and outside of a droplet, and its translational motion could actually hinder these circulations on one or multiple sites within and outside the droplet (Chang and Berg, 1983).

Table 6.2. Changes in the dispersion characteristics as then field frequency increased from 70 to 60 Hz and then to 40 Hz at a field strength of 3.50 kV/cm.

Variable	**70 Hz**	**60 Hz**	**40 Hz**	**%Change 70 - 60 Hz**	**%Change 60 - 40 Hz**
Mass transfer (%)	73.20	78.13	90.99	+6%	+16%
Sauter mean diameter (μm)	224.16	209.26	209.10	-7%	~0%
Specific interfacial area (mm^{-1})	26.92	28.76	28.84	+7%	~0%
Droplet speed (m/s)	0.72	0.83	0.96	+15%	+16%
Horizontal velocity (m/s)	0.21	0.29	0.54	+38%	+86%
Relative span	1.96	1.80	1.37	-8%	-31%

Hence, it was deemed that, in the present study, the increased droplet horizontal velocity enhanced the mass transfer process mainly by increasing the droplet residence time in the column and the frequency of droplet coalescence and redispersion. The former favours mass transfer by increasing the time for mass transfer to occur. The latter favours mass transfer by inducing internal mixing during coalescence and creating new interfaces with high concentration gradients during redispersion (Davies, 1972a). The narrower droplet size distribution with decreasing frequency was also a result of the more frequent coalescence and redispersion (Chapter 5.3.2), which is also favourable to increasing the mass transfer efficiency.

Another factor that may affect the mass transfer is droplet oscillation, but in theory, the observed changes in the droplet oscillation behaviour with decreasing frequency of the AC fields would not be favourable to the mass transfer. This is because, although the oscillation amplitude increased with decreasing field frequency, the oscillation frequency decreased. Consequently, the time-averaged surface area by the increased oscillation amplitudes at the lower field frequencies may actually be smaller than those at the higher frequencies. Nonetheless, researchers have empirically shown that the beneficial effect of oscillation on mass transfer is more from the action of internal mixing rather than the increased interfacial area (Wham and Byers, 1987). This

indicated that the observed mass transfer enhancement with decreasing frequency could not be ascribed to the changes in the droplet oscillation behaviours.

Therefore, the increase in mass transfer with decreasing frequency can largely be attributed to the effect of field frequency to increase the droplet horizontal velocity, leading to a longer residence time and more frequent droplet coalescence and redispersion. The results of the present study may complement the earlier findings by Assmann (2014), who observed a similar mass-transfer trend at a lower field strength (3.0 kV/cm). He postulated that the enhanced mass transfer was mainly owing to the increased droplet speed, zigzagging and amplitude of oscillation with decreasing frequency, but provided no explanation on how the increased droplet speed and zigzagging affected the mass transfer. This explanation is important because, as discussed above, it was unlikely that the difference in the droplet oscillation behaviours significantly affected the mass transfer, or even favourably, in the present case.

The results of the present study show that fast mass transfer can be achieved when operating with small droplets with a diameter below 100 μm, as these could exhibit significant oscillation under the influence of AC fields and there was no sign of them behaving more like a rigid sphere. The mass-transfer efficiency was found to increase with increasing strength and decreasing frequency under more vigorous electrostatic field conditions when operating with smaller droplets than those studied previously by Assmann (2014). One major contribution of the present study to fill in the gap in the knowledge is that it shows a limiting condition at high-strength and low-frequency AC fields, wherein the droplets generated became too small to exhibit a significant vertical motion to settle. This leads to SPE formation, resulting in poor phase-disengagement efficiency. Therefore, these findings suggest that the most suitable AC field condition for an ESX operation is at high voltage and low frequency, to allow high mass-transfer rates but below the regime where an emulsion would form to also allow fast phase disengagement.

6.3.3 Effect of Electrostatic Fields on Mass Transfer of a Slow Kinetics System

Experiments were performed to elucidate how the strength and frequency of AC fields can be exploited in ESX for SX systems that are known to exhibit slow extraction

kinetics. The aim of these experiments was to show the effectiveness of ESX to overcome the slow extraction kinetics to further determine the potential of ESX columns as an alternative to conventional SX contactors for purification of metal ions, including those with slow kinetics. A system comprised of 2-hyroxy-5-nonylacetophenone oxime (commercially available as LIX 84-I) in ShellSol 2046 as the organic phase and cupric sulfate solution as the aqueous phase was used as the test case.

Oxime extractants are industrially well-established for copper extraction but known to have slow extraction kinetics. A pure ketoxime extractant for copper extraction was selected over a pure aldoxime (e.g. LIX® 860-I) or a mixture ketoxime-aldoxime variant (e.g. LIX® 984N) because the ketoxime extractant is the weakest extractant among the three commercial variants of the oxime extractants (Szymanowski and Borowiak-resterna, 1991; BASF, 2014), i.e., it has the slowest extraction kinetics among the three. It is recognised that conventional SX contactors other than mixer settlers are unlikely to be used in the commercial copper SX operation involving oxime extractants (Sole et al., 2013). Hence, the $CuSO_4$–LIX 84-I system was deemed to be a good representation of slow kinetics system.

Similar to cobalt extraction with CYANEX 272, the extraction reaction of copper with LIX 84-I releases hydrogen ions, which may slow the copper extraction rate from the aqueous phase. Therefore, the aqueous solution needs to be buffered to keep the pH relatively constant throughout mixing. Earlier studies suggest that a pH above 4.0 is required to achieve quantitative copper extraction with LIX 84-I in a single extraction stage from acidic sulfate solutions (Reddy and Priya, 2005; BASF, 2014). Considering that a high copper concentration in the aqueous phase would lead to excessive addition of a pH buffer, the suitable aqueous test solution composition was deemed to be 1000 mg/L Cu^{2+} from cupric sulfate with 0.22 mol/L sodium acetate and 0.38 mol/L acetic acid as buffers at pH 4.5. The test organic solution composition was 5% LIX 84-I by volume in ShellSol 2046.

The effect of the strength of AC fields on copper extraction was studied at a constant field frequency of 50 Hz. The suitable field strengths were found to be 3.5–6.0 kV/cm. The results, depicted in Figure 6.3, show that the application of AC fields enhanced mass transfer and the trend of the mass-transfer enhancement with field strength was

similar to that in the $CoSO_4$–CYANEX 272. A higher voltage was required to achieve quantitative copper extraction because the droplets were harder to break, probably due to the higher interfacial tension of the system. The droplets were observed to barely break at the 3.50 kV/cm fields, which explains why the copper extraction was rather low, i.e., the droplets only experienced a regime of feed droplet breakup (Figure 4.3(a)), wherein only a single splitting occurred throughout the length of the high-field-strength region. As the field strength increased, the breakup intensity increased, and the droplets experienced the regimes of primary and secondary droplet dispersion. Analysis of the dispersions showed that the smallest Sauter mean diameter produced in these ranges was 224 µm at the 6.0 kV/cm fields. No emulsion formation was observed, probably because the droplets were still relatively large enough, to exhibit a significant settling rate, which is consistent with the observation in the $CoSO_4$–CYANEX 272 system.

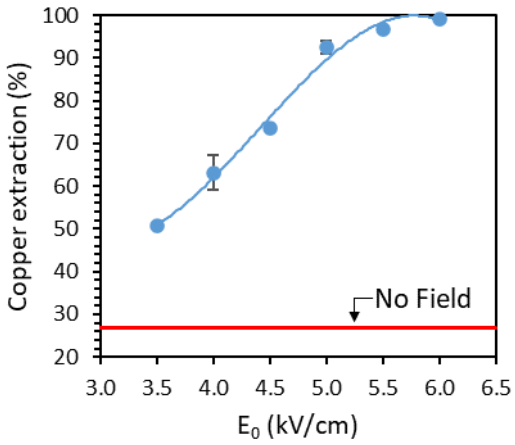

Figure 6.3. Effect of field strength on copper extraction at a constant field frequency of 50 Hz. The experiments at 3.5, 4.5 and 5.5 kV/cm were not triplicated as they show a consistent trend.

It is interesting to note that, although the droplet of the $CuSO_4$–LIX 84-I system in the 6.0 kV/cm fields had a smaller specific interfacial area than those of the $CoSO_4$–CYANEX 272 system in the 4.0 kV/cm fields, the former exhibited much faster droplet horizontal velocity (1.27 m/s) than those in the latter (0.57 m/s). Clearly, this can be attributed to the stronger electrostatic force imposed on the droplets at the higher field strengths and was probably the most significant contributor to how the ESX technique overcame the slow extraction kinetics of the system.

The effect of field frequency, ranging from 30 to 70 Hz, on the copper extraction was studied at a field strength of 5.0 kV/cm. The results, depicted in Figure 6.4, show that decreases in field frequency enhanced the mass transfer, which is consistent with the established relationship between field frequency and mass transfer.

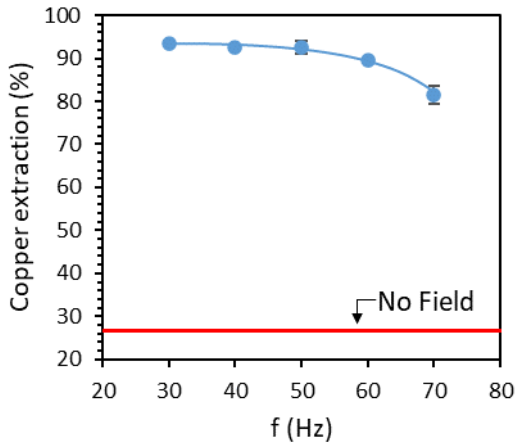

Figure 6.4. Effect of field frequency on copper extraction at a constant field strength of 5.0 kV/cm. The experiments at 40 and 60 Hz were not triplicated as they show a consistent trend.

Given that no indication of SPE would form even at the highest tested field strength, copper extraction experiments at higher aqueous flow rates up to 0.75 mL/min at a field strength of 5.0 kV/cm and a frequency of 50 Hz were performed. The results, depicted in Figure 6.5(a), show that copper extraction decreased with increasing flow rate. It was visually apparent that the extraction rate decreased largely due to the decreasing droplets' residence time in the high-field-strength region. This was substantiated by plots of the measured apparent residence time versus copper extraction, which show a linear trend, as depicted in Figure 6.5(b). Clearly, this shows that the aqueous-phase flow rate significantly affected the droplet residence time.

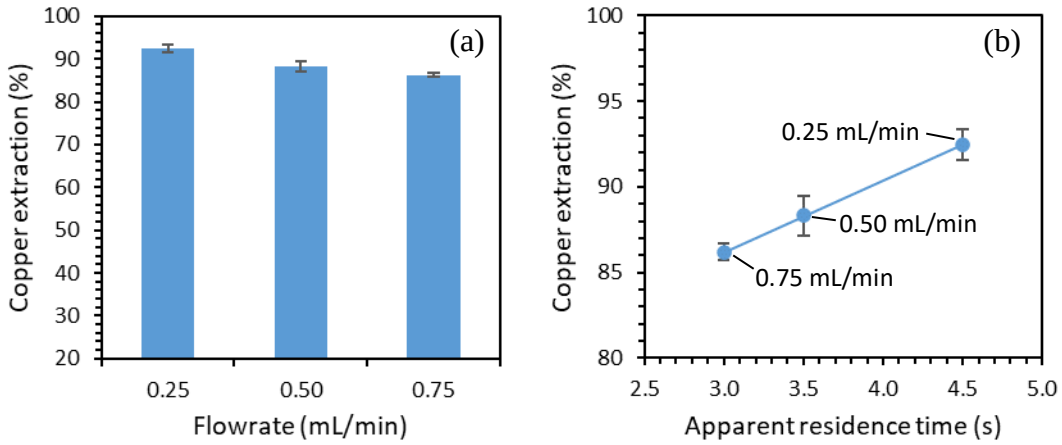

Figure 6.5. Effect of (a) flow rate on copper extraction and (b) the relationship of the residence time at varying flow rates with the copper extraction.

A direct comparison of the results of the present study with previous studies that used conventional mixing methods cannot be made to assess the relative performance of ESX compared with conventional SX as no comparable study could be found in the literature. The comparison cannot be made mainly because this ESX column was only capable of working with a very low volume of the dispersed phase relative to the continuous phase. Nevertheless, visual observation of the dispersions suggests that the almost quantitative copper extraction in the 6.0 kV/cm AC fields was achieved in less than 6 s of residence time in the high-field-strength region. This demonstrates that the ESX technique could produce a dispersion with high specific interfacial area and agitation, allowing it to overcome the slow extraction kinetics of the $CuSO_4$–LIX 84-I system. As a perspective, reports from the manufacturer of the extractant show that using their standard kinetics tests involving mixing the mixture vigorously in a baffled reactor with an overhead stirrer, higher than 90% of copper extractions using 10% LIX 84-I by volume in ShellSol® D70 were achieved only after 60 s of mixing (Kordosky et al., 1987; BASF, 2014). Moreover, the fact that the Sauter mean diameter at the highest tested field strength in the present study was still significantly larger than the apparent onset of the SPE formation indicates that mass transfer enhancement could still be increased further.

These results suggest that the ESX technique may open an opportunity for a column contactor, which requires less solvent inventory and plant footprint, to be used for copper SX. These results also suggest that there is no practical difference in the general effect of electrostatic field conditions to treat slow kinetics and fast kinetics systems in ESX.

6.4 CHAPTER SUMMARY

The effect of the strength and frequency of AC fields on mass transfer in SX was investigated. In addition to the $CoSO_4$–CYANEX 272 system, the use of ESX to enhance mass transfer in a $CuSO_4$–LIX 84-I system that is known to have slower extraction kinetics was tested. In both the tested systems, increases in the strength and decreases in the frequency of the field enhanced the mass transfer. The former enhanced the mass transfer through a compounding effect of the increasing interfacial area and droplet agitation, as clearly apparent from the decreasing droplet size and increasing droplet speed, horizontal velocity and oscillation amplitude. The latter enhanced the mass transfer largely by increasing the droplet horizontal velocity leading to longer droplet residence time and more frequent droplet coalescence and redispersion.

The trend of increasing cobalt extraction with increasing field strength (3.50–4.25 kV/cm) and decreasing field frequency (30–70 Hz) increased almost linearly when the field strength increased further than those previously studied (2.50–3.50 kV/cm), even under conditions that were near the regime where SPE forms. This demonstrates the ESX technique remains effective when operating with small droplets with a diameter mainly below 100 μm under more vigorous electrostatic field conditions than those previously studied.

The ESX technique was able to allow > 99% copper extraction in only less than 6 s under 6.0 kV/cm fields at a frequency of 50 Hz while descending through a height of the active contacting area of only 50 mm with the $CuSO_4$–LIX 84-I system. Moreover, the mass-transfer enhancement could still be increased further because the droplets appeared to be still large enough to allow the application of stronger fields before SPE started to form. This suggests that the ESX technique can overcome the slow kinetics of the systems and indicates a satisfactory mass transfer performance of the technique.

The results of the present study suggest that the most suitable AC field condition for an ESX operation is at high voltage and low frequency to allow high mass transfer rates, which is consistent with that previously proposed, but below the regime where an emulsion would form to also allow fast phase disengagement.

CHAPTER 7
CONCLUSIONS AND RECOMMENDATIONS

7.1 INTRODUCTION

The present study aimed to investigate the behaviours of smaller droplets under more vigorous electrostatic field conditions than those previously studied. Specifically, it aimed to:

1. Characterise the behaviours of the smaller droplets (< 100 μm) than those previously characterised (100–1400 μm) under the influence of electrostatic fields and determine their effect on mass transfer.
2. Determine the conditions that allow the formation of momentary emulsion under the influence of electrostatic fields and explore if and how they can be controlled to allow high mass-transfer rates and fast phase disengagement in ESX.
3. Evaluate the performance of the proposed ESX technique by performing SX of metals from aqueous solutions and determine conditions for high mass-transfer rates and fast phase disengagement.

In pursuing the first objective, experimental investigations were carried out using an identical liquid–liquid system (cobalt(II) sulfate and CYANEX 272 extractant) and a comparable experimental method to that used previously so a direct comparison could be made. The experiments were performed using an ESX column involving insulated parallel-plate electrodes with AC fields, which was deemed to be the most promising for industrial application of the technique based on the literature review. These experiments were carried out in three parts. In the first part, experiments were performed to understand the effect of the AC fields on droplet behaviours, which include breakup, motion and oscillation. In the second part, experiments were performed to understand the effect of the changes in the droplet behaviours in relation to the properties of the AC fields on the droplet size and size distribution. In the third part, experiments were then performed to understand the effect of the changes in the dispersion characteristics under the AC fields on mass transfer. The second objective was addressed from the experiments in the first part. The third objective was addressed

from the experiments in the third part, which also included experiments involving a SX system with a slow extraction kinetics.

The conclusions drawn from these experiments are summarised in the following sections. Recommendations for future research on this subject are also offered.

7.2 CONCLUSIONS

7.2.1 Effect of AC Fields on Droplet Breakup, Motion and Oscillation

- The droplet dispersion was observed to involve five breakup mechanisms; namely, jetting, necking, irregular, combination breakup and a mechanism that appeared to be emulsion-like formation, which was previously known to occur only when uninsulated electrodes were used in PDC and DC fields.
- Unlike previously reported, it was observed in the present study that a significant proportion of ultrafine droplets from the emulsion-like formation were quickly pushed away from the place they formed and spread around the column before having the chance to coalesce owing to the vigorous agitation under the tested ranges. The frequency of the breakup mechanism appeared to increase with increasing field strength, but no discernible changes could be observed with the changes in field frequency. The emulsion-like formation was observed only during the initial phase of the dispersion lasting for less than 0.3 s, wherein a significant number of large droplets were present. Hence, it was deemed difficult to control within the tested ranges to allow high mass transfer rates and fast phase disengagement.
- The combination breakup mechanism involving jetting and necking was found to be the predominant breakup mechanism under all the tested ranges. Hence, the field conditions that increased the frequency of necking also increased the frequency of jetting.
- Some droplets were observed to exhibit zigzagging, oscillation, or both owing to the periodic cycling of the applied AC fields. The amplitude of the zigzagging and oscillation increased with increasing field strength and decreasing frequency.
- The horizontal velocity of small droplets with a diameter less than 100 μm was generally smaller than the larger droplets, but it was found that the gap

between them decreased with increasing field strength to the point that it was practically negligible in the 4.25kV/cm at a frequency of 50 Hz. This behaviour was not previously observed at the lower field strengths. This observation is particularly significant because the smaller droplets are known to have smaller motions in conventional SX contactors.

- Increases in the strength and decreases in the frequency of the fields were observed to increase the frequency of droplet coalescence and redispersion, which phenomenon can be attributed to an increase in the droplet horizontal velocity.
- It was observed that droplets smaller than 100 μm in diameter also exhibited stable and unstable oscillation and generally, the smaller droplets exhibited smaller oscillation amplitude. The smallest observable droplets within the used imaging equipment, which were those with a diameter of 23 μm, were found to be able to exhibit significant oscillation within the tested ranges.
- The application of a vigorous electrostatic field could lead to the formation of an SPE. The proclivity for the emulsion to form increased with increasing field strength and decreasing frequency.

7.2.2 Effect of AC Fields on Droplet Size and Size Distribution

- The strength and frequency of the field affect the droplet size of the dispersion. The effect of the former on droplet size was more significant than the latter as it controls the maximum magnitude of the electrical stress imposed on droplets. The latter influenced the droplet size largely due to its effect on the amplitude of droplet elongation, which affects the droplet stability.
- The increase in strength and decrease in frequency of the field decreased the droplet size. Trends of the plots of the droplet Sauter mean diameter as a function of either the field strength or frequency were almost linear, analogous to that previously observed at the lower field strengths. These suggest that the droplet size of dispersions generated by AC fields can be predicted with relative ease.
- The effects of strength and frequency of the field on droplet size distribution were found to vary, depending on whether droplet size distributions are in a regime where they are unimodal or multimodal. This was not previously

observed at lower field strengths. In regimes where the droplet size distributions were multimodal, increases in strength and decreases in the frequency of the field, which increase the breakup probability, favoured the formation of narrower droplet size distributions. In regimes where these were unimodal, however, increases in field strength had a negligible effect on them. Differently, decreases in the field frequency still favoured a narrower droplet size distribution, whether the droplet size distributions were in a regime where they were unimodal or multimodal, but the changes were found to be more significant in the latter regime. These results suggest that controlling the probability of coalescence during dispersion is important to control the droplet size distribution in AC fields.

- The formation of an SPE formation was found to be related to the size of the droplets generated by the electrostatic fields that prevented them from settling. In the present case, the semi-permanent emulsion was formed when the field strength increased above 4.25 kV/cm at a field frequency of 50 Hz or when the field frequency decreased below 50 Hz at a field strength of 4.25 kV/cm. The smallest Sauter mean diameter at which the ESX technique can operate before the emulsion starts to form was found to be 115 μm, which corresponds to 54 μm in average droplet diameter.

7.2.3 Effect of AC Fields on Mass Transfer

- Increases in the strength of the AC fields enhanced the mass transfer by increasing the interfacial contact area and droplet agitation as clearly apparent from the decreasing droplet size and increasing droplet speed, horizontal velocity and oscillation amplitude.
- Decreases in the frequency of the AC fields enhanced mass transfer largely by increasing the droplet horizontal velocity, leading to longer droplet residence time and more frequent droplet coalescence and redispersion.
- The trend of the increasing cobalt extraction with increasing field strength (3.50–4.25 kV/cm) and decreasing field frequency (30–70 Hz) increased almost linearly when the field strength increased further from those previously studied (2.50–3.50 kV/cm) even under conditions that were near the regime where the SPE forms. This demonstrates the ESX technique remains effective

when operating with dispersions comprising droplets mainly smaller than 100 μm.

- The ESX technique was able to achieve > 99% copper extraction in only less than 6 s with LIX 84-I, which extractant is known to have a slow extraction kinetics for copper(II). Moreover, the mass-transfer enhancement can still be increased further as there was no indication of the SPE to form within the tested ranges. The result indicates satisfactory mass-transfer performance of the technique to overcome the slow kinetics of the system.

Overall, the results of the present study suggest that the most suitable AC field condition for an ESX operation is at high voltage and low frequency to allow high mass-transfer rates, which is consistent with that observed previously, but below the regime where an emulsion would form to also allow fast phase disengagement.

7.3 RECOMMENDATIONS

The following are some recommendations for future research to further advance the development of ESX for process metallurgy applications that were outside the scope of the present study:

- Some peripheral observations made in the present study suggested that the droplet coalescence while leaving the high-field-strength regions was enhanced. More detailed investigations of this phenomenon would be useful in the design of an ESX contactor.
- The dispersion characteristics of the two tested SX systems under the same experimental conditions were found to be markedly different. Investigations on the effect of the physical properties of the systems on the dispersion characteristics, such as droplet size, motion and oscillation, as well as on the formation of SPE would significantly assist in further developing the ESX technique.
- Further investigations to minimise the proclivity for emulsion formations are needed. The spacing between the electrodes may have a significant influence on the emulsion formation because the droplet population density decreases when the electrode spacing increases at the same feed droplet flow rate.

- The results of the present study showed that the use of insulated parallel-plate electrodes with AC fields is promising for industrial application of the technique. Hence, it is recommended that future research concentrate on developing an ESX column involving insulated parallel-plate electrodes that allow continuous counter-current operations. Experimental studies under counter-current operations will help assess the performance of the technique under conditions that are more relevant to industrial applications. It will also help to generate important data such as, for example, dispersed phase holdup and height of mass transfer unit, to determine whether the ESX technique would be a better technology than conventional SX for the purification of metal ions and impurity removal.

REFERENCES

Ajayi, OO 1978, 'A note on Taylor's electrohydrodynamic theory'. *Proceedings of the Royal Society of London. A. Mathematical and Physical Sciences,* vol. 364, no. 1719, pp. 499–507.

Allan, RS and Mason, SG 1962a, 'Particle behaviour in shear and electric fields I. Deformation and burst of fluid drops'. *Proceedings of the Royal Society of London. Series A. Mathematical and Physical Sciences,* vol. 267, no. 1328, pp. 45–61.

Allan, RS and Mason, SG 1962b, 'Particle motions in sheared suspensions. XIV. Coalescence of liquid drops in electric and shear fields'. *Journal of Colloid Science,* vol. 17, no. 4, pp. 383–408.

Assmann, S 2014, *Effect of electrostatic fields on mass transfer in solvent extraction.* PhD Thesis, Curtin University.

Atten, P 1992, 'On electrocoalescence of water droplets in an insulating liquid'. *Conference Record of the 1992 IEEE Industry Applications Society Annual Meeting,* vol. 2, pp. 1407–1411.

Atten, P 1993, 'Electrocoalescence of water droplets in an insulating liquid'. *Journal of Electrostatics,* vol. 30, pp. 259–269.

Bailes, PJ 1977, 'Electrostatic extraction for metals and non-metals'. *In:* Lucas, BH, Ritcey, GM and Smith, HW, (eds) *Proceedings of the International Solvent Extraction Conference 1977,* Toronto, Canada, pp. 233–241.

Bailes, PJ 1981, 'Solvent extraction in an electrostatic field'. *Industrial & Engineering Chemistry Process Design and Development,* vol. 20, no. 3, pp. 564–570.

Bailes, PJ and Thornton, JD 1971, 'Electrically augmented liquid–liquid extraction in two-component system I.– Single droplet studies'. *In:* Gregory, JG, Evans, B and Weston, PC, (eds) *Proceedings of the International Solvent Extraction Conference 1971,* The Hague, Netherlands, pp. 1431–1439.

Bailes, PJ and Thornton, JD 1974, 'Electrically augmented liquid–liquid extraction in two-component system I.—Multidroplet studies'. *In:* Jeffreys, GV, (ed) *Proceedings of the International Solvent Extraction Conference 1974,* Lyon, France, pp. 1011–1027.

BASF 2014, *Redbook - Mining Solutions.* BASF. pp. 8–12.

Berg, G, Lundgaard, LE, Becidan, M and Sigrnond, RS 2002, 'Instability of electrically stressed water droplets in oil'. *Proceedings of 2002 IEEE 14th International Conference on Dielectric Liquids,* Graz, Austria, pp. 220–224.

Betelú, SI, Fontelos, MA, Kindelán, U and Vantzos, O 2006, 'Singularities on charged viscous droplets'. *Physics of Fluids,* vol. 18, no. 5, pp. 051706-1–051706-4.

Brazier-Smith, PR 1971, 'Stability and shape of isolated and pairs of water drops in an electric field'. *The Physics of Fluids,* vol. 14, no. 1, pp. 1–6.

Brown, AH and Hanson, C 1965, 'Effect of oscillating electric fields on coalescence in liquid+liquid systems'. *Transactions of the Faraday Society,* vol. 61, pp. 1754–1760.

Chakraborty, M, Bhattacharya, C and Datta, S 2003, 'Effect of drop size distribution on mass transfer analysis of the extraction of nickel(II) by emulsion liquid membrane'. *Colloids and Surfaces A: Physicochemical and Engineering Aspects*, vol. 224, no. 1, pp. 65–74.

Chang, LS and Berg, JC 1983, 'Fluid flow and transfer behavior of a drop translating in an electric field at intermediate Reynolds numbers'. *International Journal of Heat and Mass Transfer,* vol. 26, no. 6, pp. 823–832.

Chang, LS, Carleson, TE and Berg, JC 1982, 'Heat and mass transfer to a translating drop in an electric field'. *International Journal of Heat and Mass Transfer,* vol. 25, no. 7, pp. 1023-1030.

Danesi, PR 2004, 'Solvent Extraction Kinetics'. In*:* Rydberg, J *et al.* (eds) *Solvent Extraction Principles and Practice, 2nd Edition.* New York, USA: Marcel Dekker, Inc., pp. 200–248.

Davies, JT 1972a, *Turbulence Phenomena: An Introduction to the Eddy Transfer of Momentum, Mass, and Heat, Particularly at Interfaces.* Academic Press. pp. 239–241.

Davies, JT 1972b, *Turbulence Phenomena: An Introduction to the Eddy Transfer of Momentum, Mass, and Heat, Particularly at Interfaces.* Academic Press. pp. 312–317.

Dehkordi, AM 2002, 'A novel two-impinging-jets reactor for copper extraction and stripping processes'. *Chemical Engineering Journal,* vol. 87, no. 2, pp. 227–238.

Dubash, N and Mestel, AJ 2007, 'Breakup behavior of a conducting drop suspended in a viscous fluid subject to an electric field'. *Physics of Fluids,* vol. 19, no. 7, pp. 072101-1–072101-13.

Duft, D, Achtzehn, T, Müller, R, Huber, BA and Leisner, T 2003, 'Rayleigh jets from levitated microdroplets'. *Nature,* vol. 421, no. 6919, pp. 128–128.

Edge, RM and Grant, CD 1971, 'The terminal velocity and frequency of oscillation of drops in pure systems'. *Chemical Engineering Science,* vol. 26, no. 7, pp. 1001–1012.

Elghazaly, HMA and Castle, GSP 1987, 'Analysis of the multisibling instability of charged liquid Drops'. *IEEE Transactions on Industry Applications,* vol. IA-23, no. 1, pp. 108–113.

Elperin, T and Fominykh, A 2006, 'Mass transfer during solute extraction from a fluid sphere with internal circulation in the presence of alternating electric field'. *Chemical Engineering and Processing: Process Intensification,* vol. 45, no. 7, pp. 578–585.

Eow, JS and Ghadiri, M 2002, 'Electrostatic enhancement of coalescence of water droplets in oil: a review of the technology'. *Chemical Engineering Journal,* vol. 85, no. 2, pp. 357–368.

Eow, JS and Ghadiri, M 2003, 'Motion, deformation and break-up of aqueous drops in oils under high electric field strengths'. *Chemical Engineering and Processing: Process Intensification,* vol. 42, no. 4, pp. 259–272.

Eow, JS, Ghadiri, M, Sharif, AO and Williams, TJ 2001, 'Electrostatic enhancement of coalescence of water droplets in oil: a review of the current understanding'. *Chemical Engineering Journal,* vol. 84, no. 3, pp. 173–192.

Garton, CG and Krasucki, Z 1964, 'Bubbles in insulating liquids: stability in an electric field'. *Proceedings of the Royal Society of London. Series A. Mathematical and Physical Sciences,* vol. 280, no. 1381, pp. 211–226.

Gong, H, Peng, Y, Shang, H, Yang, Z and Zhang, X 2015, 'Non-linear vibration of a water drop subjected to high-voltage pulsed electric field in oil: Estimation of stretching deformation and resonance frequency'. *Chemical Engineering Science,* vol. 128, pp. 21–27.

Guo, C, He, L and Xin, Y 2015, 'Deformation and breakup of aqueous drops in viscous oil under a uniform AC electric field'. *Journal of Electrostatics,* vol. 77, pp. 27–34.

Ha, J-W and Yang, S-M 1998, 'Effect of nonionic surfactant on the deformation and breakup of a drop in an electric field'. *Journal of Colloid and Interface Science,* vol. 206, no. 1, pp. 195–204.

Ha, J-W and Yang, S-M 2000, 'Deformation and breakup of newtonian and non-newtonian conducting drops in an electric field'. *Journal of Fluid Mechanics,* vol. 405, pp. 131–156.

Hadamard, JS 1911, 'Mouvement permanent lent d'une sphère liquide et visqueuse dans un liquide visqueux'. *Comptes rendus hebdomadaires des séances de l'Académie des sciences.,* vol. 152, pp. 1735–1738.

He, W, Chang, JS and Baird, MHI 1997, 'Enhancement of interphase mass transfer by a pulsed electric field'. *Journal of Electrostatics,* vol. 40, pp. 259–264.

Hendricks, CD 1973, 'Charging Macroscopic Particles'. In*:* Moore, AD (ed) *Electrostatics and Its Applications.* New York: John Wiley and Sons, pp. 57–85.

Kaji, N, Mori, YH and Tochitani, Y 1985, 'Heat transfer enhancement due to electrically induced resonant oscillation of drops'. *Journal of Heat Transfer,* vol. 107, no. 4, pp. 788–793.

Kaji, N, Mori, YH, Tochitani, Y and Komotori, K 1980, 'Augmentation of direct-contact heat transfer to drops with an intermittent electric field'. *Journal of Heat Transfer,* vol. 102, no. 1, pp. 32–37.

Kalinske, AA and Pien, CL 1944, 'Eddy diffusion'. *Industrial & Engineering Chemistry,* vol. 36, no. 3, pp. 220–223.

Karyappa, RB, Deshmukh, SD and Thaokar, RM 2014, 'Breakup of a conducting drop in a uniform electric field'. *Journal of Fluid Mechanics,* vol. 754, no. 550–589.

Karyappa, RB, Naik, AV and Thaokar, RM 2016, 'Electroemulsification in a uniform electric field'. *Langmuir,* vol. 32, no. 1, pp. 46–54.

Kashdan, JT, Shrimpton, JS and Whybrew, A 2007, 'A digital image analysis technique for quantitative characterisation of high-speed sprays'. *Optics and Lasers in Engineering,* vol. 45, no. 1, pp. 106–115.

Klink, IM, Phillips, RJ and Dungan, SR 2011, 'Effect of emulsion drop-size distribution upon coalescence in simple shear flow: A population balance study'. *Journal of Colloid and Interface Science,* vol. 353, no. 2, pp. 467–475.

Kordosky, GA, Olafson, SM, Lewis, RG, Deffner, VL and House, JE 1987, 'A state-of-the-art discussion on the solvent extraction reagents used for the recovery of copper from dilute sulfuric acid leach solutions'. *Separation Science and Technology,* vol. 22, no. 2–3, pp. 215–232.

Kowalski, W and Ziolkowski, Z 1981, 'Increase in rate of mass transfer in extraction columns by means of an electric field'. *International Chemical Engineering,* vol. 21, no. 2, pp. 323–327.

Lac, E and Homsy, GM 2007, 'Axisymmetric deformation and stability of a viscous drop in a steady electric field'. *Journal of Fluid Mechanics,* vol. 590, pp. 239–264.

Lewis, WK and Whitman, WG 1924, 'Principles of gas absorption'. *Industrial & Engineering Chemistry,* vol. 16, no. 12, pp. 1215–1220.

Li, B, Vivacqua, V, Ghadiri, M, Sun, Z, Wang, Z and Li, X 2017, 'Droplet deformation under pulsatile electric fields'. *Chemical Engineering Research and Design,* vol. 127, no. 180-188.

Li, W, Wang, Y, Lu, HT, Mumford, KA, Smith, KH and Stevens, GW 2019, 'Comparison of mass transfer performance of pulsed columns with Tenova kinetics internals and standard disc and doughnut internals'. *Hydrometallurgy,* vol. 186, no. 132-142.

Löwe, J-M, Hinrichsen, V, Roisman, IV and Tropea, C 2020, 'Behavior of charged and uncharged drops in high alternating tangential electric fields'. *Physical Review E,* vol. 101, no. 2, pp. 023102.

Mackenzie, M 2015, 'Solvent extraction of nickel - 28 years of endeavour'. *ALTA 2015 Nickel-Cobalt-Copper Conference,* Perth, Australia, pp. 191–211.

Martin, L, Vignet, P, Fombarlet, C and Lancelot, F 1983, 'Electrical field contactor for solvent extraction'. *Separation Science and Technology,* vol. 18, no. 14–15, pp. 1455–1471.

Maruyama, M, Ishii, H and Yamaguchi, M 2003, 'Deformation and disintegration behaviour of single water drops in an oil phase in an electric field'. *Developments in Chemical Engineering and Mineral Processing,* vol. 11, no. 5–6, pp. 491–497.

Masoum, MAS and Fuchs, EF 2015, 'Chapter 1 - Introduction to Power Quality'. In*:* Masoum, MAS and Fuchs, EF (eds) *Power Quality in Power Systems and Electrical Machines.* 2nd edn. Boston: Academic Press, pp. 1–104.

Melcher, JR and Taylor, GI 1969, 'Electrohydrodynamics: A review of the role of interfacial shear stresses'. *Annual Review of Fluid Mechanics,* vol. 1, no. 1, pp. 111–146.

Mohamed, AS, Lopez-Herrera, JM, Herrada, MA, Modesto-Lopez, LB and Gañán-Calvo, AM 2016, 'Effect of a surrounding liquid environment on the electrical disruption of pendant droplets'. *Langmuir,* vol. 32, no. 27, pp. 6815–6824.

Mora, JFdl 2007, 'The fluid dynamics of Taylor cones'. *Annual Review of Fluid Mechanics*, vol. 39, no. 1, pp. 217–243.

Morrison, FA, Jr. 1977, 'Transient Heat and Mass Transfer to a Drop in an Electric Field'. *Journal of Heat Transfer*, vol. 99, no. 2, pp. 269–273.

Mugele, RA and Evans, HD 1951, 'Droplet Size Distribution in Sprays'. *Industrial & Engineering Chemistry*, vol. 43, no. 6, pp. 1317–1324.

Ng, K and Yianneskis, M 2000, 'Observations on the Distribution of Energy Dissipation in Stirred Vessels'. *Chemical Engineering Research and Design*, vol. 78, no. 3, pp. 334–341.

Noik, C, Chen, J and Dalmazzone, CSH 2006, 'Electrostatic demulsification on crude oil: A state-of-the-art review'. SPE: Society of Petroleum Engineers.

O'Konski, CT and Thacher, HC 1953, 'The distortion of aerosol droplets by an electric field'. *The Journal of Physical Chemistry*, vol. 57, no. 9, pp. 955–958.

Park, JY and Blair, LM 1975, 'The effect of coalescence on drop size distribution in an agitated liquid–liquid dispersion'. *Chemical Engineering Science*, vol. 30, no. 9, pp. 1057–1064.

Pohl, HA 1973, 'Nonuniform Field Effects: Dielectrophoresis'. In: Moore, AD (ed) *Electrostatics and Its Applications.* New York: John Wiley and Sons, pp. 337–361.

Raut, JS, Akella, S, Singh, A and Naik, VM 2009, 'Catastrophic drop breakup in electric field'. *Langmuir*, vol. 25, no. 9, pp. 4829–4834.

Rayleigh, L 1882, 'XX. On the equilibrium of liquid conducting masses charged with electricity'. *The London, Edinburgh, and Dublin Philosophical Magazine and Journal of Science*, vol. 14, no. 87, pp. 184–186.

Reddy, BR and Priya, DN 2005, 'Process development for the separation of copper(II), nickel(II) and zinc(II) from sulphate solutions by solvent extraction using LIX 84 I'. *Separation and Purification Technology*, vol. 45, no. 2, pp. 163–167.

Reeves, MJ, Bailey, AG, Howard, AG and Broan, CJ 1999, 'Factors influencing operational efficiency of an electrostatic solvent extraction system'. *In:* Taylor, DM, (ed) *Electrostatics 1999, Proceedings of the 10th International Conference*, Cambridge, UK, pp. 257–260.

Richardson, CB, Pigg, AL, Hightower, RL and Lighthill, MJ 1989, 'On the stability limit of charged droplets'. *Proceedings of the Royal Society of London. A. Mathematical and Physical Sciences*, vol. 422, no. 1863, pp. 319–328.

Ritcey, GM 1980, 'Crud in solvent extraction processing — a review of causes and treatment'. *Hydrometallurgy*, vol. 5, no. 2, pp. 97–107.

Ritcey, GM 2006, *Solvent Extraction, Principles and Application to Process Metallurgy.* Ottawa, Canada: G.M. Ritcey and Associates Inc. pp. 438–447.

Rybczyński, W 1911, 'Über die fortschreitende Bewegung einer flüssigen Kugel in einen zähen Medium'. *Bulletin international de l'Académie des sciences de Cracovie, Classe des sciences mathématiques et naturelles. Série A, Sciences mathématiques*, vol. 1, no. 40–46.

Ryce, SA and Patriarche, DA 1965, 'Energy considerations in the electrostatic dispersion of liquids'. *Canadian Journal of Physics,* vol. 43, no. 12, pp. 2192–2199.

Saranin, BA 1999, 'Some effects of the electrostatic interaction of water drops in the atmosphere'. *Technical Physics,* vol. 44, no. 12, pp. 1407–1412.

Schroeder, RR and Kintner, RC 1965, 'Oscillations of drops falling in a liquid field'. *AIChE Journal,* vol. 11, no. 1, pp. 5–8.

Schweizer, JW and Hanson, DN 1971, 'Stability limit of charged drops'. *Journal of Colloid and Interface Science,* vol. 35, no. 3, pp. 417–423.

Scott, TC 1987a, 'Surface area generation and droplet size control using pulsed electric fields'. *AIChE Journal,* vol. 33, no. 9, pp. 1557–1559.

Scott, TC 1987b, 'Visualization of flow fields and interfacial phenomena in liquid–liquid solvent extraction'. *Separation Science and Technology,* vol. 22, no. 2–3, pp. 503–511.

Scott, TC 1989, 'Use of electric fields in solvent extraction: A review and prospectus'. *Separation and Purification Methods,* vol. 18, no. 1, pp. 65–109.

Scott, TC, Basaran, OA and Byers, CH 1990, 'Characteristics of electric-field-induced oscillations of translating liquid droplets'. *Industrial & Engineering Chemistry Research,* vol. 29, no. 5, pp. 901–909.

Scott, TC, DePaoli, DW and Sisson, WG 1994, 'Further development of the electrically driven emulsion-phase contactor'. *Industrial & Engineering Chemistry Research,* vol. 33, no. 5, pp. 1237–1244.

Scott, TC and Sisson, WG 1988, 'Droplet size characteristics and energy input requirements of emulsions formed using high-intensity-pulsed electric fields'. *Separation Science and Technology,* vol. 23, no. 12–13, pp. 1541–1550.

Scott, TC and Wham, RM 1989, 'An electrically driven multistage countercurrent solvent extraction device: The emulsion-phase contactor'. *Industrial & Engineering Chemistry Research,* vol. 28, no. 1, pp. 94–97.

Shchukin, SI and Grigor'ev, AI 2000, 'Breakup of an uncharged droplet in an electrostatic field'. *Technical Physics,* vol. 45, no. 6, pp. 694–697.

Sherwood, JD 1988, 'Breakup of fluid droplets in electric and magnetic fields'. *Journal of Fluid Mechanics,* vol. 188, no. 133–146.

Singh, M, Gawande, N, Mayya, YS and Thaokar, R 2019, 'Effect of the quadrupolar trap potential on the rayleigh instability and breakup of a levitated charged droplet'. *Langmuir,* vol. 35, no. 48, pp. 15759–15768.

Sole, K, Zarate, G, Steeples, J, Tinkler, O and Robinson, T 2013, 'Global survey of copper solvent extraction operations and practices'. *Copper-Cobre 2013,* Santiago, Chile, pp. 137–148.

Steffens, MJ 2011, *Development of an Electrostatically Assisted Solvent Extraction Column.* PhD Thesis, Curtin University.

Stewart, G and Thornton, J 1967, 'Charge and velocity characteristics of electrically charged droplets. Part II: Preliminary measurement of droplet charge and velocity'. *Instn. Chem. Engrs. Symposium Series,* pp. 37–42.

Szymanowski, J and Borowiak-resterna, A 1991, 'Chemistry and analytical characterization of the effect of hydroxyoxime structure upon metal-complexing and extraction properties'. *Critical Reviews in Analytical Chemistry,* vol. 22, no. 1–2, pp. 519–566.

Taflin, DC, Ward, TL and Davis, EJ 1989, 'Electrified droplet fission and the Rayleigh limit'. *Langmuir,* vol. 5, no. 2, pp. 376–384.

Taylor, G 1964, 'Disintegration of water drops in an electric field'. *Proceedings of the Royal Society of London. Series A. Mathematical and Physical Sciences,* vol. 280, no. 1382, pp. 383–397.

Taylor, G 1966, 'Studies in electrohydrodynamics. I. The circulation produced in a drop by electrical field'. *Proceedings of the Royal Society of London. Series A. Mathematical and Physical Sciences,* vol. 291, no. 1425, pp. 159–166.

Tennakoon, S, Perera, L, Robinson, DA and Perera, S 2004, 'Flicker transfer in radial power systems'. *In:* Saha, T, (ed) *Australasian Universities Power Engineering Conference (AUPEC 2004),* Brisbane, Australia, pp. 1–6.

Torza, S, Cox, RG and Mason, SG 1971, 'Electrohydrodynamic deformation and burst of liquid drops'. *Philosophical Transactions of the Royal Society of London. Series A, Mathematical and Physical Sciences,* vol. 269, no. 1198, pp. 295–319.

Trinh, E, Zwern, A and Wang, TG 1982, 'An experimental study of small-amplitude drop oscillations in immiscible liquid systems'. *Journal of Fluid Mechanics,* vol. 115, no. 453–474.

Vacek, V and Nekovář, P 1977, 'Remarks on the behaviour of single oscillating droplets'. *The Chemical Engineering Journal,* vol. 13, no. 2, pp. 185-189.

Vancas, MF 2003, 'Pulsed column and mixer-settler applications in solvent extraction'. *JOM,* vol. 55, no. 7, pp. 43–45.

Vivacqua, V, Ghadiri, M, Abdullah, AM, Hassanpour, A, Al-Marri, MJ, Azzopardi, B, Hewakandamby, B and Kermani, B 2016, 'Linear dynamics modelling of droplet deformation in a pulsatile electric field'. *Chemical Engineering Research and Design,* vol. 114, no. 162–170.

Vizika, O and Saville, DA 1992, 'The electrohydrodynamic deformation of drops suspended in liquids in steady and oscillatory electric fields'. *Journal of Fluid Mechanics,* vol. 239, no. 1–21.

Warren, KW and Byeseda, JJ 1990, 'The electrodynamic contactor for extraction'. *In:* Sekine, T, (ed) *ISEC 1990,* Kyoto, Japan, pp. 1417–1422.

Warren, KW and Prestridge, FL 1979, *Apparatus for Application of Electrostatic Fields to Mixing and Separating Fluids.* United States patent application 4,161,439.

Wegener, M, Paul, N and Kraume, M 2014, 'Fluid dynamics and mass transfer at single droplets in liquid/liquid systems'. *International Journal of Heat and Mass Transfer,* vol. 71, no. 475–495.

Wham, RM and Byers, CH 1987, 'Mass transport from single droplets in imposed electric fields'. *Separation Science and Technology,* vol. 22, no. 2-3, pp. 447–466.

Whitman, WG 1962, 'The two film theory of gas absorption'. *International Journal of Heat and Mass Transfer,* vol. 5, no. 5, pp. 429–433.

Wigley, G, Heath, J, Pitcher, G and Whybrew, A 2000, 'Experimental analysis of the response of a PDA system to a partially atomized spray'. *10th International Symposium on Applications of Laser Techniques to Fluid Mechanics, Lisbon*.

Williams, TJ and Bailey, AG 1986, 'Changes in the size distribution of a water-in-oil emulsion due to electric field induced coalescence'. *IEEE Transactions on Industry Applications,* vol. IA-22, no. 3, pp. 536–541.

Winnikow, S and Chao, BT 1966, 'Droplet Motion in Purified Systems'. *The Physics of Fluids,* vol. 9, no. 1, pp. 50–61.

Wu, H and Patterson, GK 1989, 'Laser-Doppler measurements of turbulent-flow parameters in a stirred mixer'. *Chemical Engineering Science,* vol. 44, no. 10, pp. 2207–2221.

Yamaguchi, M, Sugaya, H and Katayama, T 1988, 'Hydrodynamic behavior of dispersed phase in a spray column with an electric field for liquid–liquid extraction'. *Journal of Chemical Engineering of Japan,* vol. 21, no. 2, pp. 179–183.

Yamaguchi, M, Sugaya, H and Katayama, T 1989, 'Liquid–liquid extraction characteristics of a spray column with a D.C. electric field'. *Journal of Chemical Engineering of Japan,* vol. 22, no. 1, pp. 25–29.

Yan, H, He, L, Luo, X, Wang, J, Huang, X, Lü, Y and Yang, D 2015, 'Investigation on transient oscillation of droplet deformation before conical breakup under alternating current electric field'. *Langmuir,* vol. 31, no. 30, pp. 8275–8283.

Yoshida, F, Yamaguchi, M and Katayama, T 1986, 'An experimental study of electrohydrodynamic dispersion from a liquid film flowing down an inclined plate into a continuous liquid phase'. *Journal of Chemical Engineering of Japan,* vol. 19, no. 1, pp. 1–7.

APPENDICES

Appendix A: Additional Information on the Motorised Positioning Table

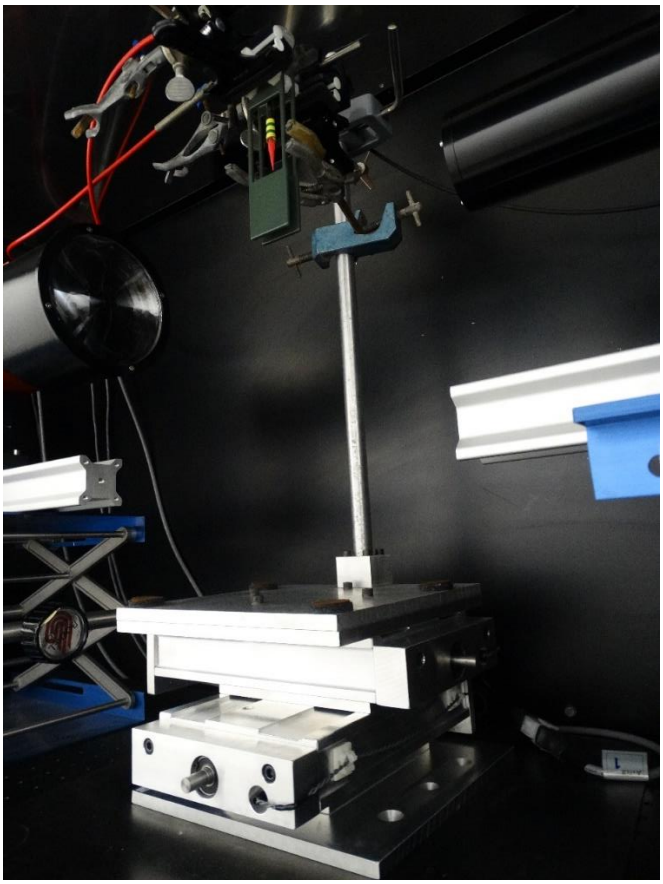

Figure A1. Photograph of the stand supporting the electrodes that was mounted on top of the motorised positioning XY table.

Figure A2. Photograph of the top plate of the motorised positioning table.

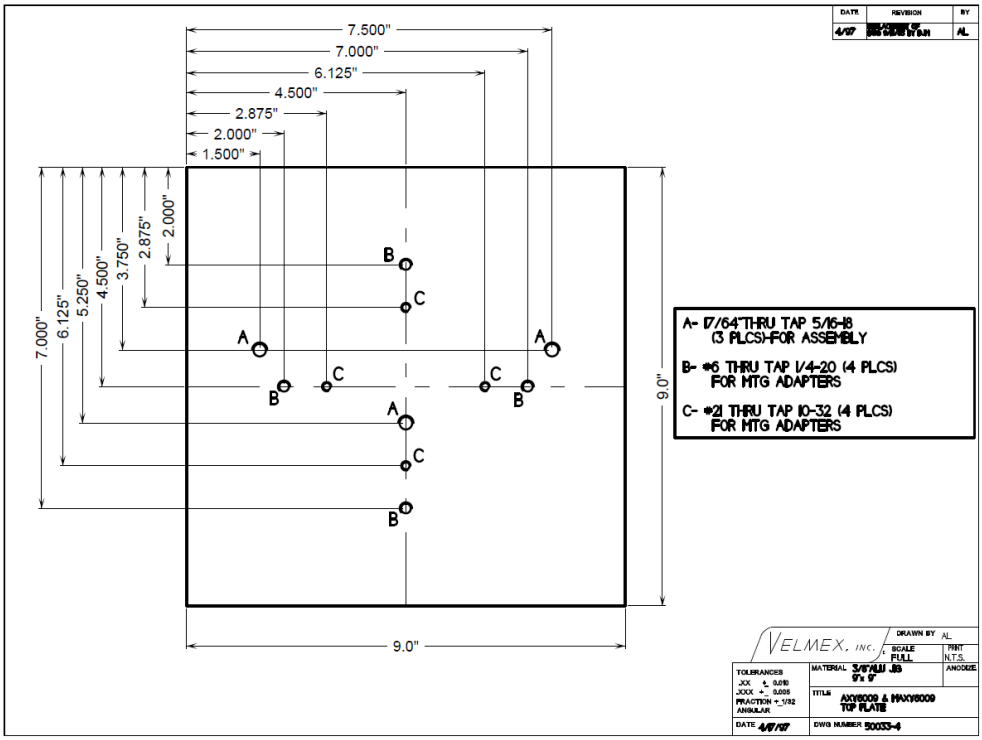

Figure A3. Schematic diagram of the top plate of the motorised positioning table from the top view.

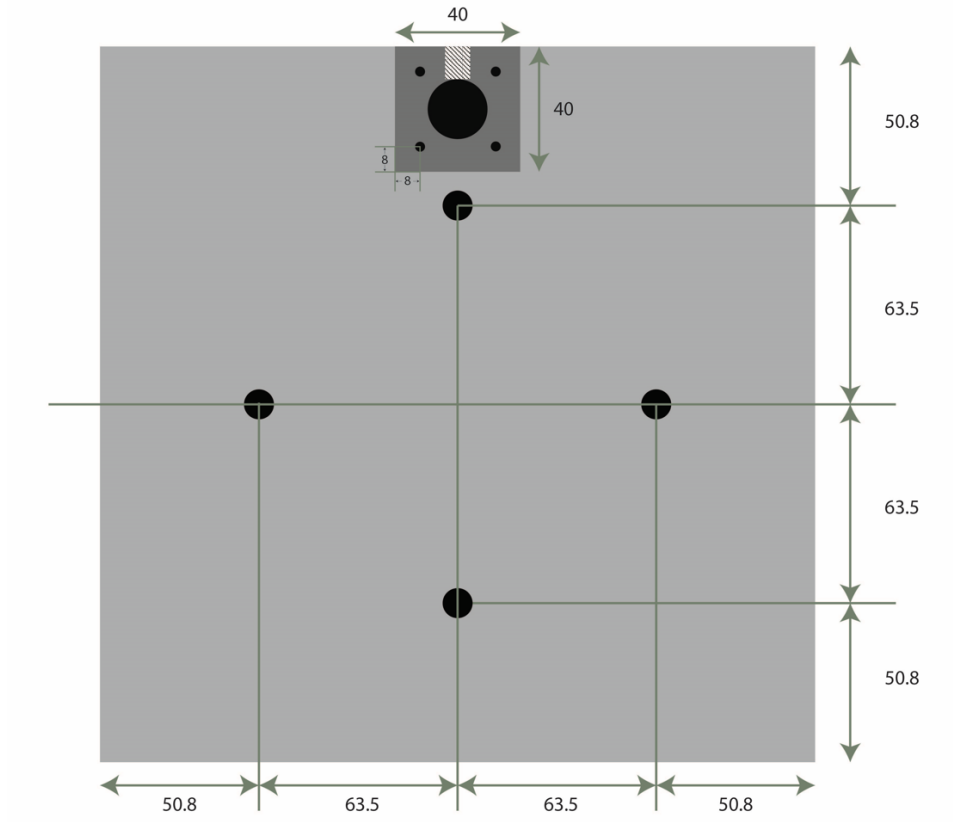

Figure A4. Schematic diagram of the mounting plate from the top view. All dimensions are in mm.

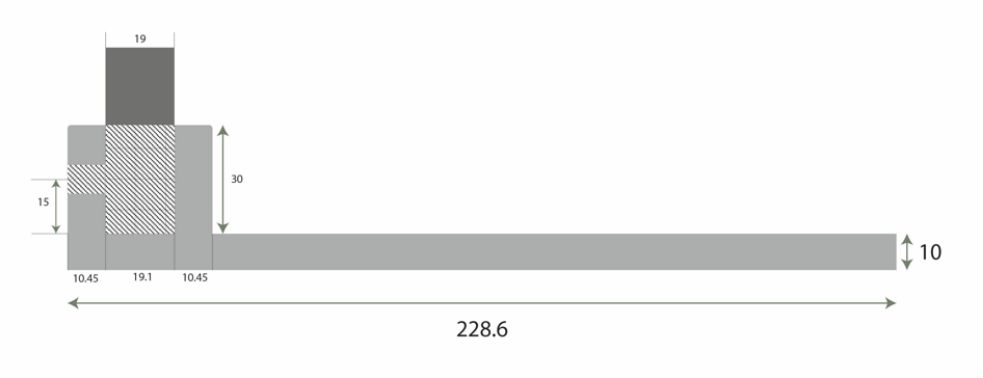

Figure A5. Schematic diagram of the mounting plate from the side view. All dimensions are in mm.

Appendix B: Additional Information on the Laser Interlock System

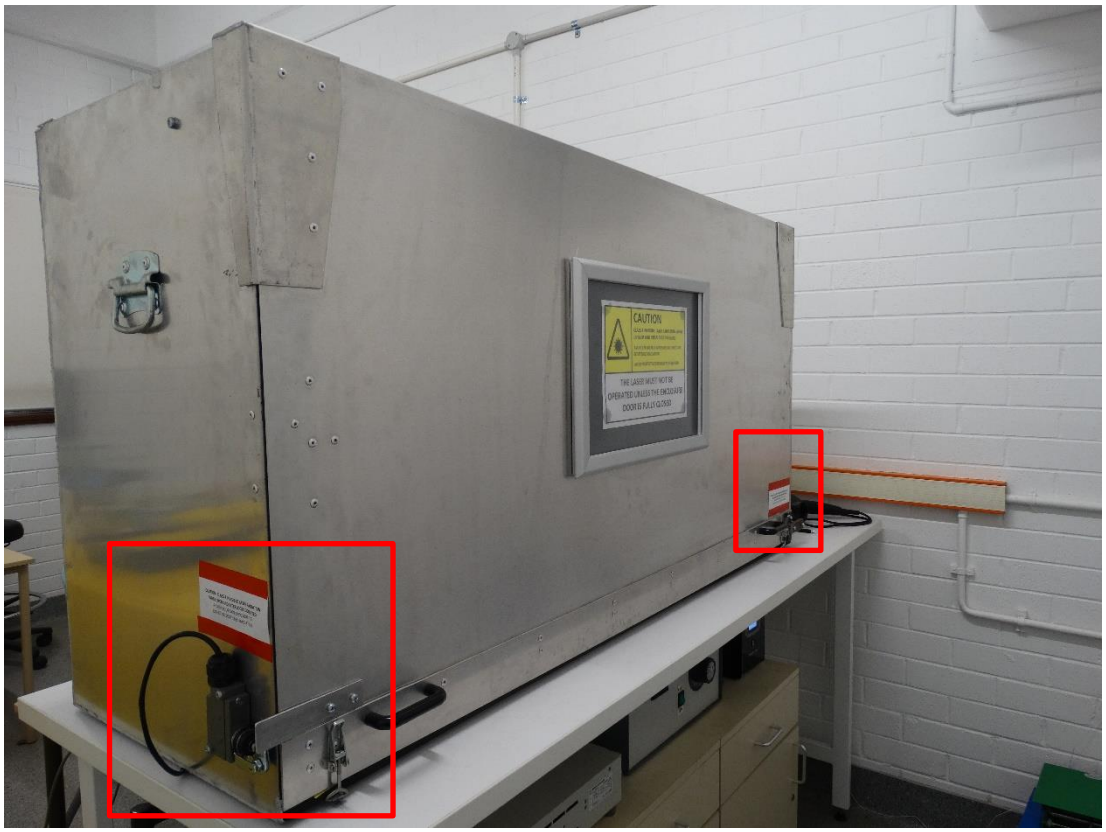

Figure B1. Photographs of the aluminium enclosure when closed. The switches that will trigger the interlock system are inside the red squares.

Figure B2. More close-up photograph of the switches that will trigger the interlock system when defeated.

Appendix C: Photographs of the Experimental Setup

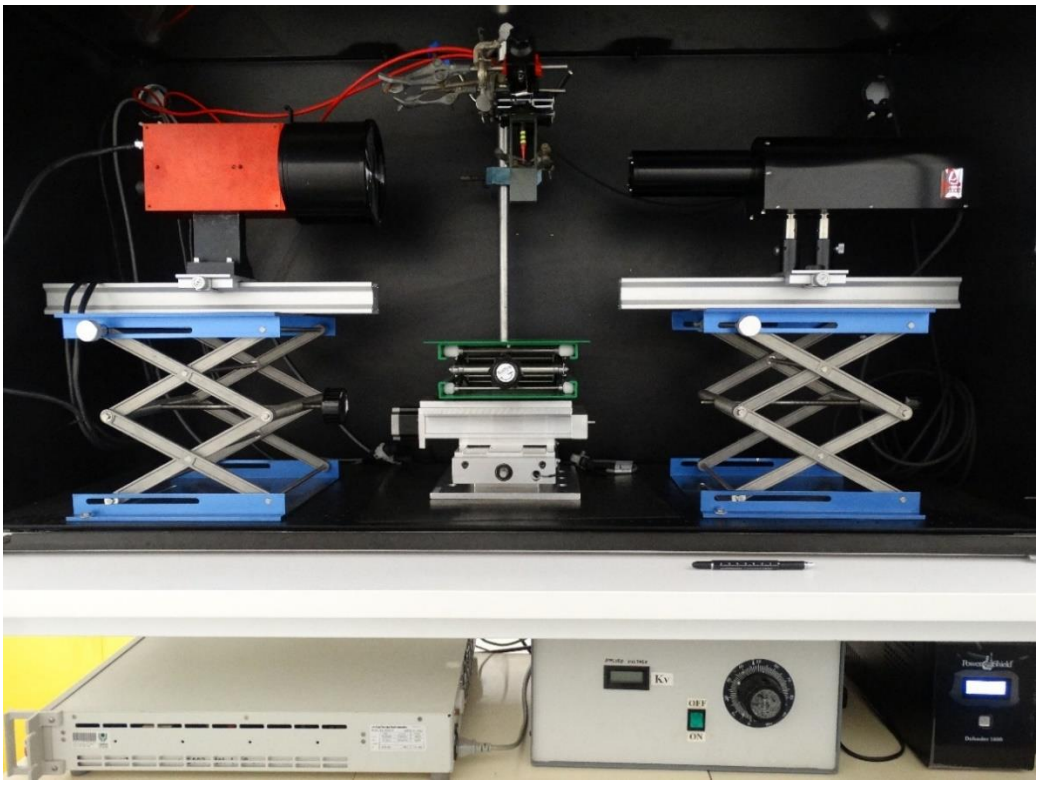

Figure C1. Photograph of the experimental setup from the front view.

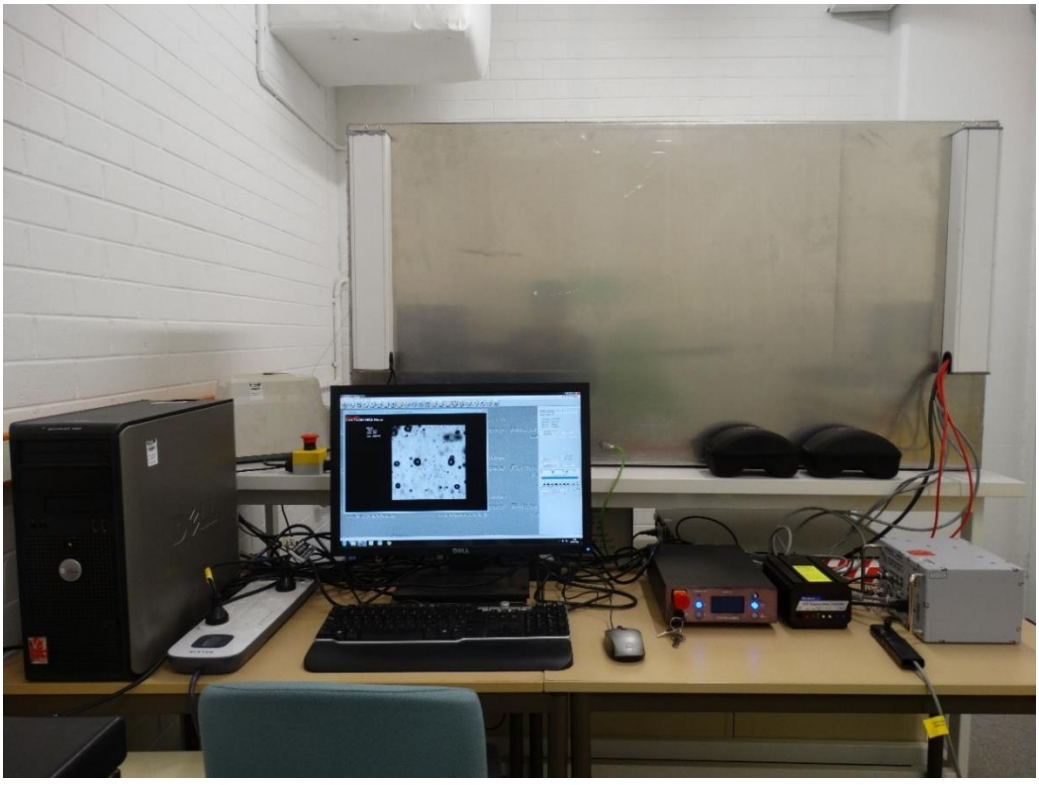

Figure C2. Photograph of the experimental setup from the back view.

Appendix D: Diagrams and Photographs of the Electrodes

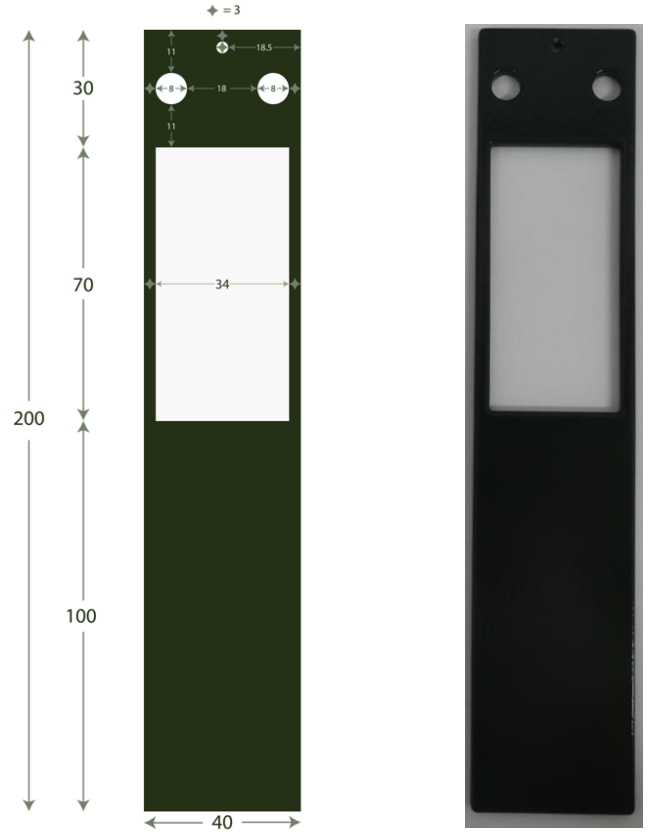

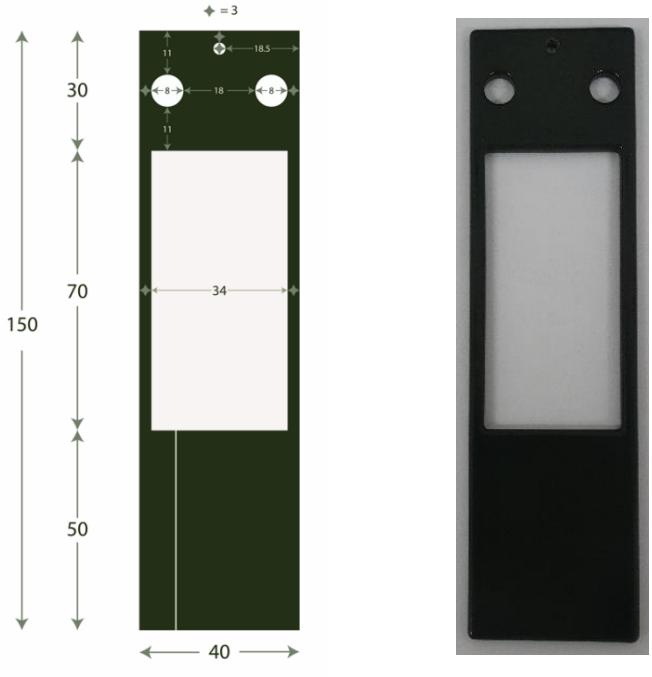

These schematic diagrams of the electrodes are redrawn from Assmann (2014). All dimensions are in mm. The electrode thickness is 3 mm. The green colour is the droplet insulation made of ethylene tetrafluoroethylene (ETFE).

Appendix E: Photographs of Dispersion Taken with Different Columns

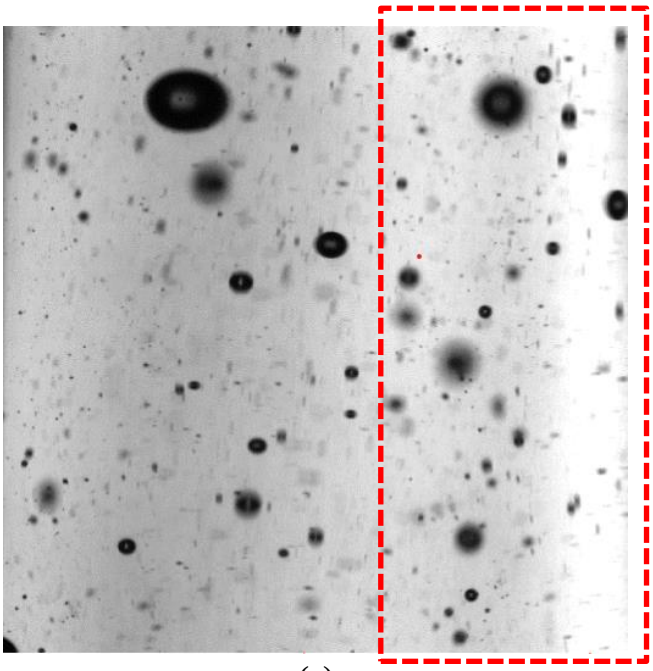

(a)

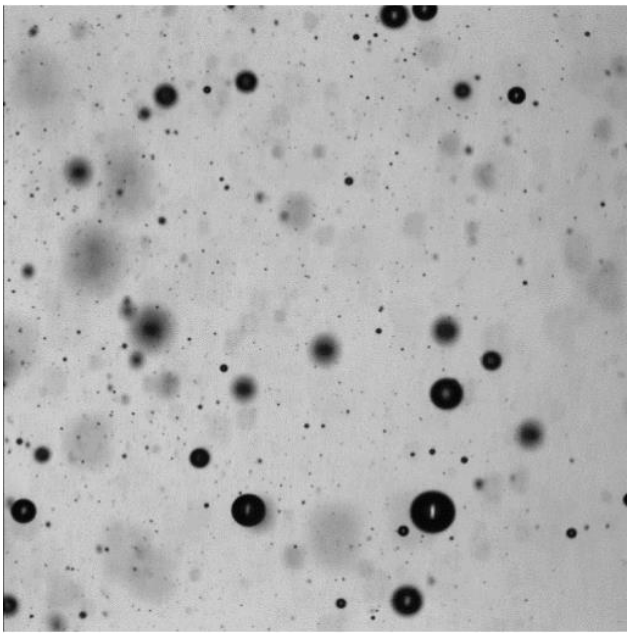

(b)

Figure E1. Examples of an image taken from (a) the extraction column and (b) the dispersion column at comparable experimental conditions. Images taken from the extraction column show significant distortions particularly in the square area.

Appendix F: Diagram and Photograph of the Extraction Column

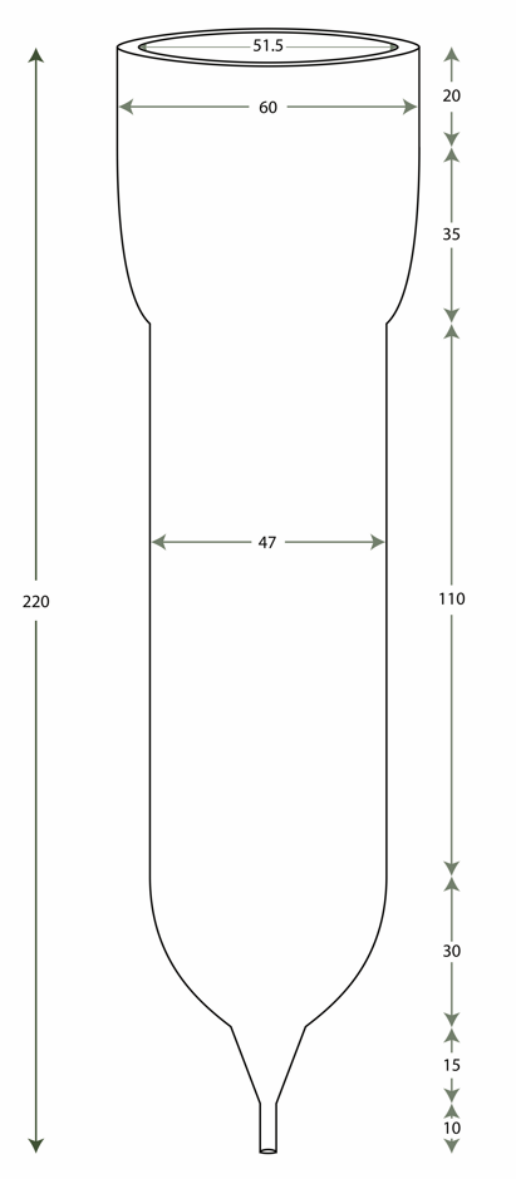

The schematic diagram of the extraction column is redrawn from Assmann (2014). All dimensions are in mm.

Appendix G: An Example of the Analysis Summary Generated by the VisiSize Software

OXFORD LASERS IMAGING SYSTEMS
VISISIZE ANALYSIS REPORT
VisiSize 6.204
C:\USERS\VISISIZE\DESKTOP\RESULTS\T1.TXT
21/01/2021 14:52
Velocity mode
Run: T1(File sequence: E15_0001 - E15_4000)

Calibration: C:\Program Files\Oxford Lasers\VisiSize\Calibration\MC2LO4x4.clb

Field Type	AC Field
Applied Voltage	3.5 kV/cm
Applied Frequency	50 Hz
Nozzle	0.26 mm
Droplet Flowrate	0.25 mL/min
Camera Magnification	4.0 Mag, SF 0.5
Pulse Duration	0.82 um
SAMPLE ANALYSIS SUMMARY (diameters in microns)	
Averages:	
Arithmetic mean	57.2
Surface mean	75.7
Volume mean	106
Sauter mean	207.8
Volume-weighted mean	407.3
Average velocity	0.8
Spread:	
Minimum diameter	23.2
Maximum diameter	967.6
Relative span	1.31
Deviation	0
Min velocity	0
Max velocity	3.8
Volume percentiles:	
10%	98.7
50%	333
90%	534.8
Sphericity	0.81

PERFORMANCE SUMMARY	
In-focus count	7067
Field of view (microns)	5186 x 3859
Focus reject %	91.3
Corrected count	142325
Probe depth (microns)	20000
Shape reject %	1.4
Video frames	2000
Probe volume (cu mm)	400.3322
Border reject %	4.96
Empty frames	178
Particle volume (cu mm)	8.88E+01
Run time (sec)	47
Particles / frame	3.5
Volume density	1.11E-04
Sample size chk (%)	0.53
Background intensity	176
Surface area (sq mm)	2563.64
Contrast	0
Micron/pixel ratio	7.538
Surface area / volume ratio	28.9
Particles/cu mm	0.18
Magnification	0.98
SYSTEM SETTINGS	
Focus rejection	ON
Border rejection	ON
DOF correction	ON
Edge contact correction	ON
Shape rejection	ON
Background intensity rejection	OFF
System details	
Micron/pixel ratio	7.538
Minimum particle area	12
Data acquisition rate	30
Maximum particle area	262144
Horizontal indents	0, 0
Shape parameter	0.5
Vertical indents	0, 0
Acceptance length	20000
Threshold	Adaptive: 75
Background rejection limits	120, 250
Diameter smoothing	None
Velocity smoothing	None
Velocity settings:	
Direction	Down
Maximum angle deviation	No limit
Interval	40
Maximum area ratio	1.1
Maximum pixel separation	20
Maximum halo area ratio	1.1

DIAMETER DISTRIBUTION TABLE									
DIAMETER (microns)		DOF FACTOR	EC FACTOR	COUNT	% NUMBER	% AREA	% VOLUME	CUM % VOL	AV. SPEED (m/s)
23	29.7	42.21	1.01	9477	6.66	0.9	0.12	0.1204	0.66
29.7	38.4	32.67	1.01	44987	31.61	6.34	1.04	1.1639	0.62
38.4	49.6	25.29	1.02	36363	25.55	8.52	1.81	2.9748	0.54
49.6	64.1	19.57	1.02	24612	17.29	9.43	2.56	5.5318	0.63
64.1	82.8	15.15	1.03	9336	6.56	6.06	2.14	7.6706	0.63
82.8	107	11.73	1.04	7356	5.17	7.84	3.54	11.2153	0.6
107	138.2	9.08	1.05	3552	2.5	6.74	4.07	15.2845	0.72
138.2	178.5	7.03	1.07	2379	1.67	7.07	5.34	20.6255	0.82
178.5	230.6	5.44	1.09	1469	1.03	7.49	7.4	28.0304	0.89
230.6	298	4.21	1.12	1277	0.9	10.9	13.95	41.9836	0.85
298	384.9	3.26	1.16	884	0.62	12.22	19.91	61.898	0.94
384.9	497.3	2.52	1.22	532	0.37	12.3	25.9	87.8015	0.92
497.3	642.5	1.95	1.3	86	0.06	3.19	8.52	96.3197	1.04
642.5	830.1	1.51	1.41	13	0.01	0.78	2.69	99.0125	1.33
830.1	1072.4	1.17	1.58	2	0	0.21	0.99	100	1

Size-Velocity Correlation :																				
	0	0.25	0.5	0.75	1	1.25	1.5	1.75	2	2.25	2.5	2.75	3	3.25	3.5	3.75	4	4.25	4.5	4.75
23	0	28	108	69	5	1	1	0	0	3	3	1	2	1	0	0	0	0	0	0
29.71	2	265	703	273	22	16	14	13	7	8	4	6	11	9	4	0	0	0	0	0
38.39	7	329	759	252	20	9	8	0	2	3	10	6	1	2	3	0	0	0	0	0
49.6	1	225	644	234	38	13	16	8	9	6	7	6	10	4	5	1	0	0	0	0
64.08	2	92	261	182	25	13	6	4	2	1	5	3	0	1	0	0	0	0	0	0
82.78	5	112	309	120	22	11	7	4	1	3	1	3	1	2	1	0	0	0	0	0
106.95	3	36	168	101	19	18	6	7	0	4	2	1	3	2	0	1	0	0	0	0
138.17	3	36	120	88	15	9	8	10	5	8	3	3	3	2	3	0	0	0	0	0
178.51	0	19	81	85	15	9	9	5	3	6	6	3	3	2	1	0	0	0	0	0
230.63	1	9	69	127	23	14	8	4	2	6	3	1	0	2	1	0	0	0	0	0
297.96	2	10	45	99	31	13	6	6	5	7	1	1	2	3	2	0	0	0	0	0
384.95	0	9	17	79	39	11	5	6	2	1	1	1	1	1	0	0	0	0	0	0
497.33	0	0	4	12	9	2	3	2	1	0	0	0	1	0	0	0	0	0	0	0
642.52	0	0	2	1	1	0	0	0	0	1	0	0	1	0	0	0	0	0	0	0
830.1	0	0	0	0	1	0	0	0	0	0	0	0	0	0	0	0	0	0	0	0
1072.44	0	0	0	0	0	0	0	0	0	0	0	0	0	0	0	0	0	0	0	0
1385.53	0	0	0	0	0	0	0	0	0	0	0	0	0	0	0	0	0	0	0	0
1790.02	0	0	0	0	0	0	0	0	0	0	0	0	0	0	0	0	0	0	0	0
2312.61	0	0	0	0	0	0	0	0	0	0	0	0	0	0	0	0	0	0	0	0
2987.75	0	0	0	0	0	0	0	0	0	0	0	0	0	0	0	0	0	0	0	0

Appendix H: An Example of the Individual Droplet Data Generated by the VisiSize Software

OXFORD LASERS IMAGING SYSTEMS
INDIVIDUAL PARTICLE DATA
VisiSize 6.204
C:\Users\Visisize\Desktop\Results\1.vsp
######
Velocity Mode

Frame	Particle ID	Diameter	Velocity	Angle	Shape Factor
1	1	154.884	0.56535	0	0.850023
1	2	31.0695	0.595931	18.4349	0.713699
1	3	41.6257	0.3769	0	0.861309
1	4	73.1843	0.3769	0	0.591714
1	5	36.0994	0.421387	-26.565	0.819591
1	6	98.3976	0.421387	26.565	0.961526
2	1	33.2656	0.421387	26.565	0.634849
2	2	41.9062	0.3769	0	0.904542
2	3	37.4603	0.3769	0	0.855454
2	4	98.4931	0.421387	26.565	0.902015
3	1	154.007	0.7538	0	0.880837
3	2	32.6683	0.3769	0	0.680895
3	3	31.9213	0.56535	0	0.715604
3	4	73.5595	0.421387	-26.565	0.550224
3	5	36.0473	0.3769	0	0.839813
4	1	67.8638	0.56535	0	0.53609
4	2	32.8172	0.421387	-26.565	0.768899
4	3	39.0041	0.3769	0	0.786979
4	4	74.9225	0.3769	0	0.58331
4	5	36.34	0.421387	-26.565	0.819591
4	6	98.8788	0.421387	-26.565	0.913639
5	1	68.0141	0.3769	0	0.542303
5	2	32.1687	0.3769	0	0.780936
5	3	31.5224	0.56535	0	0.722725
6	1	92.7758	0.56535	0	0.829588
6	2	169.243	0.56535	0	0.878288
6	3	31.3535	0.3769	0	0.82663
6	4	73.6679	0.3769	0	0.595918
7	1	93.2538	0.18845	0	0.79587
7	2	66.0786	0.3769	0	0.580543
8	1	168.525	0.56535	0	0.882758
8	2	31.275	0.3769	0	0.857872
9	1	94.332	0.595931	18.4349	0.760907

10	1	48.3314	0.18845	0	0.669856
10	2	169.083	0.421387	26.565	0.877246
10	3	26.3055	0.3769	0	0.789216
11	1	49.1781	0.3769	0	0.695952
11	2	46.7144	0.595931	-18.4349	0.766822
12	1	49.2396	0.595931	18.4349	0.695865
13	1	49.112	0.421387	-26.565	0.703168
13	2	109.266	1.19186	71.5649	0.798612
13	3	123.839	0.595931	-18.4349	0.770754
14	1	49.3023	0.421387	26.565	0.706217
15	1	48.7225	0.3769	0	0.734508
16	1	168.294	0.595931	-18.4349	0.905542
16	2	73.224	0.3769	0	0.594187
17	1	60.3203	3.03867	82.8748	0.945218
17	2	33.163	0.56535	0	0.823854
17	3	75.4928	0.266509	-44.9999	0.5449
18	1	59.8268	0.533017	44.9999	0.9289
18	2	45.7889	0.56535	0	0.657557
18	3	30.9475	0.3769	0	0.991718
18	4	73.9836	0.3769	0	0.541326
19	1	59.6139	2.29259	-80.5375	0.824948
19	2	73.9005	0.3769	0	0.57709
20	1	59.5264	1.554	-75.9636	0.889743
21	1	44.4584	0.679466	33.69	0.697208
21	2	168.599	0.3769	0	0.879071
22	1	87.36	0.3769	0	0.89015
23	1	86.7046	0.56535	0	0.925776
23	2	60.2991	0.533017	44.9999	0.936057
23	3	31.317	0.421387	26.565	0.920655
24	1	137.523	0.595931	-18.4349	0.749131
24	2	88.2592	0.595931	-18.4349	0.820388
25	1	47.8045	0.56535	0	0.790518
25	2	136.416	0.533017	-44.9999	0.871836
25	3	32.4148	0.56535	0	0.852
25	4	36.575	0.3769	0	0.694479
26	1	135.045	0.679466	33.69	0.930678
26	2	48.4	0.56535	0	0.760486
26	3	135.948	0.421387	26.565	0.835756

The list goes on until frame 4000.

Appendix I: Composition of the Buffer Solutions

I1: Composition of Buffer Solution for $CoSO_4$–CYANEX® 272 System

Acetic acid (CH_3COOH)/sodium acetate (CH_3COONa) buffer was used to maintain the pH of the aqueous solution at 5.5. The required base:acid concentration for this purpose was calculated as follows:

$$\mathrm{pH} = \mathrm{pK}_a + \log\frac{[base]}{[acid]}$$

$$5.5 = 4.74 + \log\frac{[\mathrm{CH_3COONa}]}{[\mathrm{CH_3COOH}]}$$

$$\frac{[\mathrm{CH_3COONa}]}{[\mathrm{CH_3COOH}]} = 5.8$$

Following those used by Assmann (2014), the concentrations of CH_3COONa and CH_3COOH to achieve the required base:acid ratio of 5.8 were 0.81 mol/L and 0.14 mol/L, respectively. The CH_3COONa was made by neutralising CH_3COOH with NaOH according to the following equation:

$$\mathrm{CH_3COOH_{(aq)} + NaOH_{(s)} = CH_3COONa_{(aq)} + H_2O_{(l)}}$$

Therefore, the total concentration of NaOH and CH_3COOH that were needed to make the buffer were 0.81 mol/L and 0.95 mol/L, respectively.

I2: Composition of Buffer Solution for $CuSO_4$–LIX® 84-I System

Acetic acid/sodium acetate buffer was also used for the aqueous solution in this system to maintain the pH at 4.5. The required base:acid concentration was:

$$\mathrm{pH} = \mathrm{pK}_a + \log\frac{[base]}{[acid]}$$

$$4.5 = 4.74 + \log\frac{[\mathrm{CH_3COONa}]}{[\mathrm{CH_3COOH}]}$$

$$\frac{[\mathrm{CH_3COONa}]}{[\mathrm{CH_3COOH}]} = 0.57$$

The chosen concentrations of CH_3COONa and CH_3COOH for the buffer to achieve the required base:acid ratio of 0.57 were 0.44 mol/L and 0.78 mol/L, respectively. This was deemed to be the lowest acetic acid concentration that can be used without compromising the capacity of the buffer. The acetic acid concentration needed to be as low as possible to minimise the formation of copper(II) acetate. Similar to that in the $CoSO_4$–CYANEX 272 System, the CH_3COONa was made by neutralising CH_3COOH with NaOH. The total concentration of NaOH and CH_3COOH that were needed to make the buffer were 0.22 mol/L and 0.60 mol/L, respectively.

Appendix J: Procedure for the Extraction Experiments

The dispersion experiments were performed as per steps detailed below:

1. Turn on the computer and the camera controller, and open the FastCam software.
2. Open the aluminium enclosure.
3. Fill the dispersion column with 200 mL of the prepared organic solution and then put it on the support jack between the camera and laser.
4. Raise the support jack so the electrodes are immersed in the organic solution until the surface of the solution coincides with the start of the high-field-strength region as shown in Figure J1.
5. Fill the aqueous solution reservoir with 10 mL of the prepared aqueous solution and insert the pump tubing into the reservoir.
6. Turn on the pump, prime it and ensure that the feed droplets are released approximately at the centre of the column between the electrodes.
7. Set the lens magnification to 1.0 by removing the camera splash guard and adjusting the zoom dial, and open the laser beam shutter.
8. Close the aluminium enclosure.
9. Turn on the laser controller with the key switch and go through the detailed parameter setting for the camera and laser.
10. Start the laser emission, turn on the pump and align the position of the electrodes by using the joystick controller for the positioning table so they are located at the centre of the screen and the droplets captured on the screen are in focus.
11. When the droplets are in focus, start recording to check the spacing between the electrodes and the position of the feed droplets when entering the column.
12. Replay the recording and select an image that shows a droplet between the electrode so the distance between the electrodes and the distance between the droplet and the two electrodes can be measured. An example of an image showing the correct electrode spacing and feed droplet position is shown in Figure J2.
13. If the spacing is not correct and the feed droplets are not situated correctly between the electrodes, then turn off the laser, open the enclosure, adjust the position of the electrodes and the delivery tip manually and repeat steps 8 until 12.
14. If the spacing is correct and the feed droplets are situated correctly between the electrodes, then turn off the laser, open the enclosure and set the lens magnification for the working magnification such as 1.5 or 4.0.
15. Close the aluminium enclosure.
16. Turn on the laser controller with the key switch and go through the detailed parameter setting for the camera and laser for the new lens magnification.
17. Start the laser emission, turn on the pump and align the position of the electrodes by using the joystick controller for the positioning table only so the droplets captured on the screen are in focus.

18. When the camera focus is set, turn off the pump.
19. Turn on the AC power supply and the voltage amplifier, and set the voltage and frequency of the field.
20. Turn on the pump and start recording.
21. When the recording is completed, turn off the laser controller, the AC power supply, the voltage amplifier and the pump.
22. Save 4000 frames of the recorded images into the computer.
23. Open the enclosure and shut the laser beam shutter.
24. Lower the support jack to remove the column from the enclosure without contacting the electrodes.
25. Clean the electrodes carefully using deionised water and methylated spirits so they maintain their positions to ensure that the distance between them remains constant.
26. Clean the tubing by pumping deionised water through them.
27. Transfer both the used organic and the raffinate solutions from the dispersion experiments into a waste container for disposal.
28. Clean the column using deionised water and methylated spirits.
29. Repeat Steps 3−28 to run a new experiment, but ensure that both the electrodes and the column are dried before use, or turn off the rest of the equipment and close the aluminium enclosure if finished with the experiment.

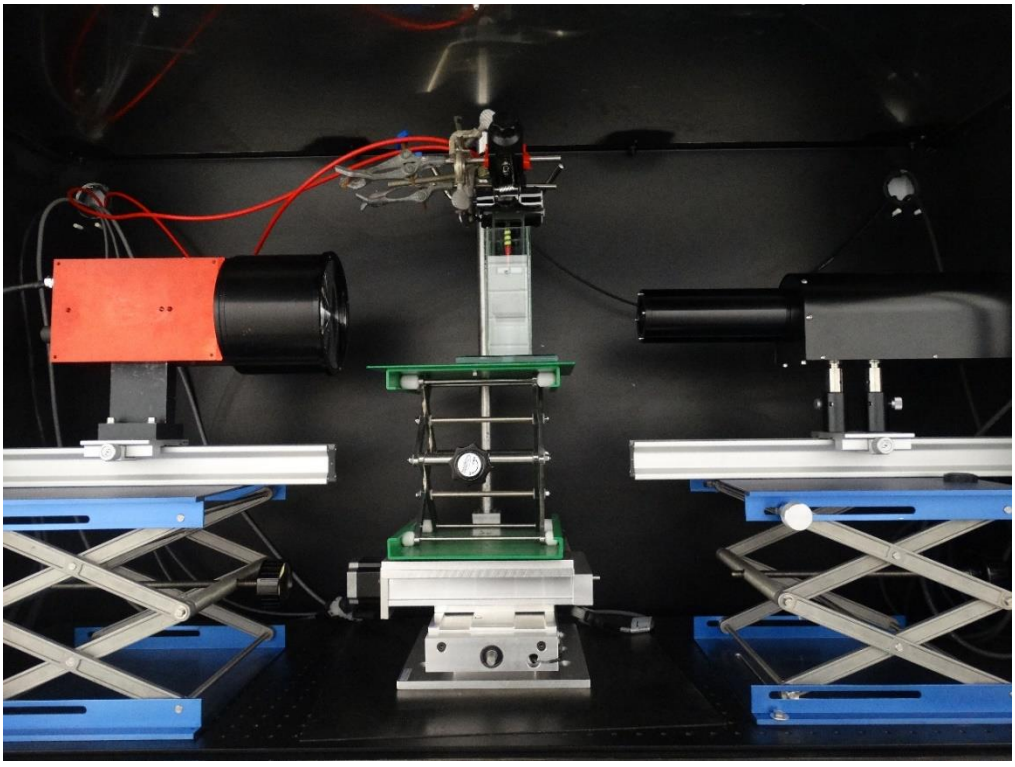

Figure J1. Photograph of the column placement during a dispersion experiment.

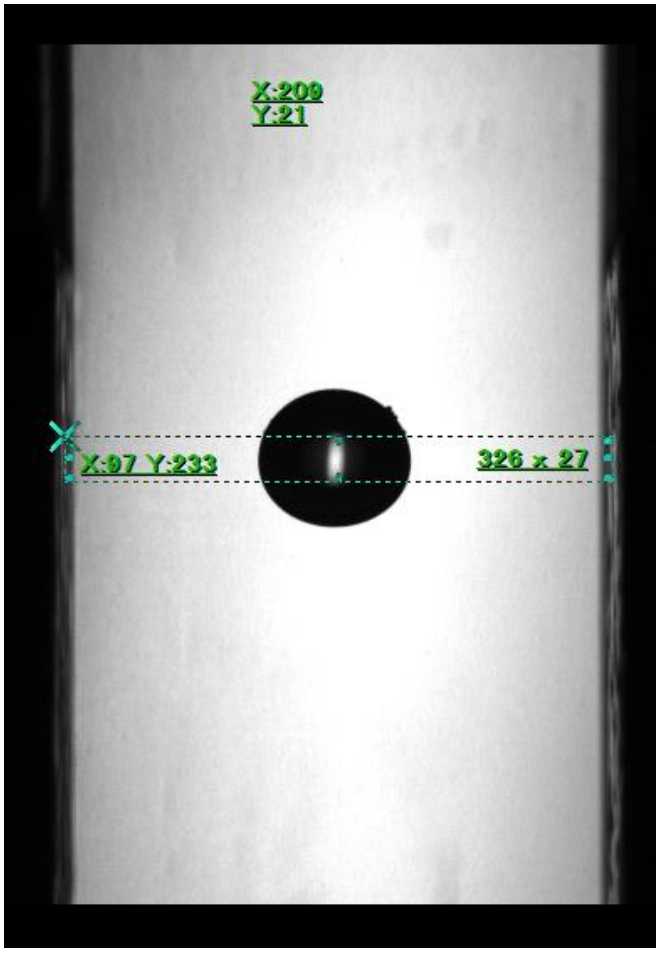

Figure J2. An example of the measurement to check the distance between the electrodes and between the droplet and the two electrodes. The image was taken using a lens magnification of 1.0, giving a pixel/micron ratio of 30.460. The 326 pixels measured by the FastCam software shows that the distance between the electrodes was 9.93 mm. The middle dots of the measurement square coincide right on the droplet's halo proving that the droplet was situated approximately at the centre of the column between the electrodes.

Appendix K: Procedure for the Extraction Experiments

The extraction experiments were performed as per steps detailed below:

1. Turn on the computer and the camera controller, and open the FastCam software.
2. Open the aluminium enclosure.
3. Fill the aqueous solution reservoir with 10 mL of the prepared aqueous solution and insert the pump tubing into the reservoir.
4. Put an empty 250-mL glass beaker on a support jack below the electrodes to collect the droplets that are used to check the camera focus.
5. Turn on the pump, prime it and ensure that the feed droplets are released approximately at the centre of the column between the electrodes.
6. Set the lens magnification to 1.0 by removing the splash guard and adjusting the zoom dial, and open the laser beam shutter.
7. Close the aluminium enclosure.
8. Turn on the laser controller with the key switch and go through the detailed parameter setting for the camera and laser.
9. Start the laser emission, turn on the pump and align the position of the electrodes by using the joystick controller for the positioning table so they are located at the centre of the screen and the droplets captured on the screen are in focus.
10. When the droplets are in focus, start recording to check the spacing between the electrodes and the position of the feed droplets when entering the column.
11. Replay the recording and select an image that shows a droplet between the electrodes so the distance between the electrodes and the distance between the droplet and the two electrodes can be measured.
12. If the spacing is not correct and the feed droplets are not situated correctly between the electrodes, then turn off the laser, open the enclosure, adjust the position of the electrodes and the delivery tip manually and repeat steps 7 until 11.
13. If the spacing is correct and the feed droplets are situated correctly between the electrodes, then turn off the laser, open the enclosure and shut the laser beam shutter.
14. Connect a polypropylene stopcock valve on the extraction column, ensure that the valve is closed and then fill the column with 80 mL of the prepared organic solution.
15. Put the column carefully into the setup so the electrodes are immersed in the organic solution until the surface of the solution coincides with the start of the high-field-strength region, and fix the column position with a clamp.
16. Connect a syringe with a syringe filter, take out its plunger and place it on the positioning table below the mouth of the valve to receive the sample when the valve is opened. Use a 5-mL glass beaker to support the syringe and a 200-mL glass beaker to surround the syringe to prevent it from tumbling as shown in Figure K1.

17. Turn on the AC power supply and the voltage amplifier, and set the voltage and frequency of the field.
18. Prepare a timer to record the experimental run time, turn on the pump and start the timer as the first feed droplet enters the column.
19. After the intended experimental time has passed, turn off the pump and ensure that no remnant droplet is hanging on the mouth of the delivery tip.
20. When the bulk of the last dispersing droplet passes the high-field-strength region, turn off the AC power supply and the voltage amplifier.
21. Open the valve carefully to drain the aqueous sample into the syringe.
22. Put the plunger back into the syringe and filter the sample into the 5-mL glass beaker.
23. Dilute the sample in 1 wt% nitric acid solution to achieve a particular dilution factor and store the sample for assay.
24. Remove the column carefully without contacting the electrodes and transfer the used organic solution into a waste container for disposal.
25. Clean the electrodes carefully using deionised water and methylated spirits so they maintain their positions to ensure that the distance between them remains constant.
26. Clean the tubing by pumping deionised water through them.
27. Clean the column using deionised water and methylated spirits.
28. Repeat Steps 3−27 to run a new experiment, but ensure that both the electrodes and the column are dry before use, or turn off the rest of the equipment and close the aluminium enclosure if finished with the experiment.

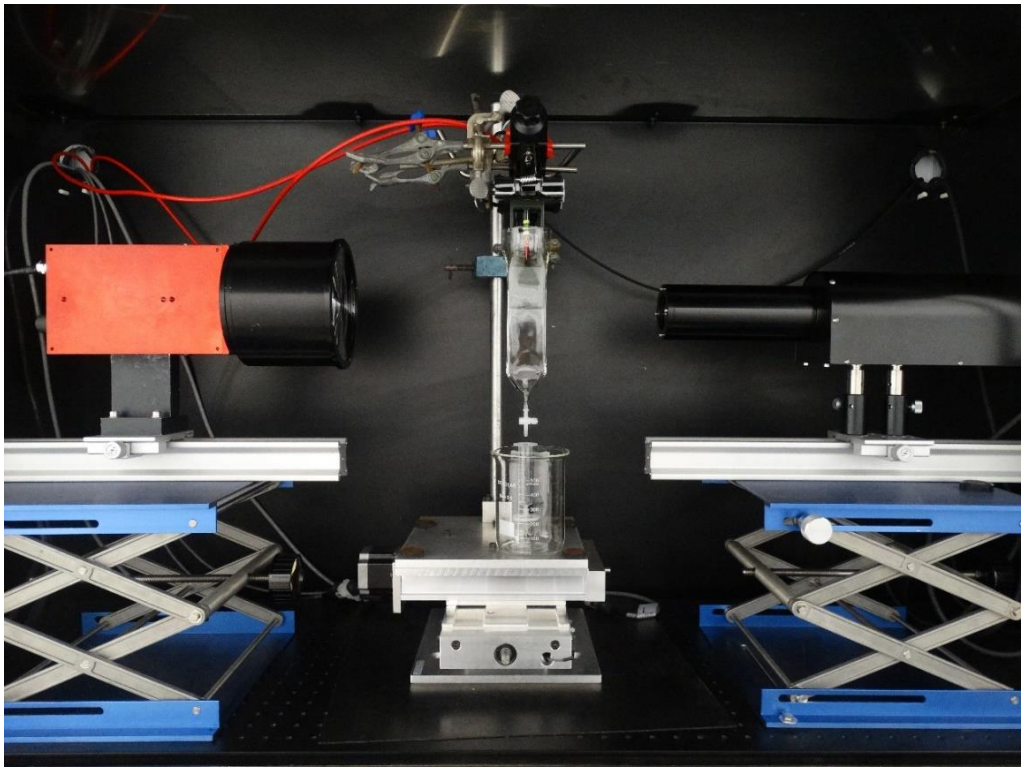

Figure K1. Photograph of the column placement during an extraction experiment.

Appendix L: Copyright Agreement to Use Copyright Materials

ELSEVIER LICENSE
TERMS AND CONDITIONS
Apr 11, 2022

This Agreement between Curtin University -- Zela Ichlas ("You") and Elsevier ("Elsevier") consists of your license details and the terms and conditions provided by Elsevier and Copyright Clearance Center.

License Number	5281831510551
License date	Apr 04, 2022
Licensed Content Publisher	Elsevier
Licensed Content Publication	International Journal of Heat and Mass Transfer
Licensed Content Title	Fluid flow and transfer behavior of a drop translating in an electric field at intermediate Reynolds numbers
Licensed Content Author	Loto S. Chang,John C. Berg
Licensed Content Date	Jun 1, 1983
Licensed Content Volume	26
Licensed Content Issue	6
Licensed Content Pages	10
Start Page	823
End Page	832
Type of Use	reuse in a thesis/dissertation
Portion	figures/tables/illustrations
Number of figures/tables/illustrations	1
Format	electronic
Are you the author of this Elsevier article?	No
Will you be translating?	No
Title	Study on Application of Electrostatic Solvent Extraction for Process Metallurgy
Institution name	Curtin University
Expected presentation date	Dec 2022

Portions	Figure 1 on page 828
Requestor Location	Curtin University 95 Egan St Kalgoorlie, Western Australia 6430 Australia Attn: Curtin University
Publisher Tax ID	GB 494 6272 12
Total	0.00 AUD
Terms and Conditions	

INTRODUCTION

1. The publisher for this copyrighted material is Elsevier. By clicking "accept" in connection with completing this licensing transaction, you agree that the following terms and conditions apply to this transaction (along with the Billing and Payment terms and conditions established by Copyright Clearance Center, Inc. ("CCC"), at the time that you opened your Rightslink account and that are available at any time at http://myaccount.copyright.com).

GENERAL TERMS

2. Elsevier hereby grants you permission to reproduce the aforementioned material subject to the terms and conditions indicated.

3. Acknowledgement: If any part of the material to be used (for example, figures) has appeared in our publication with credit or acknowledgement to another source, permission must also be sought from that source. If such permission is not obtained then that material may not be included in your publication/copies. Suitable acknowledgement to the source must be made, either as a footnote or in a reference list at the end of your publication, as follows:

"Reprinted from Publication title, Vol /edition number, Author(s), Title of article / title of chapter, Pages No., Copyright (Year), with permission from Elsevier [OR APPLICABLE SOCIETY COPYRIGHT OWNER]." Also Lancet special credit - "Reprinted from The Lancet, Vol. number, Author(s), Title of article, Pages No., Copyright (Year), with permission from Elsevier."

4. Reproduction of this material is confined to the purpose and/or media for which permission is hereby given.

5. Altering/Modifying Material: Not Permitted. However figures and illustrations may be altered/adapted minimally to serve your work. Any other abbreviations, additions, deletions and/or any other alterations shall be made only with prior written authorization of Elsevier Ltd. (Please contact Elsevier's permissions helpdesk here). No modifications can be made to any Lancet figures/tables and they must be reproduced in full.

6. If the permission fee for the requested use of our material is waived in this instance, please be advised that your future requests for Elsevier materials may attract a fee.

7. Reservation of Rights: Publisher reserves all rights not specifically granted in the combination of (i) the license details provided by you and accepted in the course of this licensing transaction, (ii) these terms and conditions and (iii) CCC's Billing and Payment terms and conditions.

8. License Contingent Upon Payment: While you may exercise the rights licensed immediately upon issuance of the license at the end of the licensing process for the transaction, provided that you have disclosed complete and accurate details of your proposed use, no license is finally effective unless and until full payment is received from you (either by publisher or by CCC) as provided in CCC's Billing and Payment terms and conditions. If full payment is not received on a timely basis, then any license preliminarily granted shall be deemed automatically revoked and shall be void as if never granted. Further, in the event that you breach any of these terms and conditions or any of CCC's Billing and Payment terms and conditions, the license is automatically revoked and shall be void as if never granted. Use of materials as described in a revoked license, as well as any use of the materials beyond the scope of an unrevoked license, may constitute copyright infringement and publisher reserves the right to take any and all action to protect its copyright in the materials.

9. Warranties: Publisher makes no representations or warranties with respect to the licensed material.

10. Indemnity: You hereby indemnify and agree to hold harmless publisher and CCC, and their respective officers, directors, employees and agents, from and against any and all claims arising out of your use of the licensed material other than as specifically authorized pursuant to this license.

11. No Transfer of License: This license is personal to you and may not be sublicensed, assigned, or transferred by you to any other person without publisher's written permission.

12. No Amendment Except in Writing: This license may not be amended except in a writing signed by both parties (or, in the case of publisher, by CCC on publisher's behalf).

13. Objection to Contrary Terms: Publisher hereby objects to any terms contained in any purchase order, acknowledgment, check endorsement or other writing prepared by you, which terms are inconsistent with these terms and conditions or CCC's Billing and Payment terms and conditions. These terms and conditions, together with CCC's Billing and Payment terms and conditions (which are incorporated herein), comprise the entire agreement between you and publisher (and CCC) concerning this licensing transaction. In the event of any conflict between your obligations established by these terms and conditions and those established by CCC's Billing and Payment terms and conditions, these terms and conditions shall control.

14. Revocation: Elsevier or Copyright Clearance Center may deny the permissions described in this License at their sole discretion, for any reason or no reason, with a full refund payable to you. Notice of such denial will be made using the contact information provided by you. Failure to receive such notice will not alter or invalidate the denial. In

no event will Elsevier or Copyright Clearance Center be responsible or liable for any costs, expenses or damage incurred by you as a result of a denial of your permission request, other than a refund of the amount(s) paid by you to Elsevier and/or Copyright Clearance Center for denied permissions.

LIMITED LICENSE

The following terms and conditions apply only to specific license types:

15. **Translation**: This permission is granted for non-exclusive world **English** rights only unless your license was granted for translation rights. If you licensed translation rights you may only translate this content into the languages you requested. A professional translator must perform all translations and reproduce the content word for word preserving the integrity of the article.

16. **Posting licensed content on any Website**: The following terms and conditions apply as follows: Licensing material from an Elsevier journal: All content posted to the web site must maintain the copyright information line on the bottom of each image; A hyper-text must be included to the Homepage of the journal from which you are licensing at http://www.sciencedirect.com/science/journal/xxxxx or the Elsevier homepage for books at http://www.elsevier.com; Central Storage: This license does not include permission for a scanned version of the material to be stored in a central repository such as that provided by Heron/XanEdu.

Licensing material from an Elsevier book: A hyper-text link must be included to the Elsevier homepage at http://www.elsevier.com . All content posted to the web site must maintain the copyright information line on the bottom of each image.

Posting licensed content on Electronic reserve: In addition to the above the following clauses are applicable: The web site must be password-protected and made available only to bona fide students registered on a relevant course. This permission is granted for 1 year only. You may obtain a new license for future website posting.

17. **For journal authors:** the following clauses are applicable in addition to the above:

Preprints:

A preprint is an author's own write-up of research results and analysis, it has not been peer-reviewed, nor has it had any other value added to it by a publisher (such as formatting, copyright, technical enhancement etc.).

Authors can share their preprints anywhere at any time. Preprints should not be added to or enhanced in any way in order to appear more like, or to substitute for, the final versions of articles however authors can update their preprints on arXiv or RePEc with their Accepted Author Manuscript (see below).

If accepted for publication, we encourage authors to link from the preprint to their formal publication via its DOI. Millions of researchers have access to the formal publications on ScienceDirect, and so links will help users to find, access, cite and use the best available

version. Please note that Cell Press, The Lancet and some society-owned have different preprint policies. Information on these policies is available on the journal homepage.

Accepted Author Manuscripts: An accepted author manuscript is the manuscript of an article that has been accepted for publication and which typically includes author-incorporated changes suggested during submission, peer review and editor-author communications.

Authors can share their accepted author manuscript:

- immediately
    - via their non-commercial person homepage or blog
    - by updating a preprint in arXiv or RePEc with the accepted manuscript
    - via their research institute or institutional repository for internal institutional uses or as part of an invitation-only research collaboration work-group
    - directly by providing copies to their students or to research collaborators for their personal use
    - for private scholarly sharing as part of an invitation-only work group on commercial sites with which Elsevier has an agreement
- After the embargo period
    - via non-commercial hosting platforms such as their institutional repository
    - via commercial sites with which Elsevier has an agreement

In all cases accepted manuscripts should:

- link to the formal publication via its DOI
- bear a CC-BY-NC-ND license - this is easy to do
- if aggregated with other manuscripts, for example in a repository or other site, be shared in alignment with our hosting policy not be added to or enhanced in any way to appear more like, or to substitute for, the published journal article.

Published journal article (JPA): A published journal article (PJA) is the definitive final record of published research that appears or will appear in the journal and embodies all value-adding publishing activities including peer review co-ordination, copy-editing, formatting, (if relevant) pagination and online enrichment.

Policies for sharing publishing journal articles differ for subscription and gold open access articles:

Subscription Articles: If you are an author, please share a link to your article rather than the full-text. Millions of researchers have access to the formal publications on ScienceDirect, and so links will help your users to find, access, cite, and use the best available version.

Theses and dissertations which contain embedded PJAs as part of the formal submission can be posted publicly by the awarding institution with DOI links back to the formal publications on ScienceDirect.

If you are affiliated with a library that subscribes to ScienceDirect you have additional private sharing rights for others' research accessed under that agreement. This includes use

for classroom teaching and internal training at the institution (including use in course packs and courseware programs), and inclusion of the article for grant funding purposes.

Gold Open Access Articles: May be shared according to the author-selected end-user license and should contain a CrossMark logo, the end user license, and a DOI link to the formal publication on ScienceDirect.

Please refer to Elsevier's posting policy for further information.

18. **For book authors** the following clauses are applicable in addition to the above: Authors are permitted to place a brief summary of their work online only. You are not allowed to download and post the published electronic version of your chapter, nor may you scan the printed edition to create an electronic version. **Posting to a repository:** Authors are permitted to post a summary of their chapter only in their institution's repository.

19. **Thesis/Dissertation**: If your license is for use in a thesis/dissertation your thesis may be submitted to your institution in either print or electronic form. Should your thesis be published commercially, please reapply for permission. These requirements include permission for the Library and Archives of Canada to supply single copies, on demand, of the complete thesis and include permission for Proquest/UMI to supply single copies, on demand, of the complete thesis. Should your thesis be published commercially, please reapply for permission. Theses and dissertations which contain embedded PJAs as part of the formal submission can be posted publicly by the awarding institution with DOI links back to the formal publications on ScienceDirect.

Elsevier Open Access Terms and Conditions

You can publish open access with Elsevier in hundreds of open access journals or in nearly 2000 established subscription journals that support open access publishing. Permitted third party re-use of these open access articles is defined by the author's choice of Creative Commons user license. See our open access license policy for more information.

Terms & Conditions applicable to all Open Access articles published with Elsevier:

Any reuse of the article must not represent the author as endorsing the adaptation of the article nor should the article be modified in such a way as to damage the author's honour or reputation. If any changes have been made, such changes must be clearly indicated.

The author(s) must be appropriately credited and we ask that you include the end user license and a DOI link to the formal publication on ScienceDirect.

If any part of the material to be used (for example, figures) has appeared in our publication with credit or acknowledgement to another source it is the responsibility of the user to ensure their reuse complies with the terms and conditions determined by the rights holder.

Additional Terms & Conditions applicable to each Creative Commons user license:

CC BY: The CC-BY license allows users to copy, to create extracts, abstracts and new works from the Article, to alter and revise the Article and to make commercial use of the